PLOS ONE

RESEARCH ARTICLE

Empirical models for anatomical and physiological changes in a human mother and fetus during pregnancy and gestation

Dustin F. Kapraun[1]*, **John F. Wambaugh**[2], **R. Woodrow Setzer**[2], **Richard S. Judson**[2]

1 National Center for Environmental Assessment, US Environmental Protection Agency, Research Triangle Park, North Carolina, United States of America, **2** National Center for Computational Toxicology, US Environmental Protection Agency, Research Triangle Park, North Carolina, United States of America

* kapraun.dustin@epa.gov

Citation: Kapraun DF, Wambaugh JF, Setzer RW, Judson RS (2019) Empirical models for anatomical and physiological changes in a human mother and fetus during pregnancy and gestation. PLoS ONE 14(5): e0215906. https://doi.org/10.1371/journal.pone.0215906

Editor: Frank T. Spradley, University of Mississippi Medical Center, UNITED STATES

Received: October 18, 2018

Accepted: April 10, 2019

Published: May 2, 2019

Data Availability Statement: All relevant data are within the manuscript and its Supporting Information files.

Funding: This work was supported in part by an appointment (DFK) to the Research Participation Program at the National Center for Computational Toxicology administered by the Oak Ridge Institute for Science and Education (ORISE). through an interagency agreement between the US Department of Energy and the US Environmental Protection Agency. ORISE did not play any role in

Abstract

Many parameters treated as constants in traditional physiologically based pharmacokinetic models must be formulated as time-varying quantities when modeling pregnancy and gestation due to the dramatic physiological and anatomical changes that occur during this period. While several collections of empirical models for such parameters have been published, each has shortcomings. We sought to create a repository of empirical models for tissue volumes, blood flow rates, and other quantities that undergo substantial changes in a human mother and her fetus during the time between conception and birth, and to address deficiencies with similar, previously published repositories. We used maximum likelihood estimation to calibrate various models for the time-varying quantities of interest, and then used the Akaike information criterion to select an optimal model for each quantity. For quantities of interest for which time-course data were not available, we constructed composite models using percentages and/or models describing related quantities. In this way, we developed a comprehensive collection of formulae describing parameters essential for constructing a PBPK model of a human mother and her fetus throughout the approximately 40 weeks of pregnancy and gestation. We included models describing blood flow rates through various fetal blood routes that have no counterparts in adults. Our repository of mathematical models for anatomical and physiological quantities of interest provides a basis for PBPK models of human pregnancy and gestation, and as such, it can ultimately be used to support decision-making with respect to optimal pharmacological dosing and risk assessment for pregnant women and their developing fetuses. *The views expressed in this article are those of the authors and do not necessarily represent the views or policies of the U.S. Environmental Protection Agency.*

the study design, data collection and analysis, decision to publish, or preparation of the manuscript. More information about ORISE is available at https://orise.orau.gov/.

Competing interests: The authors have declared that no competing interests exist.

Introduction

Human health chemical risk assessments frequently consider pregnant women as a subpopulation of interest based on the relatively high exposure rates and/or susceptibility of this group to various compounds [1, 2]. Unfortunately, pregnant women are generally underrepresented in pharmaceutical clinical studies [3] and non-therapeutic chemicals are rarely studied in humans at any life-stage [4–6]. In order to assess the risk posed by a chemical, pharmacokinetic (PK) modeling can be used to relate chemical exposure to potential toxicity in tissues [7]. PK models describe chemical absorption, distribution, metabolism, and elimination by the body [8, 9]. Furthermore, such models allow one to quantify the tissue concentrations resulting from external doses, whether they are controlled (e.g., doses administered in a clinical trial or animal toxicity study [10]) or uncontrolled (e.g., through complex environmental exposures [11]).

During gestation there are windows of toxic susceptibility during which chemical insults may induce life-long adverse effects [2, 9, 12–14]. Mathematical PK models provide a means for predicting fetal tissue exposures to chemicals [12, 15]. Given that PK data in pregnant women and in utero infants are unavailable for most chemicals, models are needed to estimate doses of concern based on data collected for non-pregnant adults or from animals [12]. Physiologically based PK (PBPK) models offer an attractive option for extrapolating information in applications such as human health risk assessments [16–18]. Furthermore, PBPK models can be used to understand and potentially replace some of the default uncertainty factors that are typically applied when using toxicity data to establish a reference dose [12, 19].

Taking into account an external dose (such as an amount that is consumed orally, applied dermally, or inhaled from ambient air), a PBPK model utilizes information about absorption into the body, distribution and storage throughout the body's tissues, metabolism within particular tissues, and excretion from the body to estimate internal doses (amounts or concentrations) at various sites within the body [20]. In other words, a PBPK model predicts concentrations in various tissues (e.g., adipose and brain tissues) represented by "compartments" of known volume that are connected by "flows", most typically of blood [21, 22]. Barton et al. [23] identified many ways in which PBPK models may be used for extrapolation, including across life-stages [15, 24]. For the current manuscript, we constructed mathematical models describing anatomical and physiological changes associated with human pregnancy and gestation, as we contend that such models must be an integral part of any PBPK model that describes the kinetics of a chemical in a mother and her fetus over a significant portion of the pregnancy.

Several different collections of time-varying formulae describing quantities related to human pregnancy and gestation have already been published, and most recently Dallmann et al. [3] performed a meta-analysis of the literature in order to construct such a set of time-dependent formulae. Prior to this, Luecke and coauthors [9, 15, 25–27] developed a collection of formulae describing anatomical and physiological changes related to pregnancy and gestation. This latter collection of models has been particularly influential, with more than one hundred citations in peer-reviewed publications related to PBPK models. The following list describes some of the publications and research groups that have provided one or more formulae related to human gestation and pregnancy:

- Wosilait et al. [27] constructed an empirical model for human embryonic and fetal growth during in utero development that was based on four data sets covering various periods of gestation that were published between 1909 and 1975.
- Luecke et al. [15] published a general human pregnancy PBPK model that uses the fetal mass model of Wosilait et al. [27]. In the context of the PBPK model, Luecke et al. [15] provided a

collection of models for changes in maternal and fetal tissue volumes and blood flow rates that are based upon allometric scaling of the fetal mass, but they did not describe the methods and data that were used to calibrate these models. Those authors cited a "submitted" article ("Luecke et al., '93b") as the source of the models, but the manuscript of the same title that was ultimately published [25] only described the models and data sources for time-varying masses of fetal tissues (not for fetal blood flow rates, maternal tissue masses, or maternal blood flow rates).

- Abduljalil et al. [28] and Gaohua et al. [29] described empirical models for many of the anatomical and physiological changes that occur in a human mother during pregnancy. For their maternal models, these authors compiled an extensive list of published studies to build a large combined data set for various anatomical and physiological changes that occur in human, singleton, low-risk, normal pregnancies. Abduljalil et al. [28] also developed a model for fetal volume and Gaohua et al. [29] constructed models for the volume of and blood flow rates to a "fetoplacental unit", which they consider as a single lumped compartment in their human pregnancy PBPK model. For each quantity of interest, Abduljalil et al. [28] used the coefficient of determination (R^2) to select an optimal model from among several polynomial models, but using this measure of goodness of fit tends to bias the model selection process by favoring models with more parameters [30].
- El-Masri et al. [31] published a "life-stage" PBPK model for humans that includes a PBPK model for pregnancy and gestation. Therein, the authors provided some models for time-dependent parameters, but did not describe their methods for doing so. They also cited and used some models of Luecke et al. [25], which have already been described in this list.
- Dallmann et al. [3] curated a data set and used it to fit models for anatomical and physiological changes that occur in women and their fetuses during pregnancy. In this analysis, the authors considered changes to fetal mass (as well as mass of total body water, intra- and extra-cellular water, proteins, and lipids), cord blood flow, and hematocrit, but they did not provide formulae for other fetal changes. In contrast to models constructed by others, the models of Dallmann et al. [3] use "fetal age" (i.e., time since fertilization of the ovum) instead of "gestational age" (time since the first day of the final menstrual period prior to conception) as the independent variable.
- Zhang et al. [32] published a PBPK model for a human mother and fetus and introduced novel models for volume of and blood flow to several fetal compartments not included in the other collections of formulae named here in this list. Like Abduljalil et al. [28], Zhang et al. [32] used the coefficient of determination (R^2) to select optimal models; as asserted previously, using this measure of goodness of fit tends to bias the model selection process [30]. Furthermore, Zhang et al. [32] do not completely describe all fetal blood flow rates relevant to their PBPK model; for example, they do not provide formulae for blood flow through the "ductus venosus/foramen ovale" or to the fetal "rest of body", both of which are depicted in their PBPK model schematic Fig 1 [32]. Finally, several of the models provided by Zhang et al. [32] are only valid during relatively brief periods of pregnancy (e.g., "10–20 weeks" for "fetal brain blood flow") and they make no recommendation about extrapolating the models for use in other periods of pregnancy, though they, themselves, seem to have performed PBPK model simulations for times well outside these periods (e.g., up to "40 weeks").
- Abduljalil et al. [33] described empirical models for organ and tissue volumes of a human fetus during gestation. To construct the models, these authors compiled a data set from published studies on embryonic and fetal tissue growth and composition during in utero

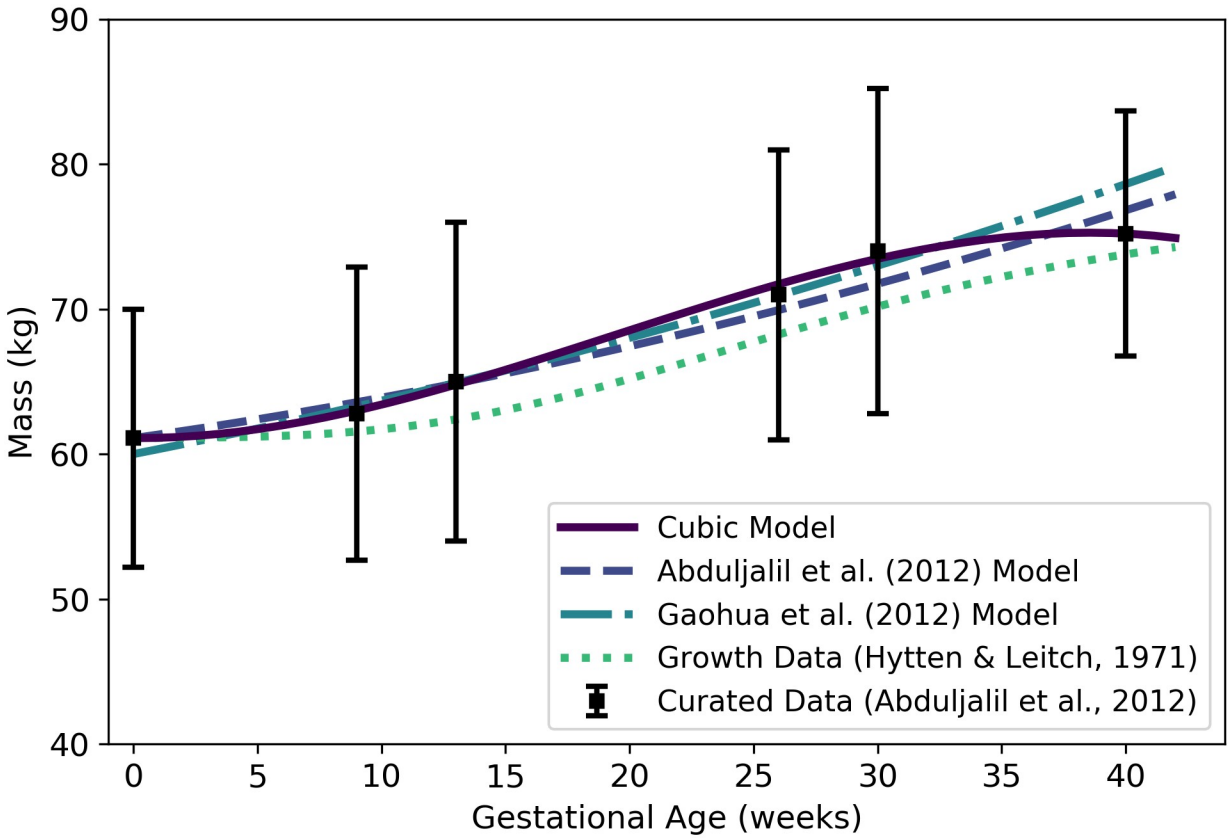

Fig 1. Mass of a human mother vs. gestational age. The cubic model (solid line) given by Eq 1 was selected as the most parsimonious model in our analysis. The models of Abduljalil et al. [28] and Gaohua et al. [29], both quadratic, were calibrated using the same curated data set [28] used by us. The maternal mass gain data (or "growth data") depicted here were modified from the source [48] to account for an assumed initial mass as described in the text. Note that all models depicted here describe the mass of the entire maternal body plus the products of conception (including the fetus, placenta, and amniotic fluid).

https://doi.org/10.1371/journal.pone.0215906.g001

development. Like Dallmann et al. [3], but in contrast to their own previous work [28], these authors used fetal age rather than gestational age as the independent variable in their models.

In Table 1, we provide an itemized comparison of the various publications in the preceding list.

We developed the current manuscript en route to producing a PBPK model for a human mother and fetus because we were not able to find in the literature useful models for all the time-varying quantities of interest that we needed to construct such a PBPK model. This manuscript expands on previous work by constructing and selecting empirical models for anatomical and physiological changes in a human mother and fetus that either (1) have not been described mathematically in previous similar collections of human pregnancy models (i.e., models for blood flow rates to maternal adipose tissue, gut, liver, and thyroid, and to the fetal lung, gut, kidney, brain, liver, and thyroid, and through the fetal ductus arteriosus and the foramen ovale); (2) have been described mathematically, but by models that appear to give unreasonably high or low values when compared with data (i.e., the Luecke et al. [15] models for maternal plasma volume, amniotic fluid volume, and fetal lung mass, the Gaohua et al. [29] model for maternal adipose mass, the Dallmann et al. [3] model for maternal glomerular

Table 1. Itemized comparison of selected publications that contain one or more formulae related to human gestation and pregnancy.

Manuscript	[27]	[15]	[25]	[28]	[29]	[31]	[3]	[32]	[33]	Current
Presents original data*	N	N	N	N	N	N	N	N	N	N
Presents original compiled data* set(s)	Y	N	N	Y	N	N	Y	Y	Y	N
Presents original models† based on compiled data sets of Abduljalil et al. [28]	N	N	N	Y	Y	N	N	N	N	Y
Presents original models† based on compiled data sets of Abduljalil et al. [33]	N	N	N	N	N	N	N	N	Y	Y
(+) Employs and thoroughly describes rigorous statistical methods for parameter‡ estimation	Y	N	Y	N	N	N	Y	N	Y	Y
(+) Employs and thoroughly describes rigorous statistical methods for model† selection	N	N	N	N	N	N	Y	N	Y	Y
(+) Presents original models† for multiple maternal compartments	N	Y	N	Y	Y	Y	Y	N	N	Y
(+) Presents original models† for multiple fetal compartments	N	Y	Y	N	N	Y	N	Y	Y	Y
(+) Presents models that reflect a biologically accurate depiction of the fetal circulatory system§	N	N	N	N	N	Y	N	N¶	N	Y
(+) Presents explicit models† for "rest of body" compartments that yield feasible (e.g., non-negative) values for all relevant time points	N	N	N	N	N	N	N	Y	N	Y
(+) Systematically compares original models† with previously published models†	N	N	N	N	N	N	N	N	N	Y
(-) Presents models that contain errors or inconsistencies identified in the current manuscript	N	Y	N	N	Y	N	Y	Y	Y	N

The labels "(+)" and "(-)" on the descriptions in the first column indicate features of models that are desirable or not desirable, respectively. Throughout the table, the symbols "Y" and "N" indicate a "yes" (positive) or "no" (negative) response, respectively, to the question implied by the corresponding entry in the first column.

*Refers to data describing compartment volumes, blood flow rates to compartments, glomerular filtration rates, and/or hematocrits in a human mother and/or fetus during pregnancy/gestation.

†Refers to models describing compartment volumes, blood flow rates to compartments, glomerular filtration rates, and/or hematocrits in a human mother and/or fetus during pregnancy/gestation. Note that here the term "models" does not refer to PBPK model(s).

‡Refers to parameters in time- or mass-dependent models for compartment volumes, blood flow rates to compartments, glomerular filtration rates, and/or hematocrits in a human mother and/or fetus during pregnancy/gestation.

§In this context, a "biologically accurate depiction of the fetal circulatory system" refers to one that explicitly acknowledges the existence of fetal blood vessels and routes (including the ductus arteriosus, ductus venosus, and foramen ovale) that do not occur in the adult circulatory system.

¶Zhang et al. [32] present a model for flow through the ductus venosus, but do not present models for flow through the ductus arteriosus or the foramen ovale.

https://doi.org/10.1371/journal.pone.0215906.t001

filtration, and the Abduljalil et al. [33] model for fetal kidney mass); or (3) have been described mathematically, but using model parameterization and selection methods that are either not statistically rigorous (e.g., the models of Abduljalil et al. [28] and Zhang et al. [32]) or not described at all (e.g., the models of Luecke et al. [15] and Gaohua et al. [29]). Wherever possible, we have endeavored to compare our models to those presented elsewhere. Also, we include herein mathematical descriptions for "rest of body" volumes and blood flow rates that incorporate mass balance principles, whereas the aforementioned published collections (with the notable exception of Zhang et al. [32]) do not. These efforts have resulted in a comprehensive collection of empirical models for important time-varying quantities that one should consider when constructing a PBPK model of human gestation and pregnancy.

Methods

Data sets

We used both curated (multiple-source) data sets and original (single-source) data sets to calibrate empirical models for various anatomical and physiological quantities that vary during gestation. In particular, we relied heavily on composite data sets published by Abduljalil et al. [28] and Abduljalil et al. [33]; for those quantities not described in these two sources (e.g., fetal blood flow rates), we located data from other published studies. Also, for cases in which data were only available in a graphical form, we used the WebPlotDigitizer data extraction tool [34] to convert the graphically-presented data into numerical data. The sources for the specific data

sets used to calibrate models for each quantity of interest are identified in Table 2, and additional details are given in the Results section.

Some data sets are based on gestational age, or time since the last menstruation, whereas others are based on fetal age, or time since fertilization of the ovum. For purposes data analysis and model comparison, we assumed that gestational age equals fetal age plus two weeks [42] to convert data and models based on fetal age to time scales based on gestational age.

Models

We examined four basic types of models to describe changes in masses, volumes, percentages (such as hematocrits) and rates (such as blood flow and glomerular filtration rates) that occur during the singleton pregnancy of an "average" healthy woman. In particular, we considered polynomial models (up to degree 3), Gompertz models, logistic models, and allometric power law models. For quantities expected to have initial values (i.e., values at the beginning of gestation) of zero (such as fetal body mass), we examined pure Gompertz and logistic growth models as candidate models, whereas for quantities expected to have initial values substantially greater than zero (such as maternal body mass) we examined modified Gompertz and logistic growth models that include an additional parameter describing a "baseline" value for the quantity of interest. In these models, the additional parameter is an additive constant that does not influence the rate of growth. For some of the quantities considered, power law models were used to relate the quantity to a body mass (i.e., the maternal or fetal mass). When the quantity in question had an initial value substantially greater than zero but the related body mass did not (as for fetal body mass), we examined modified power law models that include an additional parameter describing a baseline value. Formulae and references for all models we considered are provided in Table 3.

Model calibration

In considering any particular model and any given quantity of interest (e.g., maternal body mass), we used data to identify the model parameters $\{\theta_0, \theta_1, \ldots\}$ that allow one to estimate the quantity of interest as a function y of an independent variable t (e.g., a gestational age or body mass) and said parameters (cf. Table 3). The data sets utilized included means, standard deviations, and sample sizes paired with times (gestational ages) or body masses. For data sets in which standard deviations and samples sizes were unavailable, we assumed a 20% coefficient of variation and a sample size of one for each data point. We used a standard maximum likelihood approach to obtain a maximum likelihood estimate (MLE) for the model parameters. Further details are provided in the Supporting Information (S1 File).

Model selection

After obtaining the MLE for each model for a given data set and quantity of interest, we chose the most parsimonious model by applying the Akaike information criterion (AIC) [47]. We computed the AIC score of each model as

$$\mathrm{AIC} = 2k - 2\ell(\hat{\theta}; \mathcal{D}),$$

where k is the number of parameters in the model, $\hat{\theta}$ is the MLE, $\mathcal{D}$ represents the data, and ℓ denotes the log-likelihood function. The model with the lowest AIC score was then selected as the most parsimonious model. For those cases in which the most parsimonious model gave negative values for the quantity of interest at any point in the domain of applicability (e.g., for

Table 2. Data sources, preferred models, and relevant figures for various quantities of interest.

Symbol	Quantity	Units	Data Source	Preferred Equation	Figure
W^{m}	Maternal mass	kg	Abduljalil et al. [28]	1	1
W^{f}	Fetal mass or volume	g or mL	Abduljalil et al. [28]	2	2
W^{m}_{adip}	Maternal adipose tissue mass	kg	Abduljalil et al. [28]	3	3
V^{m}_{adip}	Maternal adipose tissue volume	L	Abduljalil et al. [28]	4	N/A
V^{m}_{plas}	Maternal plasma volume	L	Abduljalil et al. [28]	5	4
V^{m}_{rbcs}	Maternal red blood cell volume	L	Abduljalil et al. [28]	7	5
V^{m}_{plac}	Placenta volume	mL	Abduljalil et al. [28]	8	6
V^{m}_{amnf}	Amniotic fluid volume	mL	Abduljalil et al. [28]	9	7
V^{m}_{rest}	Maternal "rest of body" volume	L	N/A	12	8
Q^{m}_{artb}	Maternal cardiac output	L/h	Abduljalil et al. [28]	13	9
Q^{m}_{adip}	Maternal blood flow to adipose tissue	L/h	ICRP [35]	14	N/A
Q^{m}_{bran}	Maternal blood flow to brain	L/h	ICRP [35]	15	N/A
Q^{m}_{kidn}	Maternal blood flow to kidneys	L/h	Abduljalil et al. [28]	17	10
Q^{m}_{gutx}	Maternal blood flow to gut	L/h	ICRP [35]	18	N/A
Q^{m}_{livr}	Maternal blood flow to liver	L/h	ICRP [35]	19	N/A
Q^{m}_{thyr}	Maternal blood flow to thyroid	L/h	ICRP [35]	20	N/A
Q^{m}_{plac}	Maternal blood flow to placenta	L/h	Wang and Zhao [36]	22	11
Q^{m}_{rest}	Maternal blood flow to "rest of body"	L/h	N/A	23	12
H^{m}	Maternal hematocrit	percent	Abduljalil et al. [28]	24	13
k^{m}_{kidn}	Maternal glomerular filtration rate	mL/min	Abduljalil et al. [28]	26	14
W^{f}_{bran}	Fetal brain mass	g	Abduljalil et al. [33]	29	15
V^{f}_{bran}	Fetal brain volume	mL	ICRP [35]	30	N/A
W^{f}_{livr}	Fetal liver mass	g	Abduljalil et al. [33]	32	16
V^{f}_{livr}	Fetal liver volume	mL	Overmoyer et al. [37]	33	N/A
W^{f}_{kidn}	Fetal kidney mass	g	Abduljalil et al. [33]	35	17
V^{f}_{kidn}	Fetal kidney volume	mL	ICRP [35]	36	N/A
W^{f}_{lung}	Fetal lung mass	g	Abduljalil et al. [33]	37	18
V^{f}_{lung}	Fetal lung volume	mL	ICRP [35]	38	N/A
W^{f}_{thyr}	Fetal thyroid mass	g	Abduljalil et al. [33]	39	19
V^{f}_{thyr}	Fetal thyroid volume	mL	ICRP [35]	40	N/A
W^{f}_{gutx}	Fetal gut mass	g	Abduljalil et al. [33]	41	20
V^{f}_{gutx}	Fetal gut volume	mL	ICRP [35]	42	N/A
V^{f}_{rest}	Fetal "rest of body" volume	mL	N/A	43	21
Q^{f}_{rvtl}	Fetal blood flow through right ventricle	mL/min	Kiserud et al. [38]	44	22
Q^{f}_{lvtl}	Fetal blood flow through left ventricle	mL/min	Kiserud et al. [38]	45	23
Q^{f}_{DA}	Fetal blood flow through ductus arteriosus	mL/min	Mielke and Benda [39]	46	24
Q^{f}_{artb}	Fetal blood flow to arterial blood	mL/min	N/A	47	N/A
Q^{f}_{lung}	Fetal blood flow to lung	mL/min	N/A	48	N/A
Q^{f}_{FO}	Fetal blood flow through foramen ovale	mL/min	N/A	49	N/A
Q^{f}_{plac}	Fetal blood flow to placenta	mL/min	Kiserud et al. [40]	50	25
Q^{f}_{DV}	Fetal blood flow through ductus venosus	mL/min	Kiserud et al. [40]	51	26
Q^{f}_{gutx}	Fetal blood flow to gut	mL/min	N/A	52	N/A
Q^{f}_{kidn}	Fetal blood flow to kidneys	mL/min	N/A	53	N/A
Q^{f}_{bran}	Fetal blood flow to brain	mL/min	N/A	54	N/A

(*Continued*)

Table 2. (Continued)

Symbol	Quantity	Units	Data Source	Preferred Equation	Figure
Q^{f}_{livr}	Fetal blood flow to liver	mL/min	N/A	55	N/A
Q^{f}_{thyr}	Fetal blood flow to thyroid	mL/min	N/A	56	N/A
Q^{f}_{rest}	Fetal blood flow to "rest of body"	mL/min	N/A	57	28
H^{f}	Fetal hematocrit	mL/min	Ohls [41]	59	29

https://doi.org/10.1371/journal.pone.0215906.t002

gestational ages from 0 to 42 weeks), the model with the next lowest AIC and that did not produce negative values was identified as the "preferred" model.

We remark that we have not attempted to statistically compare our models to other published models. This is because, in many cases, the other models were developed using different data sets. In selecting models, we compared our candidate models to one another (but not to any other published models) using robust statistical methods designed to assess parsimony and agreement with a specific data set; in each case, we then proposed a preferred model. We have provided representations of models published by other authors in our various figures for purposes of visual comparison only. Thus, readers can see in which cases our models appear to be very similar or very dissimilar to other published models.

Composite models

For some important anatomical and physiological quantities, raw data expressed as values vs. gestational ages were not available. For such quantities (e.g., maternal blood flow to adipose tissue and fetal blood flow through the foramen ovale), we constructed composite models. That is, in each such case, we used information about relationships between the quantity of interest and other modeled quantities, possibly along with proportionality constants or relative percentages, to construct a model for the quantity of interest.

Table 3. Types of models used to describe changes in masses, volumes, percentages, and physiological rates during pregnancy and gestation.

Model	Formula	Reference(s)
Linear	$y(t;\theta) = \theta_0 + \theta_1 t$	—
Linear Growth	$y(t;\theta) = \theta_0 t$	—
Quadratic	$y(t;\theta) = \theta_0 + \theta_1 t + \theta_2 t^2$	—
Quadratic Growth	$y(t;\theta) = \theta_0 t + \theta_1 t^2$	—
Cubic	$y(t;\theta) = \theta_0 + \theta_1 t + \theta_2 t^2 + \theta_3 t^3$	—
Cubic Growth	$y(t;\theta) = \theta_0 t + \theta_1 t^2 + \theta_2 t^3$	—
Gompertz	$y(t;\theta) = \theta_0 \cdot \exp\left[\frac{\theta_1}{\theta_2}(1 - \exp[-\theta_2 t])\right]$	[43–45]
Modified Gompertz	$y(t;\theta) = \theta_0 \cdot \exp\left[\frac{\theta_1}{\theta_2}(1 - \exp[-\theta_2 t])\right] + \theta_3$	—
Logistic	$y(t;\theta) = \frac{\theta_0}{1+\exp[-\theta_1(t-\theta_2)]}$	[46]
Modified Logistic	$y(t;\theta) = \frac{\theta_0}{1+\exp[-\theta_1(t-\theta_2)]} + \theta_3$	—
Power Law	$y(x;\theta) = \theta_0 x^{\theta_1}$	—
Modified Power Law	$y(x;\theta) = \theta_0 x^{\theta_1} + \theta_2$	—
Luecke Power Law	$y(x;\theta) = \theta_0 x^{\theta_1 + \theta_2 \cdot \ln(x)}$	[25]
Modified Luecke Power Law	$y(x;\theta) = \theta_0 x^{\theta_1 + \theta_2 \cdot \ln(x)} + \theta_3$	—

https://doi.org/10.1371/journal.pone.0215906.t003

Programming details

For all analyses described herein, we used Python 3.6.4 with the NumPy (version 1.13.3), SciPy (version 0.19.1), Matplotlib (version 2.1.2), and PIL (version 5.0.0) packages. Scripts are available in the Supporting Information (S2 File).

Naming conventions

We have used mathematical symbols to denote various quantities of interest throughout this manuscript. For example, $V^{\mathrm{m}}_{\mathrm{adip}}$ represents the volume of the adipose tissue in the mother. In general, a superscript on such a symbol will be "m" in the case a maternal quantity and "f" in the case of a fetal quantity. When present, the subscript on such a symbol is typically a four-letter code and it indicates a particular physiological compartment. A list of compartment codes is provided in Table 4. For symbols representing blood flow rates through temporary blood vessels or routes in the fetus, the subscript is an upper-case two-letter code indicating the specific blood vessel or route. In particular, "DA", "DV", and "FO" indicate the ductus arteriosus, ductus venosus, and foramen ovale, respectively.

Results

For each quantity of interest discussed in this section, we describe: (1) the data we used for model calibration, (2) the model selected by us after considering both parsimony and plausibility, and (3) previously published models for the same quantity of interest. Our recommended, or "preferred", models for all quantities of interest are identified by equation number in Table 2.

Maternal mass

To identify an optimal model for the mass of an average woman throughout gestation, we used data curated by Abduljalil et al. [28] to calibrate linear, quadratic, and cubic functions (i.e.,

Table 4. Four-letter codes used to represent compartments in a human mother or fetus.

Code	Compartment
artb	Arterial Blood
venb	Venous Blood
plas	Plasma
rbcs	Red Blood Cells
adip	Adipose
lung	Lungs
thyr	Thyroid
kidn	Kidneys
gutx	Gut
livr	Liver
plac	Placenta
amnf	Amniotic Fluid
bran	Brain
ratm	Right Atrium
rvtl	Right Ventricle
latm	Left Atrium
lvtl	Left Ventricle
rest	Rest of Body

These codes appear as subscripts in mathematical symbols throughout this manuscript.

https://doi.org/10.1371/journal.pone.0215906.t004

Table 5. Maternal mass models (mass in kg vs. gestational age in weeks).

Model	$\hat{\theta}_0$	$\hat{\theta}_1$	$\hat{\theta}_2$	$\hat{\theta}_3$	$\ell(\hat{\theta})$	AIC
Linear	61.093	0.35761	—	—	-30314.7	60633.4
Quadratic	61.019	0.42287	-1.6429×10^{-3}	—	-30312.4	60630.8
Cubic	**61.103**	**-0.010614**	**0.029161**	**5.0203×10^{-4}**	**-30298.0**	**60603.9**
Modified Gompertz	0.078155	0.54404	0.10286	61.023	-30299.2	60606.5
Modified Logistic	15.780	0.14502	19.055	60.166	-30298.8	60605.6

For each model considered, the maximum likelihood parameter estimates ($\hat{\theta}$), log-likelihood ($\ell(\hat{\theta})$), and AIC are provided. The row describing the selected model is shown in boldface.

https://doi.org/10.1371/journal.pone.0215906.t005

polynomial functions of degree 1, 2, and 3), as well as modified Gompertz and logistic functions. The cubic model, which had the lowest AIC, gives the mass (kg) of an average pregnant woman as

$$W^{\mathrm{m}}(t) = 61.103 - 0.010614t + 0.029161t^2 - (5.0203 \times 10^{-4})t^3, \quad (1)$$

where t is the gestational age (weeks) of her fetus. Table 5 shows the maximum likelihood estimates of the parameter values for all models considered along with the associated log-likelihood and AIC values. The cubic model of Eq 1 is shown in Fig 1. It is important to note that "maternal mass" includes the mass of the fetus, the placenta, and the amniotic fluid.

Abduljalil et al. [28] and Gaohua et al. [29] both selected quadratic models to give the mass (in kg) of a pregnant woman as a function of gestational age t (in weeks). In both cases, the authors used the same maternal mass data used by us [28] in order to obtain their models. These two models are also shown in Fig 1.

Even without considering the starting mass of a woman, there is tremendous variability in mass *gain* trends of women during pregnancy. For example, some women have gained 23 kg or more at term, while others have actually experienced a *reduction* in total body mass [49]. Hytten and Leitch [48] depicted data summarizing the mean mass gain during pregnancy of 2868 normotensive primigravidae (i.e., women who were pregnant for the first time and who maintained blood pressure in the normal range throughout their pregnancies). Unfortunately, the actual data are not provided by Hytten and Leitch [48], so we were unable to calibrate models to that data as discussed in the Methods section. To compare the trend shown by Hytten and Leitch [48] with our model and the models of Abduljalil et al. [28] and Gaohua et al. [29], we captured data points from their graphical depiction of the data trend curve, calibrated a Gompertz growth curve to fit those points, then added an initial mass of 61.1 kg to match the initial mass of the Abduljalil et al. [28] model. The resulting curve is shown for purposes of comparison in Fig 1.

Fetal mass

To identify an optimal model for the *volume* of an average human fetus throughout gestation, we used data curated by Abduljalil et al. [28]. The Gompertz model, which had the lowest AIC, gives the volume (mL) of an average human fetus as

$$W^{\mathrm{f}}(t) = 0.0018282 \times \exp\left[\frac{1.1735}{0.077577} \times (1 - \exp[-0.077577t])\right], \quad (2)$$

where t is the gestational age (weeks). Since the average density of a human fetus is approximately 1 g/mL throughout gestation [50], $W^{\mathrm{f}}(t)$ also represents the *mass* (g) of the fetus at a

Table 6. Fetal mass models (mass in g vs. gestational age in weeks).

Model	$\hat{\theta}_0$	$\hat{\theta}_1$	$\hat{\theta}_2$	$\hat{\theta}_3$	$\ell(\hat{\theta})$	AIC
Linear Growth	2.0609	—	—	—	-1.3×10^6	2.6×10^6
Quadratic Growth	-14.715	2.4326	—	—	-288832	577668
Cubic Growth	0.11563	0.061459	0.045199	—	-285330	570666
Gompertz	**0.0018282**	**1.1735**	**0.077577**	—	**-258093**	**516193**
Logistic	3680.3	0.29875	31.205	—	-259854	519714

For each model considered, the maximum likelihood parameter estimates ($\hat{\theta}$), log-likelihood ($\ell(\hat{\theta})$), and AIC are provided. The row describing the selected model is shown in boldface.

https://doi.org/10.1371/journal.pone.0215906.t006

given gestational age. Table 6 shows the maximum likelihood estimates of the parameter values for all models considered along with the associated log-likelihood and AIC values. Fig 2 shows the Gompertz model of Eq 2 and three published models for human fetal mass [3, 27, 28].

Like us, Abduljalil et al. [28] and Wosilait et al. [27] both selected Gompertz models to give the volume (mL) of a human fetus as a function of gestational age $\boldsymbol{t}$ (weeks). The model of Abduljalil et al. [28] was calibrated using the same curated data set [28] used by us, but we were unable to reproduce the Gompertz model parameters reported by them. Nevertheless, as illustrated in Fig 2, our Gompertz model and the Abduljalil et al. [28] model predict similar fetal volumes for most gestational ages. The model of Wosilait et al. [27], also depicted in Fig 2, was calibrated using a different data set; thus, it is not surprising that they obtained different Gompertz model parameters and different predicted fetal volumes. Dallmann et al. [3] used a log-logistic model for fetal volume that was calibrated with yet another curated data set.

Maternal compartment volumes

While volumes of many maternal organs and tissues remain approximately constant throughout pregnancy, several of these undergo dramatic changes. In particular, the volumes of adipose tissue and blood components (plasma and red blood cells) generally increase as pregnancy progresses. In addition, the "products of conception", which include the placenta and the amniotic fluid, increase in size as pregnancy progresses and therefore contribute to maternal mass gain [48].

Adipose tissue. For the *mass* of the adipose (fat) tissue of an average woman throughout pregnancy, we used data curated by Abduljalil et al. [28] to calibrate various models. In calibrating the polynomial models and the modified Gompertz and logistic models, we used the total maternal fat mass (mean and standard deviation) vs. gestational age data exactly as tabulated by Abduljalil et al. [28]. In an alternative approach, we followed the working assumption of Luecke et al. [15] that maternal fat mass gain correlates with fetal mass; that is, we considered allometric relationships between these two quantities. Using Eq 2, we calculated a fetal mass for each gestational age data point that was tabulated [28] for total maternal fat mass. We then calibrated modified versions of the power law and Luecke power law models (cf. Table 3) using data for the total maternal fat mass (mean and standard deviation) vs. (calculated) fetal mass. Of all models considered, the linear model had the lowest AIC. This model gives the mass (kg) of the adipose tissue of an average pregnant woman as

$$W^{\mathrm{m}}_{\mathrm{adip}}(t) = 17.067 + 0.14937t, \tag{3}$$

where t is the gestational age (weeks). Since the mean density of human adipose tissue is

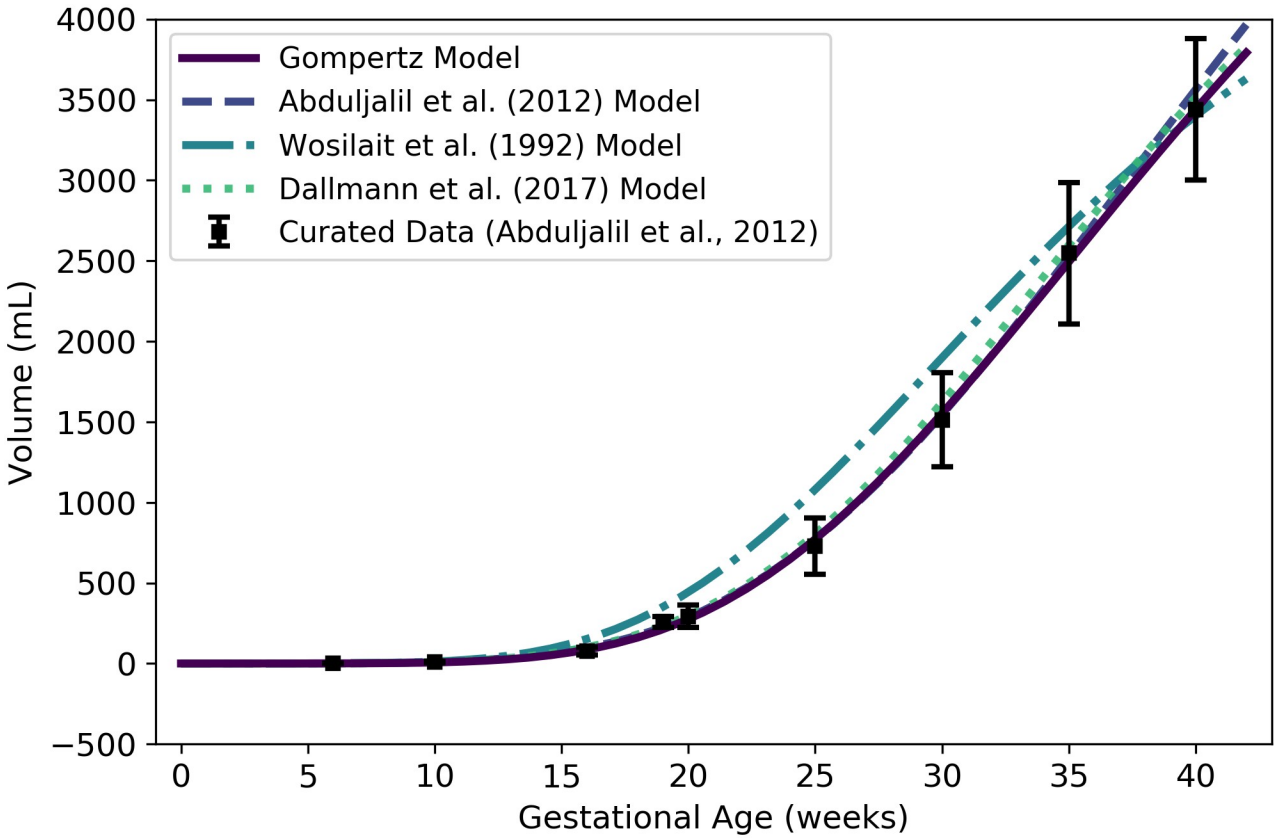

Fig 2. Volume (mL) or mass (g) of a human fetus vs. gestational age. The Gompertz model (solid line) given by Eq 2 was selected as the most parsimonious model in our analysis. The models of Abduljalil et al. [28] and Wosilait et al. [27] were also Gompertz models, though the model parameters used by those authors were different. Dallmann et al. [3] used a log-logistic model for fetal volume. The model of Abduljalil et al. [28] was calibrated using the same curated data set [28] used by us, while the models of Wosilait et al. [27] and Dallmann et al. [3] were calibrated using different data sets.

https://doi.org/10.1371/journal.pone.0215906.g002

0.950 kg/L [51], the *volume* of the maternal adipose tissue (L) can be computed as

$$V^{\mathrm{m}}_{\mathrm{adip}}(t) = \frac{1}{0.950} \cdot W^{\mathrm{m}}_{\mathrm{adip}}(t). \tag{4}$$

Table 7 shows the maximum likelihood estimates of the parameter values for all models considered along with the associated log-likelihood and AIC values. The linear model of Eq 3 and several other models for maternal fat mass are shown in Fig 3.

Abduljalil et al. [28] and Gaohua et al. [29] each selected quadratic models to give the mass (kg) of adipose tissue in a pregnant woman as a function of gestational age t (weeks). In both cases, the authors used the same maternal total fat mass data used by us [28] to obtain their models. Gaohua et al. [29] claim that their model gives the total fat mass (kg) vs. gestational age, but the masses predicted for various gestational ages are about 50% larger than the mean data values upon which the model is based. In an effort to explain this discrepancy, we hypothesized that the Gaohua et al. [29] quadratic model for maternal fat mass is actually a model for the *percentage* of the mother's body mass that is fat. Thus, to obtain fat mass values for comparison, we divided the values predicted by their model by 100 and then multiplied the resulting values by corresponding values from the maternal mass vs. gestational age model that these

Table 7. Maternal fat mass models (mass in kg vs. fetal mass in kg for power law models, mass in kg vs. gestational age in weeks for all other models).

Model	$\hat{\theta}_0$	$\hat{\theta}_1$	$\hat{\theta}_2$	$\hat{\theta}_3$	$\ell(\hat{\theta})$	AIC
Linear	**17.067**	**0.14937**	—	—	**-3221.24**	**6446.48**
Quadratic	17.249	0.11990	7.2110×10^{-4}	—	-3221.13	6448.26
Cubic	17.165	0.19050	-0.0046448	9.6148×10^{-5}	-3220.99	6449.98
Modified Gompertz	20.402	0.0058803	-0.0042400	-3.1426	-3221.12	6450.24
Modified Logistic	104.49	0.0070722	152.86	-9.3414	-3221.18	6450.36
Modified Power Law	4.0204	0.26566	17.224	—	-3221.90	6449.80
Modified Luecke Power Law	4.3011	0.25439	0.0064128	16.904	-3221.77	6451.54

For each model considered, the maximum likelihood parameter estimates ($\hat{\theta}$), log-likelihood ($\ell(\hat{\theta})$), and AIC are provided. The row describing the selected model is shown in boldface.

https://doi.org/10.1371/journal.pone.0215906.t007

authors provide in the same manuscript [29]. That is, in Fig 3, the model labeled "Gaohua et al. (2012) Model" differs from the model described by those authors.

Luecke et al. [15] constructed a model for maternal fat mass *gain*, so to compare its predictions with those of the other models, we added an initial mass of 17.14 kg (the mean value for non-pregnant women from the data set curated by Abduljalil et al. [28]) to the predicted mass

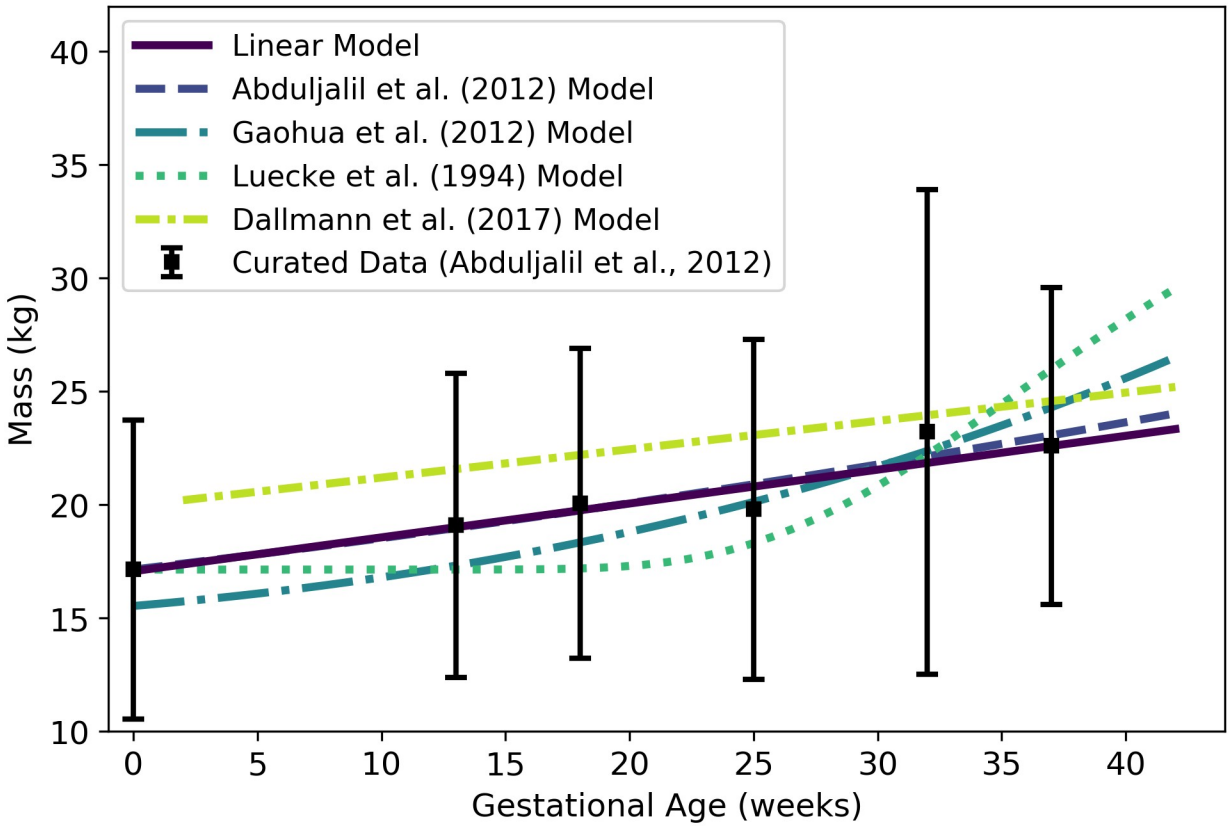

Fig 3. Adipose tissue mass of a human mother vs. gestational age. The linear model (solid line) given by Eq 3 was selected as the most parsimonious model in our analysis. The models of Abduljalil et al. [28] and Gaohua et al. [29], both quadratic, were calibrated using the same curated data set [28] used by us. The latter of these models was modified as described in the text. The model of Luecke et al. [15] was calibrated using different data. It predicts maternal fat mass as a function of total fetal mass, and was interpreted as described in the text. Dallmann et al. [3] also selected a linear model, but they calibrated their model with different data.

https://doi.org/10.1371/journal.pone.0215906.g003

Table 8. Percent of total body mass and density (references listed) for various human organs and tissues.

Compartment	Code	Percent (%) of Total Body Mass*		Density (kg/L)	Density Reference
		Male	Female†		
Adipose	adip	19.9	37.5	0.95	Martin et al. [51]
Brain	bran	1.99	2.17	1.04	ICRP [35]
Thyroid	thyr	0.0274	0.0283	1.05	ICRP [35]
Kidneys	kidn	0.425	0.458	1.05	ICRP [35]
Gut‡	gutx	1.66	1.90	1.045	ICRP [35]
Liver	livr	2.47	2.33	1.05	Overmoyer et al. [37]
Lungs	lung	1.64	1.58	1.05	ICRP [35]
Arterial Blood	artb	—	—	1.06	ICRP [35]
Venous Blood	venb	—	—	1.06	ICRP [35]
Placenta	plac	—	—	1.02	Del Nero et al. [53]
Amniotic Fluid	amnf	—	—	1.01	Uyeno [54]

*Percentages were computed using reference masses from Table 2.8 of ICRP (2002).

†Percentages listed in this column are for a non-pregnant woman.

‡The values listed for the "Gut" assume this compartment comprises the esophagus, stomach, small intestine, and large intestine.

https://doi.org/10.1371/journal.pone.0215906.t008

gain values. The model of Luecke et al. [15], modified as just described to account for an initial maternal fat mass, is shown in Fig 3. For earlier gestational ages, this model predicts maternal fat masses considerably lower than the data values curated by Abduljalil et al. [28]. This may be because the model is a power law based on fetal mass, which does not increase substantially (from an initial mass of about zero) until about 15 weeks, whereas the data suggest that maternal fat mass *does* begin to increase substantially between conception and 13 weeks.

Note that the total fat mass predicted (by our preferred linear model) for a woman at conception, $W^{\mathrm{m}}_{\mathrm{adip}}(0) = 17.067\,\mathrm{kg}$, represents about 27.9% of the total body mass, $W^{\mathrm{m}}(0) = 61.103$ kg. This represents a considerable deviation from the figure of 37.5% reported in Table 8 for adipose body mass percentage for women, but note that that number represents an average for *all* women [35]. The individuals that have been included in studies of pregnancy [3, 28], appear to have a lower mean body fat percentage than the population of all women, or even all women of childbearing age [52].

Plasma. Plasma is one of the two major constituents of blood. We used the curated data of Abduljalil et al. [28] to calibrate various models for plasma volume in a human mother during pregnancy. The modified logistic model, which we found to be the best of the candidate models based on AIC, gives the plasma volume (L) of the mother as

$$V^{\mathrm{m}}_{\mathrm{plas}}(t) = \frac{\mathbf{1.2406}}{\mathbf{1} + \exp[-\mathbf{0.31338}(t - \mathbf{17.813})]} + \mathbf{2.4958}. \tag{5}$$

where t is the gestational age (weeks). Table 9 shows the maximum likelihood estimates of the parameter values for all models considered along with the associated log-likelihood and AIC values. We remark that the modified Luecke power law model yielded a lower AIC (365.07 vs. 365.13), but the AIC difference is too small to recommend one model over the other. Furthermore, the modified Luecke power law relates maternal plasma volume to fetal mass whereas the modified logistic model relates maternal plasma volume directly to gestational age; thus, the latter model has the advantage of not requiring an (intermediate) estimate of fetal mass at each time point of interest. Fig 4 shows the modified logistic model of Eq 5 and several other models for maternal plasma volume. (Fig 4 does not show the modified Luecke power law

Table 9. Maternal plasma volume models (volume in L vs. fetal mass in kg for power law models, volume in L vs. gestational age in weeks for all other models).

Model	$\hat{\theta}_0$	$\hat{\theta}_1$	$\hat{\theta}_2$	$\hat{\theta}_3$	$\ell(\hat{\theta})$	AIC
Linear	2.4661	0.034724	—	—	-214.34	432.69
Quadratic	2.4700	0.032771	5.2886×10^{-5}	—	-214.24	434.47
Cubic	2.4985	-0.03542	0.0053774	-9.4192×10^{-5}	-180.995	369.99
Modified Gompertz	5.3111×10^{-6}	1.9825	0.15982	2.4919	-180.72	369.44
Modified Logistic	**1.2406**	**0.31338**	**17.813**	**2.4958**	**-178.57**	**365.13**
Modified Power Law	0.97923	0.27860	2.4588	—	-195.73	397.46
Modified Luecke Power Law	1.1650	0.14125	-0.083058	2.5002	-178.534	365.07

For each model considered, the maximum likelihood parameter estimates ($\hat{\theta}$), log-likelihood ($\ell(\hat{\theta})$), and AIC are provided. The row describing the selected model is shown in boldface.

https://doi.org/10.1371/journal.pone.0215906.t009

model, but values predicted by that model and the modified logistic model differ by less than 2% throughout the period from 0 to 42 gestational weeks.)

We remark that some longitudinal studies of human subjects have shown that plasma volume typically decreases slightly at the end of pregnancy [55–58]. When applied to the aggregated data set [28] our model selection process led us to choose a model for plasma volume

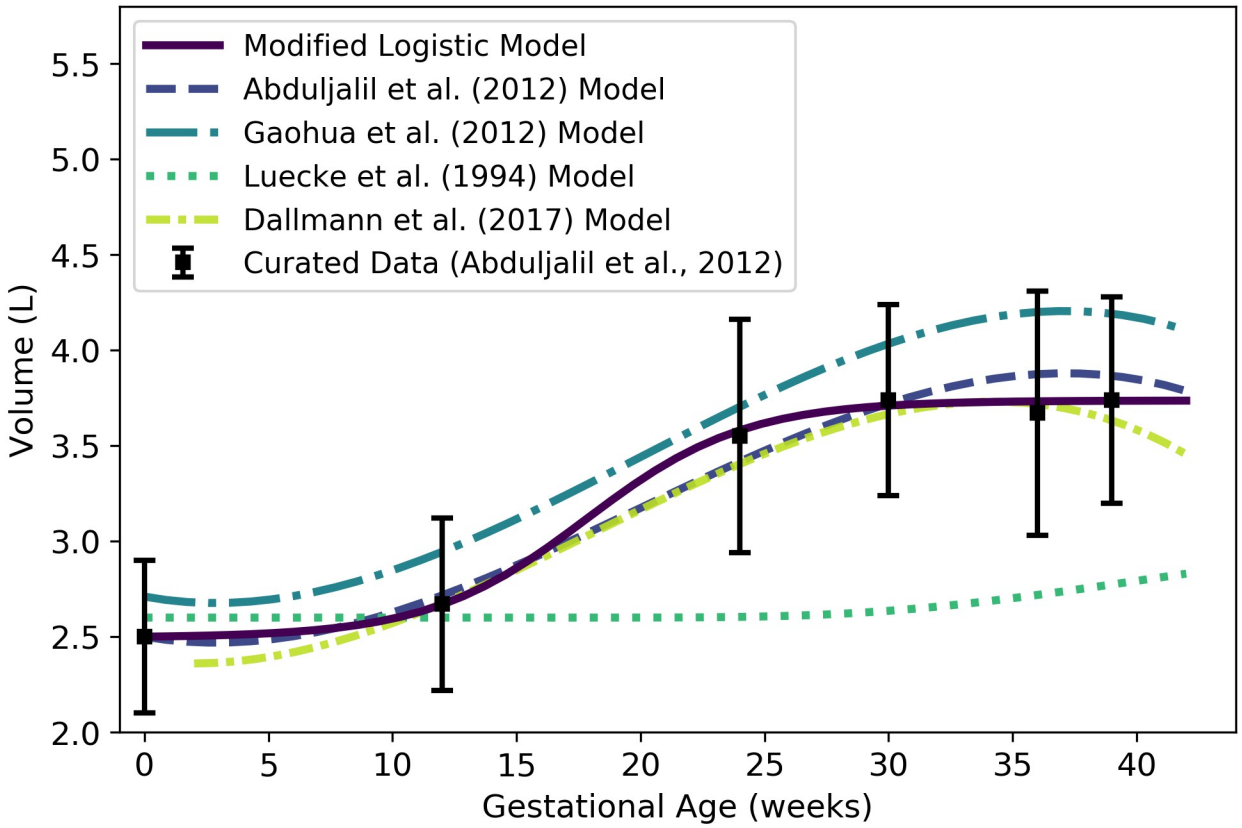

Fig 4. Maternal plasma volume vs. gestational age. The modified logistic model (solid line) given by Eq 5 was selected as the most parsimonious model in our analysis. The models of Abduljalil et al. [28] and Gaohua et al. [29], both cubic polynomials, were calibrated using the same curated data set [28] used by us. The model of Luecke et al. [15] was calibrated using different data. It assumes an initial maternal plasma volume of 2.6 L (or an initial plasma mass of 2.6 kg) and predicts an increase in maternal plasma volume (or mass) as a function of total fetal mass. Dallmann et al. [3] calibrated their cubic model with different data.

https://doi.org/10.1371/journal.pone.0215906.g004

Table 10. Maternal RBC volume models (volume in L vs. fetal mass in kg for power law models, volume in L vs. gestational age in weeks for all other models).

Model	$\hat{\theta}_0$	$\hat{\theta}_1$	$\hat{\theta}_2$	$\hat{\theta}_3$	$\ell(\hat{\theta})$	AIC
Linear	1.4555	0.01101	—	—	3597.70	-7191.41
Quadratic	1.4741	0.007927	7.7997×10^{-5}	—	3612.98	-7219.95
Cubic	1.4918	-0.0070658	0.0011160	-1.7512×10^{-5}	3660.39	-7312.78
Modified Gompertz	1.9369×10^{-5}	1.1786	0.11792	1.4925	3679.15	-7350.31
Modified Logistic	**0.32704**	**0.62555**	**21.452**	**1.5169**	**3753.96**	**-7499.93**
Modified Power Law	0.27569	0.33366	1.4802	—	3662.1	7318.19
Modified Luecke Power Law	0.28532	0.37478	-0.18321	1.5109	3693.36	-7378.72

For each model considered, the maximum likelihood parameter estimates ($\hat{\theta}$), log-likelihood ($\ell(\hat{\theta})$), and AIC are provided. The row describing the selected model is shown in boldface.

https://doi.org/10.1371/journal.pone.0215906.t010

(Eq 5) that does not predict such decrease, though some of the alternative models presented in the literature do [3, 28, 29].

Red blood cells. Red blood cells (RBCs) make up the other major component of human blood. We used curated data from Abduljalil et al. [28] to calibrate various models for RBC volume in a human mother during pregnancy. We selected the modified logistic model given by

$$V^{\mathrm{m}}_{\mathrm{rbcs}}(t) = \frac{\mathbf{0.32704}}{\mathbf{1} + \exp[\mathbf{-0.62555}(t - \mathbf{21.452})]} + \mathbf{1.5169} \tag{6}$$

as the most parsimonious of the candidate models. Here, $V^{\mathrm{m}}_{\mathrm{rbcs}}(t)$ denotes the volume (L) of the RBCs at gestation age t (weeks). Table 10 shows the maximum likelihood estimates of the parameter values for all models considered along with the associated log-likelihood and AIC values.

Through analysis of data sets describing maternal plasma volume, RBC volume, and hematocrit [28], we independently obtained models for each of these quantities (cf. Eqs 5, 6 and 24). However, as one might expect when independently constructing models of interrelated quantities, the models that arose are not perfectly consistent. Because hematocrit represents the volume percentage of RBCs in whole blood, and because whole blood is mostly made up of plasma and RBCs (with only a small fraction made up of white blood cells and platelets), we can estimate the volume (L) of RBCs in maternal blood as

$$V^{\mathrm{m}}_{\mathrm{rbcs}}(t) = \frac{H^{\mathrm{m}}(t)}{1 - H^{\mathrm{m}}(t)} \cdot V^{\mathrm{m}}_{\mathrm{plas}}(t), \tag{7}$$

where $H^{\mathrm{m}}(t)$ and $V^{\mathrm{m}}_{\mathrm{plas}}(t)$ represent the maternal hematocrit and plasma volume (L) at gestation age t (weeks). Thus, if one uses the models for maternal plasma volume, RBC volume, and hematocrit given by Eqs 5, 7 and 24, respectively, the model predictions will be consistent with one another. The modified logistic model of Eq 6, the alternate hematocrit-based model of Eq 7, and three published models for maternal RBC volume [3, 28, 29] are shown in Fig 5.

Placenta. We used the curated data of Abduljalil et al. [28] to calibrate various models for human placenta volume. The cubic growth model given by

$$V^{\mathrm{m}}_{\mathrm{plac}}(t) = \mathbf{-1.7646}t + \mathbf{0.91775}t^2 - \mathbf{0.011543}t^3 \tag{8}$$

was selected as the most parsimonious model for placenta volume (mL) at gestational age t (weeks). Table 11 shows the maximum likelihood estimates of the parameter values for all

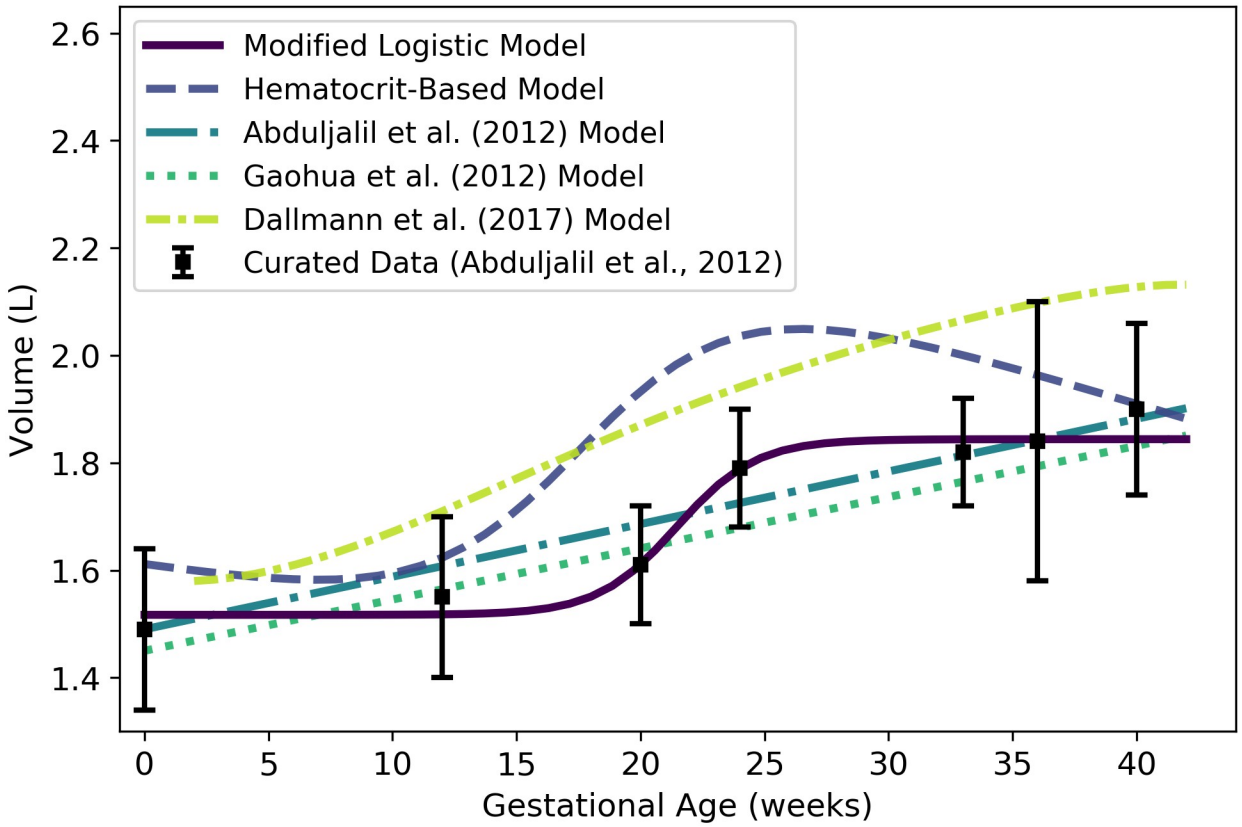

Fig 5. Maternal RBC volume vs. gestational age. The modified logistic model (solid line) given by Eq 6 was selected as the most parsimonious model in our analysis, but the hematocrit-based model (second in legend) of Eq 7 ensures consistency with models for plasma volume (Eq 5) and hematocrit (Eq 24). The models of Abduljalil et al. [28] and Gaohua et al. [29], both of which are linear models, were calibrated using the same curated data set [28] used by us. Dallmann et al. [3] did not create a model for maternal RBC volume, so the model attributed to them here is algebraically derived from their models for plasma volume and hematocrit.

https://doi.org/10.1371/journal.pone.0215906.g005

models considered along with the associated log-likelihood and AIC values. Fig 6 shows the cubic growth model of Eq 8 and three published models for placenta volume [3, 15, 28].

It is worth noting that Eq 8 yields negative volumes for the placenta for gestational ages less than about 1.97 weeks; thus, this equation should not be used to estimate placental volume during that time frame. In any case, conception does not occur until a gestational age of about

Table 11. Placenta volume models (volume in mL vs. fetal mass in kg for power law models, volume in mL vs. gestational age in weeks for all other models).

Model	$\hat{\theta}_0$	$\hat{\theta}_1$	$\hat{\theta}_2$	$\hat{\theta}_3$	$\ell(\hat{\theta})$	AIC
Linear Growth	16.395	—	—	—	-78521.5	157045
Quadratic Growth	8.3802	0.20441	—	—	-78222.9	156450
Cubic Growth	**-1.7646**	**0.91775**	**-0.011543**	**—**	**-78114.3**	**156235**
Gompertz	5.4388	0.33757	0.065182	—	-78119.3	156245
Logistic	802.77	0.12491	27.831	—	-78146.5	156299
Power Law	398.05	0.40647	—	—	-78131.6	156267
Luecke Power Law	389.55	0.4129	0.0096187	—	-78125.4	156257

For each model considered, the maximum likelihood parameter estimates ($\hat{\theta}$), log-likelihood ($\ell(\hat{\theta})$), and AIC are provided. The row describing the selected model is shown in boldface.

https://doi.org/10.1371/journal.pone.0215906.t011

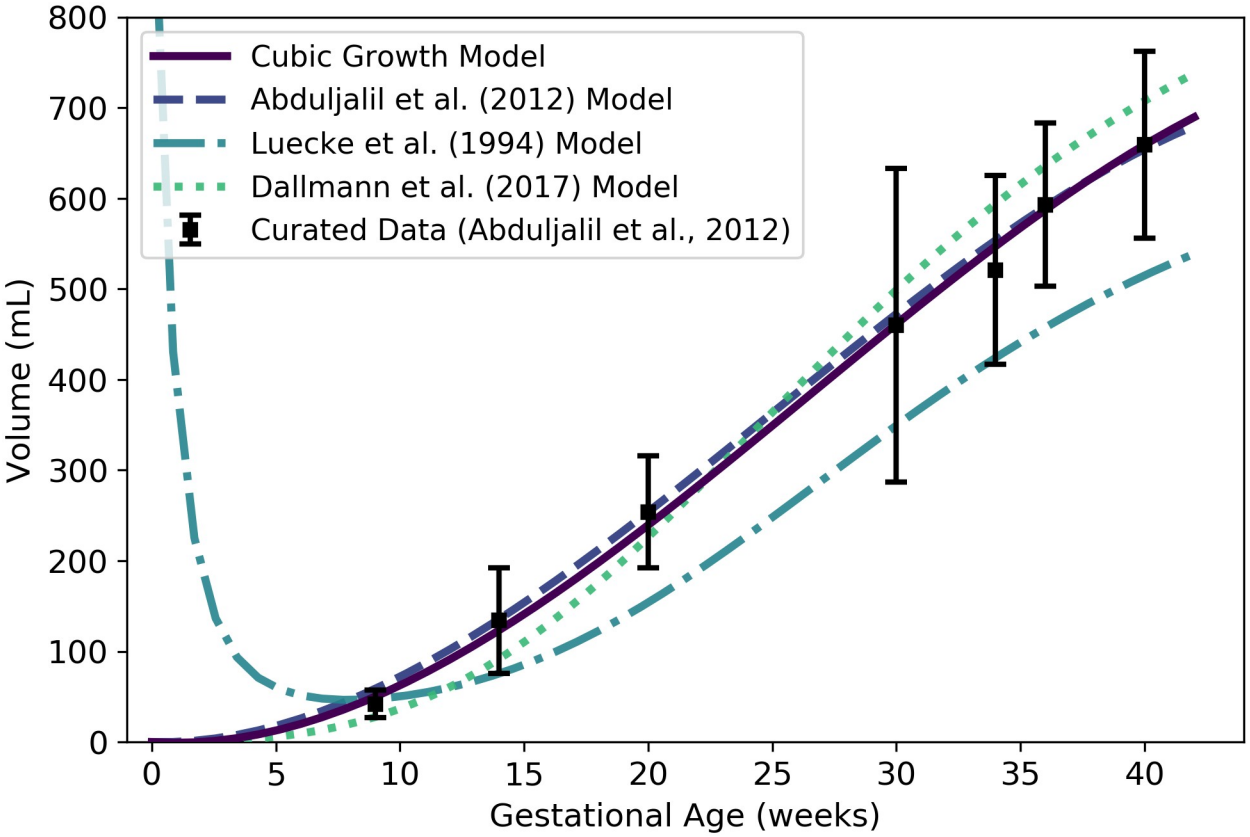

Fig 6. Placenta volume vs. gestational age. The cubic growth model (solid line) given by Eq 8 was selected as the most parsimonious model in our analysis. The model of Abduljalil et al. [28], also a cubic polynomial model, was calibrated using the same curated data set [28] used by us. The model of Luecke et al. [15] was calibrated using different data and assumes a relationship between placenta volume and fetal mass. Dallmann et al. [3] calibrated their cubic model with different data.

https://doi.org/10.1371/journal.pone.0215906.g006

2 weeks, so neither the placenta nor the embryo, itself, come into existence until after that time. At a fetal age of about 4 days, or a gestational age of about 18 days, the cells in the periphery of the blastocyst (i.e., the early embryo) become distinguishable as a trophoblast; this trophoblast is a precursor to the fetal component of the placenta [42]. We propose that Eq 8 be used to estimate the volume of the placenta after 2 weeks, but it should not be considered accurate until 9 weeks (the time of the first data point of Abduljalil et al. [28]).

Amniotic fluid. We used the curated data of Abduljalil et al. [28] to calibrate various models for human amniotic fluid volume. The logistic model given by

$$V^{\mathrm{m}}_{\mathrm{amnf}}(t) = \frac{\mathbf{822.34}}{\mathbf{1} + \exp[-\mathbf{0.26988}(t - \mathbf{20.150})]} \tag{9}$$

was selected as the most parsimonious model for amniotic fluid volume (mL) at gestational age t (weeks). Table 12 shows the maximum likelihood estimates of the parameter values for all models considered along with the associated log-likelihood and AIC values. The logistic model of Eq 9 and three published models for amniotic fluid volume [3, 15, 28] are shown in Fig 7.

Eq 9 yields nonnegative values for amniotic fluid volume on the time domain of interest ($t > 0$); however, as with the placenta volume model, it is worth noting that conception does not occur until a gestational age of about 2 weeks and so none of the products of conception

Table 12. Amniotic fluid volume models (volume in mL vs. fetal mass in kg for power law models, volume in mL vs. gestational age in weeks for all other models).

Model	$\hat{\theta}_0$	$\hat{\theta}_1$	$\hat{\theta}_2$	$\hat{\theta}_3$	$\ell(\hat{\theta})$	AIC
Linear Growth	9.3837	—	—	—	-1122.31	2246.62
Quadratic Growth	-0.045477	0.61316	—	—	-824.80	1653.6
Cubic Growth	-15.702	2.4783	-0.039285	—	-759.30	1524.61
Gompertz	0.041998	1.2118	0.12121	—	-750.239	1506.48
Logistic	**822.34**	**0.26988**	**20.150**	**—**	**-739.00**	**1484.00**
Power Law	535.45	0.43942	—	—	-774.08	1552.16
Luecke Power Law	611.83	0.31801	-0.038286	—	-753.05	1512.10

For each model considered, the maximum likelihood parameter estimates ($\hat{\theta}$), log-likelihood ($\ell(\hat{\theta})$), and AIC are provided. The row describing the selected model is shown in boldface.

https://doi.org/10.1371/journal.pone.0215906.t012

(including amniotic fluid) exist until after that time. To be clear, Eq 9 should not be used to estimate the volume of the amniotic fluid prior to 2 weeks, and should not be considered accurate until 9 weeks (the time of the first data point of Abduljalil et al. [28]).

In Fig 7, we present two versions of the amniotic fluid volume model of Luecke et al. [15]. The first version shown ("Luecke et al. (1994) Model") represents a Luecke power law model

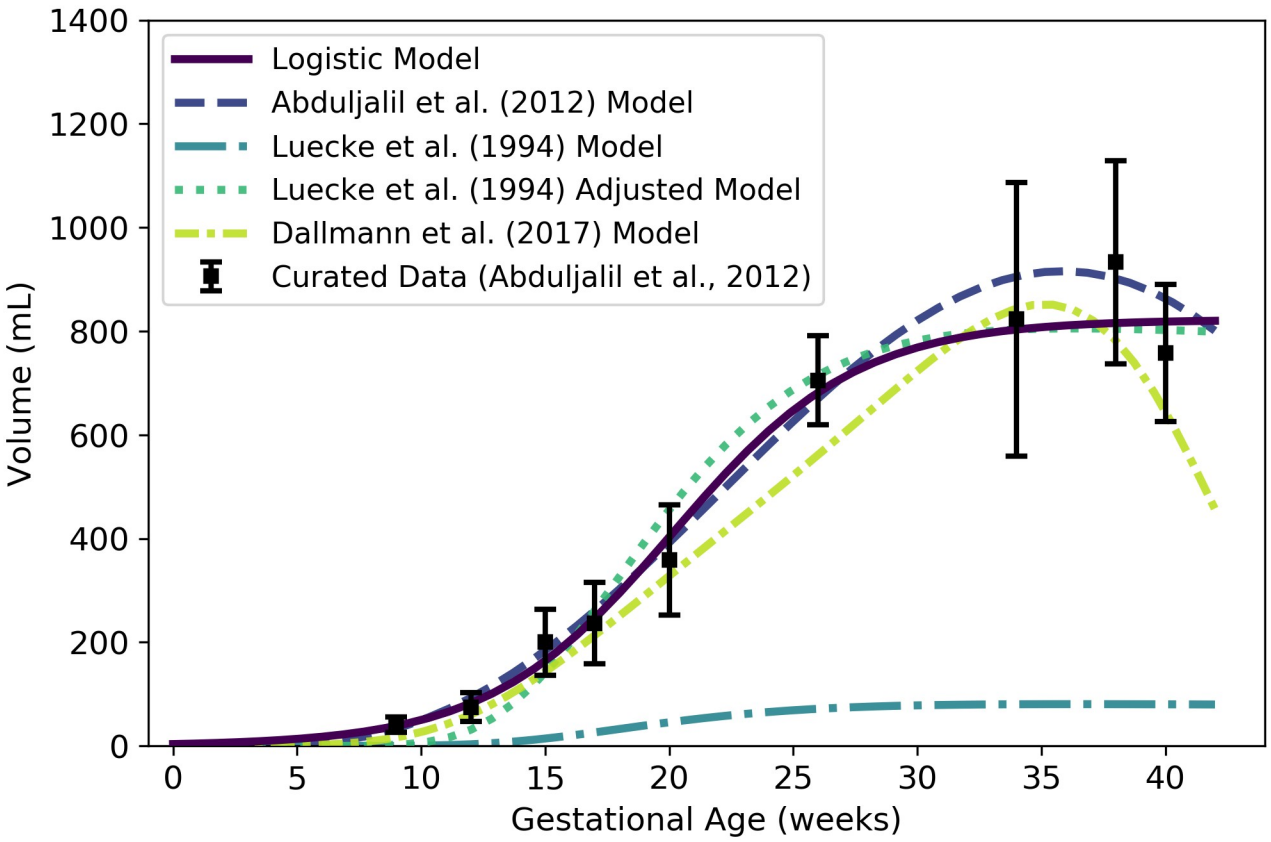

Fig 7. Amniotic fluid volume vs. gestational age. The logistic model (solid line) given by Eq 9 was selected as the most parsimonious model in our analysis. The model of Abduljalil et al. [28], which is a fifth degree polynomial model, was calibrated using the same curated data set [28] used by us. The model of Luecke et al. [15] was calibrated using different data and assumes a relationship between amniotic fluid volume and fetal mass. That model is shown here both as originally stated (in the publication) and after correcting a presumed error (to obtain the "Adjusted Model") as described in the text. Dallmann et al. [3] calibrated their fourth degree polynomial model with different data.

https://doi.org/10.1371/journal.pone.0215906.g007

Table 13. Volumes of (some) maternal compartments that do not change during pregnancy.

Compartment	Symbol	Value (L)
Brain	$V^{\mathrm{m}}_{\mathrm{bran}}$	1.2749
Thyroid	$V^{\mathrm{m}}_{\mathrm{thyr}}$	0.016469
Kidneys	$V^{\mathrm{m}}_{\mathrm{kidn}}$	0.26653
Gut	$V^{\mathrm{m}}_{\mathrm{gutx}}$	1.1110
Liver	$V^{\mathrm{m}}_{\mathrm{livr}}$	1.3559
Lungs	$V^{\mathrm{m}}_{\mathrm{lung}}$	0.91945

https://doi.org/10.1371/journal.pone.0215906.t013

(cf. Table 3) with coefficient values as shown in Table 3 of Luecke et al. [15]. Since that model seems to under-predict amniotic fluid volumes by an order of magnitude, we hypothesized that the first coefficient printed in their table ($\boldsymbol{\theta_0 = 0.002941}$) may have been off by a factor of 10. We therefore increased that coefficient by a factor of 10 ($\boldsymbol{\theta_0 = 0.02941}$) to obtain the second model version ("Luecke et al. (1994) Adjusted Model") shown in Fig 7.

Other specific compartments. Any given PBPK model may include compartments that correspond to specific organs and tissues in the mother that do not vary significantly during a normal pregnancy. To obtain volumes for such compartments that coincide with the time-varying volumes already described, we examined reference values for total body masses of "typical" women and the masses of various organs and tissues in such women as reported by the ICRP [35]. We used these to compute the percent of total body mass accounted for by various tissues. These percentages, along with densities associated with various organs and tissues, are displayed in Table 8. We calculated the static compartment volumes for a typical pregnant woman by multiplying the non-pregnant body mass ($W^{\mathrm{m}}(0) = 61.103$ kg) by the female mass percentage of the relevant tissue or organ and dividing by the relevant density. The volumes obtained for maternal brain, thyroid, kidneys, gut, liver, and lungs are shown in Table 13.

Rest of body. We used the principle of mass balance to obtain a formula for the volume of a "rest of body" compartment comprising all mass in the pregnant female body that has not been accounted for in one of the specific compartments already described. Assuming that the fat-free mass of the mother has an average density of 1.1 g/mL throughout pregnancy [59], the total volume (L) of the maternal fat-free mass is

$$\boldsymbol{V^{\mathrm{m}}_{\mathrm{ffmx}}(t)} = \begin{cases} \dfrac{1}{1.1}\left[\boldsymbol{W^{\mathrm{m}}(t) - W^{\mathrm{m}}_{\mathrm{adip}}(t)}\right] & \boldsymbol{t < 2}, \\ \dfrac{1}{1.1}\left[\boldsymbol{W^{\mathrm{m}}(t) - W^{\mathrm{m}}_{\mathrm{adip}}(t) - \dfrac{1}{1000}\left(W^{\mathrm{f}}(t) + 1.02 \cdot V^{\mathrm{m}}_{\mathrm{plac}}(t) + 1.01 \cdot V^{\mathrm{m}}_{\mathrm{amnf}}(t)\right)}\right] & \boldsymbol{t \geq 2}. \end{cases} \tag{10}$$

Here, we have assumed that the products of conception appear at gestational age 2 weeks, and that the densities of the placenta and amniotic fluid are 1.02 g/mL [53] and 1.01 g/mL [54], respectively (cf. Table 8). (We further assumed that W^{m}, W^{f}, $W^{\mathrm{m}}_{\mathrm{adip}}$, $V^{\mathrm{m}}_{\mathrm{plac}}$, and $V^{\mathrm{m}}_{\mathrm{amnf}}$ are described by Eqs 1, 2, 3, 8 and 9, respectively.) Also, the total volume (L) of all the specific maternal compartments, excluding adipose tissue, is

$$V^{\mathrm{m}}_{\mathrm{allx}}(t) = V^{\mathrm{m}}_{\mathrm{plas}}(t) + V^{\mathrm{m}}_{\mathrm{rbcs}}(t) + V^{\mathrm{m}}_{\mathrm{bran}} + V^{\mathrm{m}}_{\mathrm{thyr}} + V^{\mathrm{m}}_{\mathrm{kidn}} + V^{\mathrm{m}}_{\mathrm{gutx}} + V^{\mathrm{m}}_{\mathrm{livr}} + V^{\mathrm{m}}_{\mathrm{lung}}. \tag{11}$$

(We assumed that the quantities on the right-hand side of this equation are described by Eqs 5 and 7 and the values listed in Table 13.) Thus, the volume of the maternal rest of body

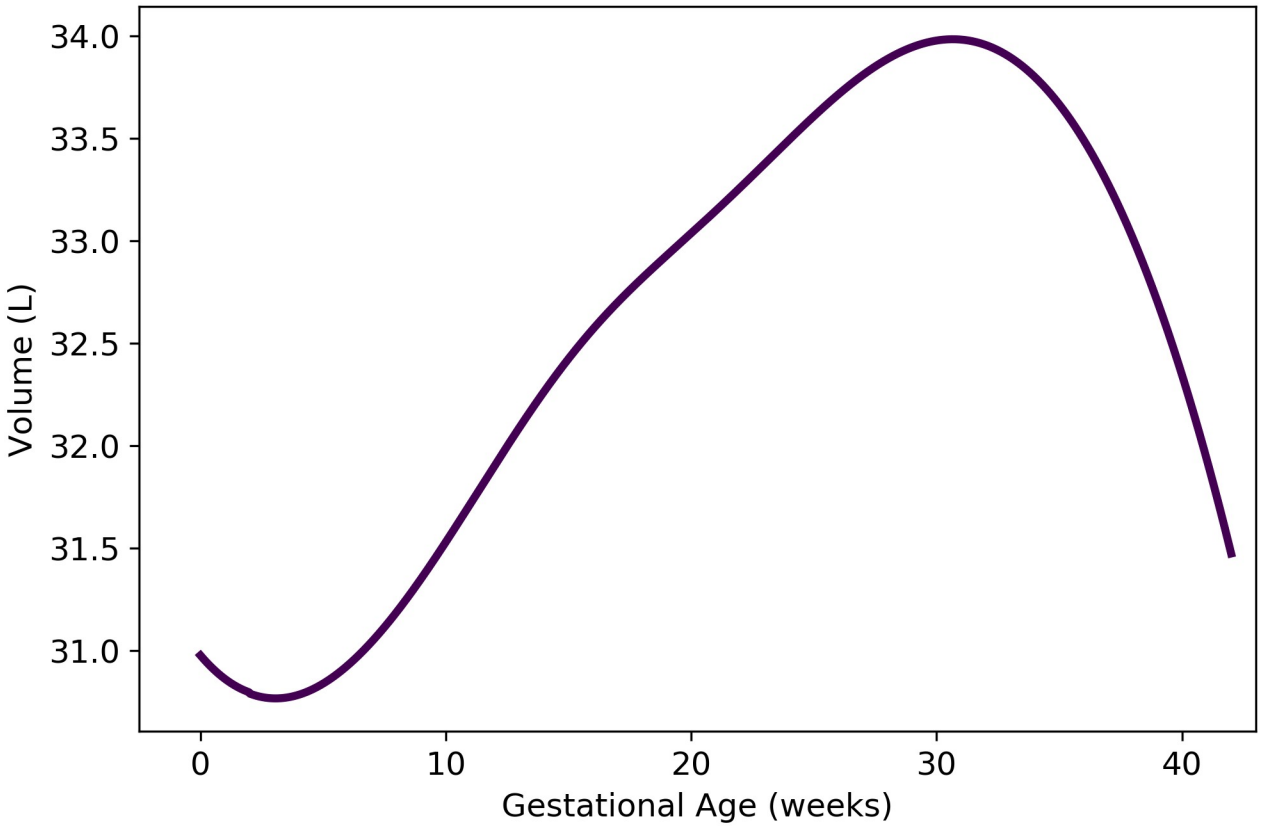

Fig 8. Volume of maternal "rest of body" compartment vs. gestational age. The formula for the depicted model, which is based on mass balance, is provided as Eq 12.

https://doi.org/10.1371/journal.pone.0215906.g008

compartment (L) is

$$V^{\mathrm{m}}_{\mathrm{rest}}(t) = V^{\mathrm{m}}_{\mathrm{ffmx}}(t) - V^{\mathrm{m}}_{\mathrm{allx}}(t), \tag{12}$$

where t is the gestational age (weeks). As shown in Fig 8, Eq 12 results in volumes for the maternal rest of body compartment that fluctuate between approximately 31 and 34 L during pregnancy.

Maternal blood flow rates

During pregnancy, a woman experiences an increase in cardiac output as well as significant changes in the relative blood flow rates to various organs and tissues [35]. We first provide an expression for the maternal cardiac output, which corresponds to the quantity we denote $Q^{\mathrm{m}}_{\mathrm{artb}}$ (the blood flow rate into the mother's arterial blood compartment). Then, we describe flow rates to the other maternal compartments as proportions of the cardiac output. As shown in Table 2.44 from Section 12.2.7 of the ICRP [35] report, the percentage of cardiac output directed to any particular organ or tissue can change as pregnancy progresses. For blood flow rates for which time course data were not available, we assumed that the change from the "non-pregnant" percentage to the near-term "pregnant" percentage (as reported in that table) occurs in a linear fashion between 0 and 40 weeks of gestational age; i.e., the percentage is a linear function of the gestational age. Hereafter, we refer to such models as "linear transition models".

Table 14. Maternal cardiac output models (flow rate in L/h vs. maternal mass in kg for power law models, flow rate in L/h vs. gestational age in weeks for all other models).

Model	$\hat{\theta}_0$	$\hat{\theta}_1$	$\hat{\theta}_2$	$\hat{\theta}_3$	$\ell(\hat{\theta})$	AIC
Linear	309.15	3.1963	—	—	-5195.06	10394.1
Quadratic	300.24	6.4348	-0.094905	—	-5178.48	10363.0
Cubic	**301.78**	**3.2512**	**0.15947**	**-0.0047059**	**-5175.96**	**10359.9**
Modified Gompertz	18.903	0.21568	0.11022	282.19	-5179.72	10367.4
Modified Logistic	167.03	0.12506	6.0723	247.93	-5179.64	10367.3
Power Law	0.81619	1.4473	—	—	-5200.06	10404.1
Luecke Power Law	0.081119	2.5485	-0.13127	—	-5199.52	10405.0

For each model considered, the maximum likelihood parameter estimates ($\hat{\theta}$), log-likelihood ($\ell(\hat{\theta})$), and AIC are provided. The row describing the selected model is shown in boldface.

https://doi.org/10.1371/journal.pone.0215906.t014

Cardiac output. We used the curated data of Abduljalil et al. [28] to calibrate various models for maternal cardiac output. We assume this to be both the total flow rate into the maternal arterial blood compartment (hence the use here of the symbol $Q^{\mathrm{m}}_{\mathrm{artb}}$) and the total flow rate into the maternal venous blood compartment. We selected the cubic model given by

$$\boldsymbol{Q}^{\mathrm{m}}_{\mathrm{artb}}(\boldsymbol{t}) = \mathbf{301.78} + \mathbf{3.2512}\boldsymbol{t} + \mathbf{0.15947}\boldsymbol{t}^2 - \mathbf{0.0047059}\boldsymbol{t}^3 \tag{13}$$

as the most parsimonious for maternal cardiac output (L/h) at gestational age $\boldsymbol{t}$ (weeks). Table 14 shows the maximum likelihood estimates of the parameter values for all models considered along with the associated log-likelihood and AIC values. Fig 9 shows the cubic model of Eq 13 along with several other models for maternal cardiac output.

Adipose tissue. Assuming the blood flow rate into the maternal adipose tissue transitions linearly from 8.5% of cardiac output at 0 weeks to 7.8% near term [35], this flow rate (L/h) is given by

$$Q^{\mathrm{m}}_{\mathrm{adip}}(t) = \frac{1}{100} \times \left[8.5 + \left(\frac{7.8 - 8.5}{40}\right)t\right] \times Q^{\mathrm{m}}_{\mathrm{artb}}(t), \tag{14}$$

where t is the gestational age (weeks), where we have assumed "near term" corresponds to 40 weeks of gestational age.

Brain. Assuming the blood flow rate into the maternal brain transitions linearly from 12.0% of cardiac output at 0 weeks to 8.8% near term [35], this flow rate (L/h) is given by

$$Q^{\mathrm{m}}_{\mathrm{bran}}(t) = \frac{1}{100} \times \left[12.0 + \left(\frac{8.8 - 12.0}{40}\right)t\right] \times Q^{\mathrm{m}}_{\mathrm{artb}}(t), \tag{15}$$

where t is the gestational age (weeks).

Kidneys. Assuming the blood flow rate into the kidneys transitions linearly from 17.0% of cardiac output at 0 weeks to 16.6% near term [35], this flow rate (L/h) is given by

$$Q^{\mathrm{m}}_{\mathrm{kidn}}(t) = \frac{1}{100} \times \left[17.0 + \left(\frac{16.6 - 17.0}{40}\right)t\right] \times Q^{\mathrm{m}}_{\mathrm{artb}}(t), \tag{16}$$

where t is the gestational age (weeks).

Since Abduljalil et al. [28] curated data for blood flow to the maternal kidneys during gestation, we also calibrated various models from Table 3 to describe kidney blood flow using this

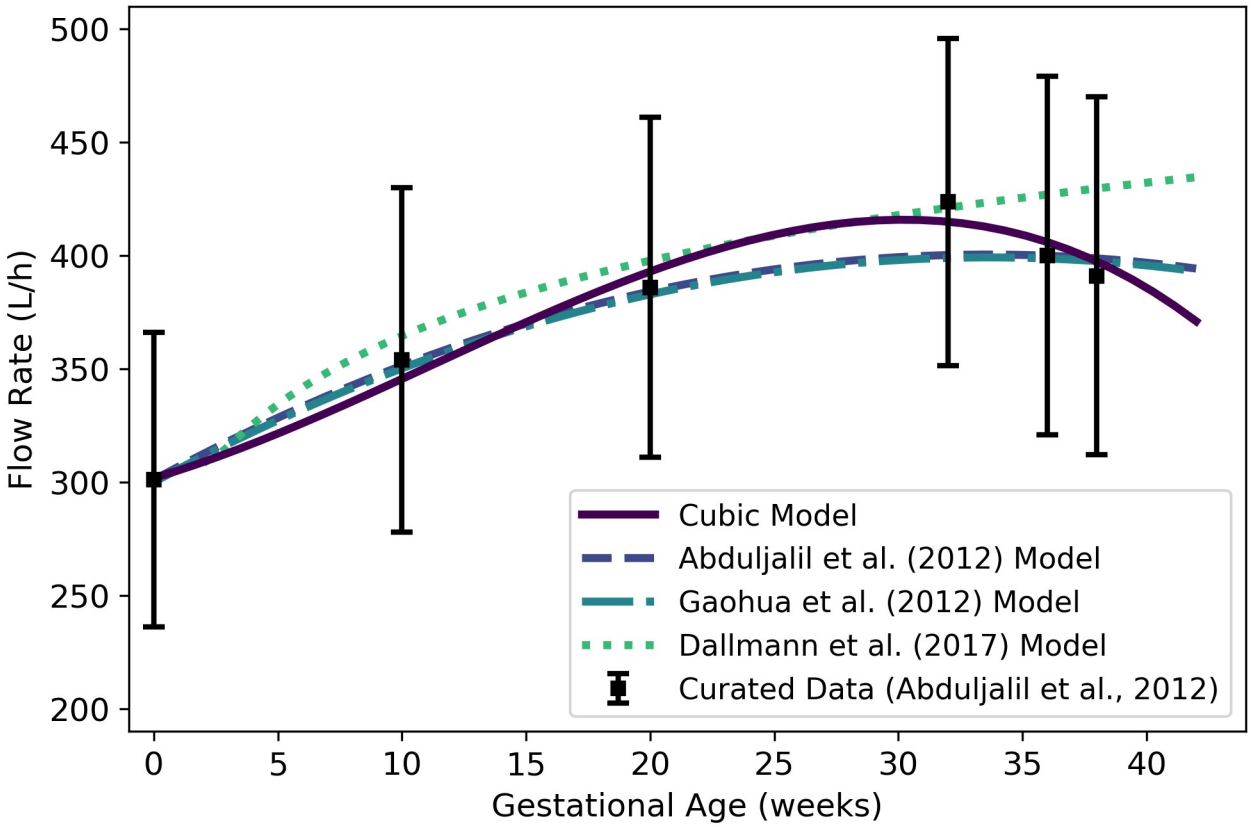

Fig 9. Maternal cardiac output vs. gestational age. The cubic model (solid line) given by Eq 13 was selected as the most parsimonious model in our analysis. The models of Abduljalil et al. [28] and Gaohua et al. [29], both of which are quadratic models, were calibrated using the same curated data set [28] used by us. Dallmann et al. [3] calibrated their model with different data.

https://doi.org/10.1371/journal.pone.0215906.g009

data set. We selected the cubic model given by

$$Q^{\mathrm{m}}_{\mathrm{kidn}}(t) = 53.248 + 3.6447t - 0.15357t^2 + 0.0016968t^3, \tag{17}$$

where $Q^{\mathrm{m}}_{\mathrm{kidn}}(t)$ is the flow rate (L/h) at gestational age t (weeks), as the most parsimonious of the candidate models. Table 15 shows the maximum likelihood estimates of the parameter

Table 15. Maternal kidney blood flow models (flow rate in L/h vs. maternal mass in kg for power law models, flow rate in L/h vs. gestational age in weeks for all other models).

Model	$\hat{\theta}_0$	$\hat{\theta}_1$	$\hat{\theta}_2$	$\hat{\theta}_3$	$\ell(\hat{\theta})$	AIC
Linear	59.979	0.41969	—	—	-944.39	1892.78
Quadratic	54.042	2.6204	-0.065712	—	-894.31	1794.63
Cubic	**53.248**	**3.6447**	**-0.15357**	**0.0016968**	**-891.88**	**1791.76**
Modified Gompertz	9.6979	2.0563	1.8668	43.402	-901.80	1811.59
Modified Logistic	38.466	1.6729	0.015416	34.115	-901.80	1811.59
Power Law	1.8508	0.85156	—	—	-950.55	1905.09
Luecke Power Law	4.9856×10^{-5}	5.8656	-0.59716	—	-948.88	1903.76

For each model considered, the maximum likelihood parameter estimates ($\hat{\theta}$), log-likelihood ($\ell(\hat{\theta})$), and AIC are provided. The row describing the selected model is shown in boldface.

https://doi.org/10.1371/journal.pone.0215906.t015

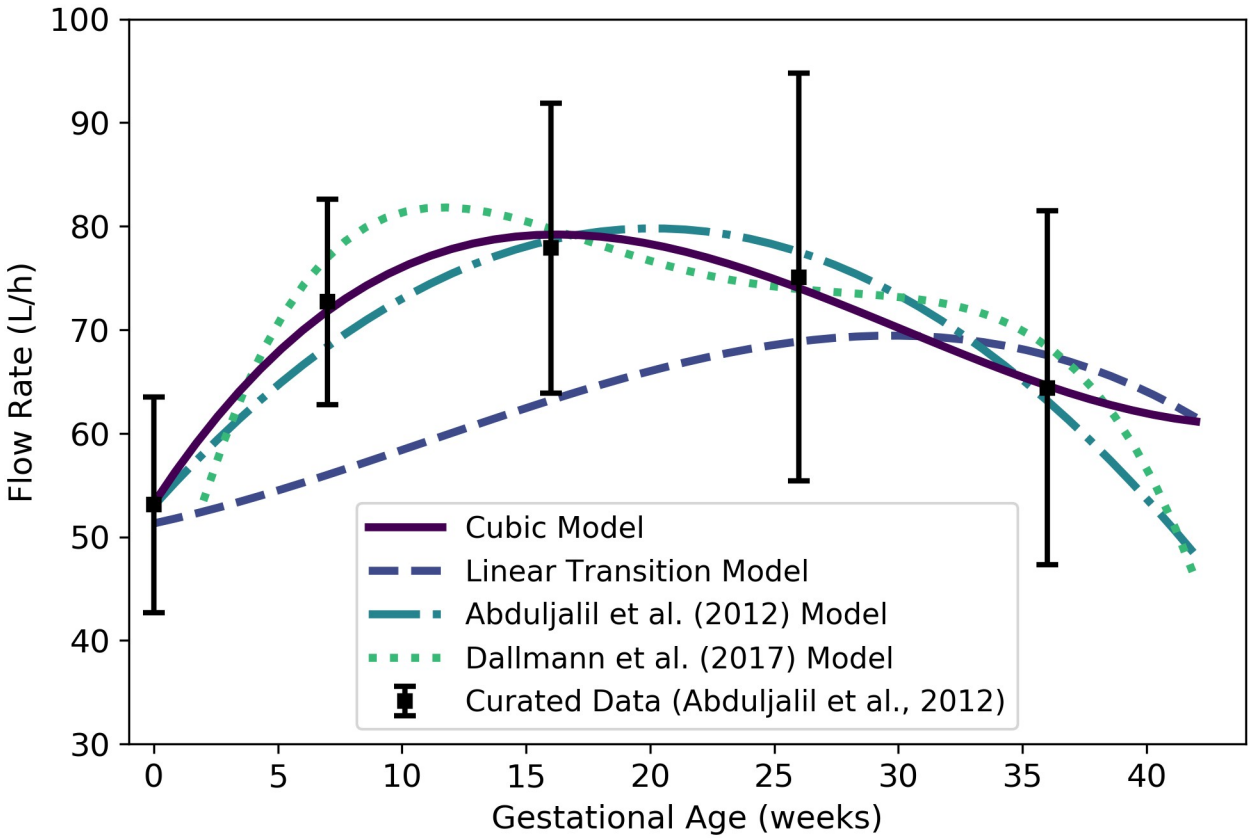

Fig 10. Maternal kidney blood flow vs. gestational age. The cubic model (solid line) given by Eq 17 was selected as the most parsimonious model in our analysis. The linear transition model given by Eq 16 is also shown. The model of Abduljalil et al. [28], which is a quadratic model, was calibrated using the same curated data set [28] used by us. Dallmann et al. [3] calibrated their model with different data.

https://doi.org/10.1371/journal.pone.0215906.g010

values for all models considered along with the associated log-likelihood and AIC values. Both the cubic model of Eq 17 and the "linear transition" model of Eq 16 are depicted in Fig 10 along with two other models [3, 28] for blood flow to the maternal kidneys.

Gut. Assuming the blood flow rate into the gut compartment transitions linearly from 17.0% of cardiac output at 0 weeks to 12.5% at 40 weeks [35], this flow rate (L/h) is given by

$$Q^{\mathrm{m}}_{\mathrm{gutx}}(t) = \frac{1}{100} \times \left[17.0 + \left(\frac{12.5 - 17.0}{40}\right)t\right] \times Q^{\mathrm{m}}_{\mathrm{artb}}(t), \tag{18}$$

where t is the gestational age (weeks).

Liver. Assuming the blood flow rate into the liver transitions linearly from 27.0% of cardiac output at 0 weeks to 20.0% at 40 weeks [35], this flow rate (L/h) is given by

$$Q^{\mathrm{m}}_{\mathrm{livr}}(t) = \frac{1}{100} \times \left[27.0 + \left(\frac{20.0 - 27.0}{40}\right)t\right] \times Q^{\mathrm{m}}_{\mathrm{artb}}(t), \tag{19}$$

where t is the gestational age (weeks).

Thyroid. Assuming the blood flow rate into the thyroid transitions linearly from 1.5% of cardiac output at 0 weeks to 1.1% at 40 weeks [35], this flow rate (L/h) is given by

$$Q^{\mathrm{m}}_{\mathrm{thyr}}(t) = \frac{1}{100} \times \left[1.5 + \left(\frac{1.1 - 1.5}{40}\right)t\right] \times Q^{\mathrm{m}}_{\mathrm{artb}}(t), \tag{20}$$

where t is the gestational age (weeks).

Placenta. Because the placenta is not listed in Table 2.44 of the ICRP [35] report, we constructed a model for maternal blood flow to the placenta by assuming that the percentage of maternal cardiac output reported for the uterus is actually a percentage for "uteroplacental" blood flow. According to Wang and Zhao [36], maternal blood flows to the placenta at about 600 to 700 mL/min (or 36 to 42 L/h) at term (end-of-pregnancy), accounting for 80% of the uteroplacental blood flow. Also, it is believed that uteroplacental circulation is established at 11 to 12 days post-fertilization, corresponding to a gestational age of about 3.6 weeks [42] (although one pair of researchers has claimed that they were unable to demonstrate "true intervillous blood flow" before 12 weeks of gestation [60]). If we assume that the blood flow rate to the uteroplacental region transitions linearly from 0.4% of cardiac output at 0 weeks to 12.0% at term [35], and further assume the proportion of this blood that flows directly to the placenta transitions from 0% at 3.6 weeks to 80% at 40 weeks, then the flow rate (L/h) to the placenta can be estimated using the linear transition model

$$Q^{\mathrm{m}}_{\mathrm{plac}}(t) = \begin{cases} 0.0 & t < 3.6, \\ \left(\frac{0.8}{36.4}\right)(t - 3.6) \times \frac{1}{100} \times \left[0.4 + \left(\frac{12.0 - 0.4}{40}\right)t\right] \times Q^{\mathrm{m}}_{\mathrm{artb}}(t) & t \geq 3.6, \end{cases} \tag{21}$$

where t is the gestational age (weeks). This model is flawed in that it predicts unrealistically low values (considerably less than 36 L/h) close to term. Thus, as an alternative, we propose a model that sets maternal blood flow to the placenta proportional to the placenta volume with a proportionality constant (0.059176) selected to ensure that the maternal blood flow rate is equal to the midpoint of the range given by Wang and Zhao [36] (39 L/h) at term (40 weeks). This model is given by

$$Q^{\mathrm{m}}_{\mathrm{plac}}(t) = \begin{cases} 0.0 & t < 3.6, \\ 0.059176 \times V^{\mathrm{m}}_{\mathrm{plac}}(t) & t \geq 3.6, \end{cases} \tag{22}$$

where $Q^{\mathrm{m}}_{\mathrm{plac}}(t)$ is the flow rate (L/h) to the placenta and $V^{\mathrm{m}}_{\mathrm{plac}}(t)$ is the volume (mL) of the placenta (cf. Eq 8) at gestational age t (weeks). Fig 11 shows the linear transition model of Eq 21, the proportional-to-volume model of Eq 22, and three published models [3, 29, 32] for maternal blood flow to the placenta. We remark that the Dallmann et al. [3] model yields zero flow up until 10.14 weeks (well after the placenta has formed) and the Zhang et al. [32] model yields a flow of 1.71 L/h at 0 weeks (well before the placenta has formed). Also Gaohua et al. [29] did not cite a data source or provide a method for generating their model.

Rest of body. We used the principle of conservation of flow to obtain a formula for the blood flow rate to the maternal rest of body compartment. Thus, the flow rate to the rest of body compartment (in L/h) is given by

$$\begin{aligned} Q^{\mathrm{m}}_{\mathrm{rest}}(t) = \; & Q^{\mathrm{m}}_{\mathrm{artb}}(t) - [Q^{\mathrm{m}}_{\mathrm{adip}}(t)] + Q^{\mathrm{m}}_{\mathrm{bran}}(t) + Q^{\mathrm{m}}_{\mathrm{kidn}}(t) + Q^{\mathrm{m}}_{\mathrm{gutx}}(t) \\ & + Q^{\mathrm{m}}_{\mathrm{livr}}(t) + Q^{\mathrm{m}}_{\mathrm{thyr}}(t) + (Q^{\mathrm{m}}_{\mathrm{plac}}(t)), \end{aligned} \tag{23}$$

where t is the gestational age (in weeks) and $Q^{\mathrm{m}}_{\mathrm{artb}}$, $Q^{\mathrm{m}}_{\mathrm{adip}}$, $Q^{\mathrm{m}}_{\mathrm{bran}}$, $Q^{\mathrm{m}}_{\mathrm{kidn}}$, $Q^{\mathrm{m}}_{\mathrm{gutx}}$, $Q^{\mathrm{m}}_{\mathrm{livr}}$, $Q^{\mathrm{m}}_{\mathrm{thyr}}$, and $Q^{\mathrm{m}}_{\mathrm{plac}}$ are given by Eqs 13, 14, 15, 17, 18, 19, 20 and 22, respectively. As shown in Fig 12, Eq 23 results

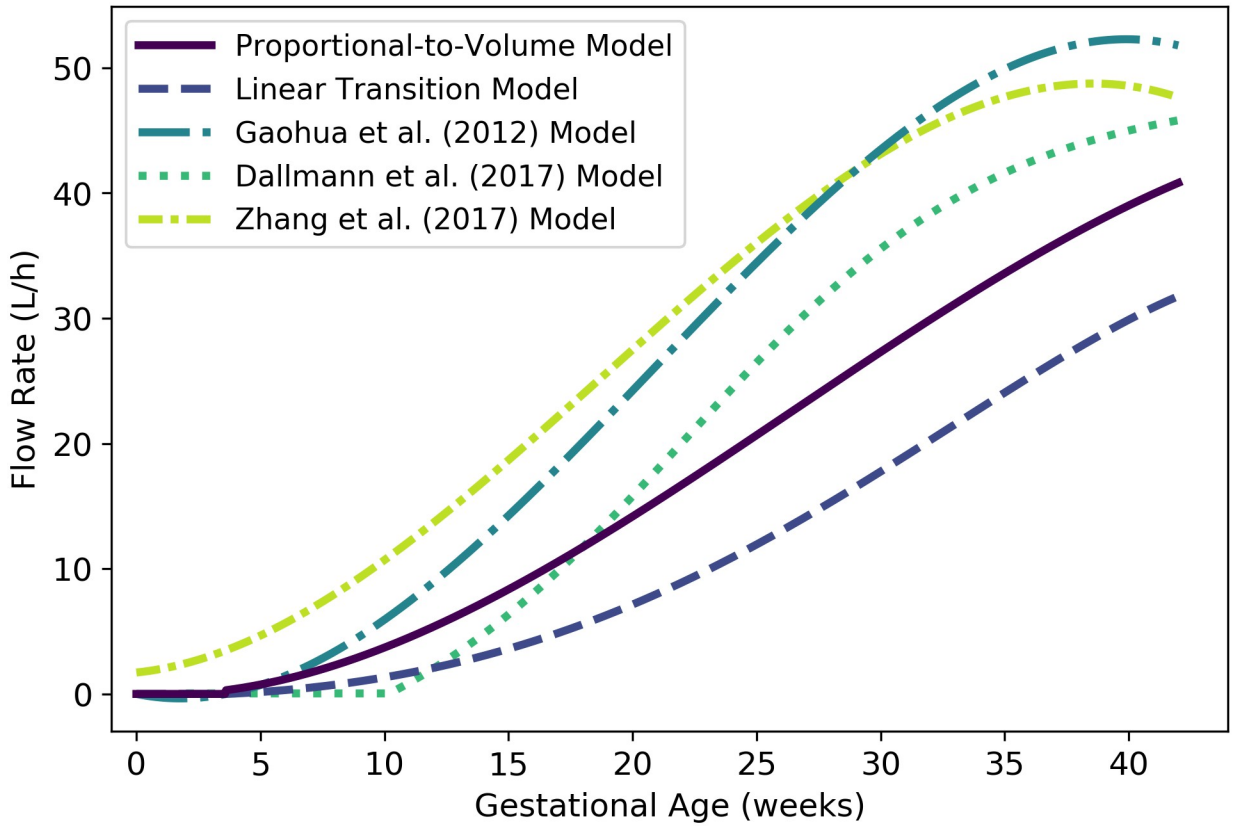

Fig 11. Maternal blood flow to the placenta vs. gestational age. The proportional-to-volume model (solid line) given by Eq 22, the linear transition model given by Eq 21, and two published models [3, 29, 32] are shown.

https://doi.org/10.1371/journal.pone.0215906.g011

in flow rates to the maternal rest of body compartment that fluctuate between approximately 47 and 97 L/h during pregnancy.

Other maternal physiological parameters

Hematocrit. We used the curated data of Abduljalil et al. [28] to calibrate various models for maternal hematocrit. The quadratic model given by

$$H^{\mathrm{m}}(t) = 39.192 - 0.10562t - (7.1045 \times 10^{-4})t^2 \tag{24}$$

was selected as the most parsimonious model for hematocrit (as a percentage) at gestational age t (weeks). Table 16 shows the maximum likelihood estimates of the parameter values for all models considered along with the associated log-likelihood and AIC values. The quadratic model of Eq 24 and several other models [3, 28, 29] for maternal hematocrit are shown in Fig 13.

Because hematocrit represents the volume percentage of red blood cells in whole blood, and because whole blood is mostly made up of plasma and red blood cells (with only a small fraction made up of white blood cells and platelets), we can estimate the hematocrit using our models for maternal plasma volume, $V^{\mathrm{m}}_{\mathrm{plas}}$, and maternal red blood cell volume, $V^{\mathrm{m}}_{\mathrm{rbcs}}$. That is,

Fig 12. Maternal blood flow to the "rest of body" compartment vs. gestational age (cf. Eq 23).

https://doi.org/10.1371/journal.pone.0215906.g012

another model for hematocrit is given by

$$\boldsymbol{H}^{\mathrm{m}}(\boldsymbol{t}) = \frac{\boldsymbol{V}^{\mathrm{m}}_{\mathrm{rbcs}}(\boldsymbol{t})}{\boldsymbol{V}^{\mathrm{m}}_{\mathrm{plas}}(\boldsymbol{t}) + \boldsymbol{V}^{\mathrm{m}}_{\mathrm{rbcs}}(\boldsymbol{t})}, \tag{25}$$

where $\boldsymbol{t}$ is the gestational age (weeks) and $\boldsymbol{V}^{\mathrm{m}}_{\mathrm{plas}}(\boldsymbol{t})$ and $\boldsymbol{V}^{\mathrm{m}}_{\mathrm{rbcs}}$ represent the maternal plasma and red blood cells volumes given by Eqs 5 and 6, respectively, at gestational week $\boldsymbol{t}$. We refer the hematocrit model of Eq 25 as the "ratio model" in Fig 13. There, we see that the ratio model

Table 16. Maternal hematocrit models (percentage vs. maternal mass in kg for power law models, percentage vs. gestational age in weeks for all other models).

Model	$\hat{\boldsymbol{\theta}}_0$	$\hat{\boldsymbol{\theta}}_1$	$\hat{\boldsymbol{\theta}}_2$	$\hat{\boldsymbol{\theta}}_3$	$\boldsymbol{\ell}(\hat{\boldsymbol{\theta}})$	AIC
Linear	39.400	-0.13373	—	—	-11567.9	23139.8
Quadratic	**39.192**	**-0.10562**	**-7.1045×10^{-4}**	**—**	**-11566.3**	**23138.5**
Cubic	39.175	-0.098154	-0.0012141	8.7385×10^{-6}	-11566.2	23140.4
Modified Gompertz	-12.358	0.29062	1.3862	51.498	-11825.5	23659.0
Modified Logistic	-75.243	0.0090404	129.80	57.099	-11566.9	23141.7
Power Law	402.84	-0.56685	—	—	-11577.1	23158.2
Luecke Power Law	1.0551	2.2505	-0.33372	—	-11575.7	23157.4

For each model considered, the maximum likelihood parameter estimates ($\hat{\theta}$), log-likelihood ($\ell(\hat{\theta})$), and AIC are provided. The row describing the selected model is shown in boldface.

https://doi.org/10.1371/journal.pone.0215906.t016

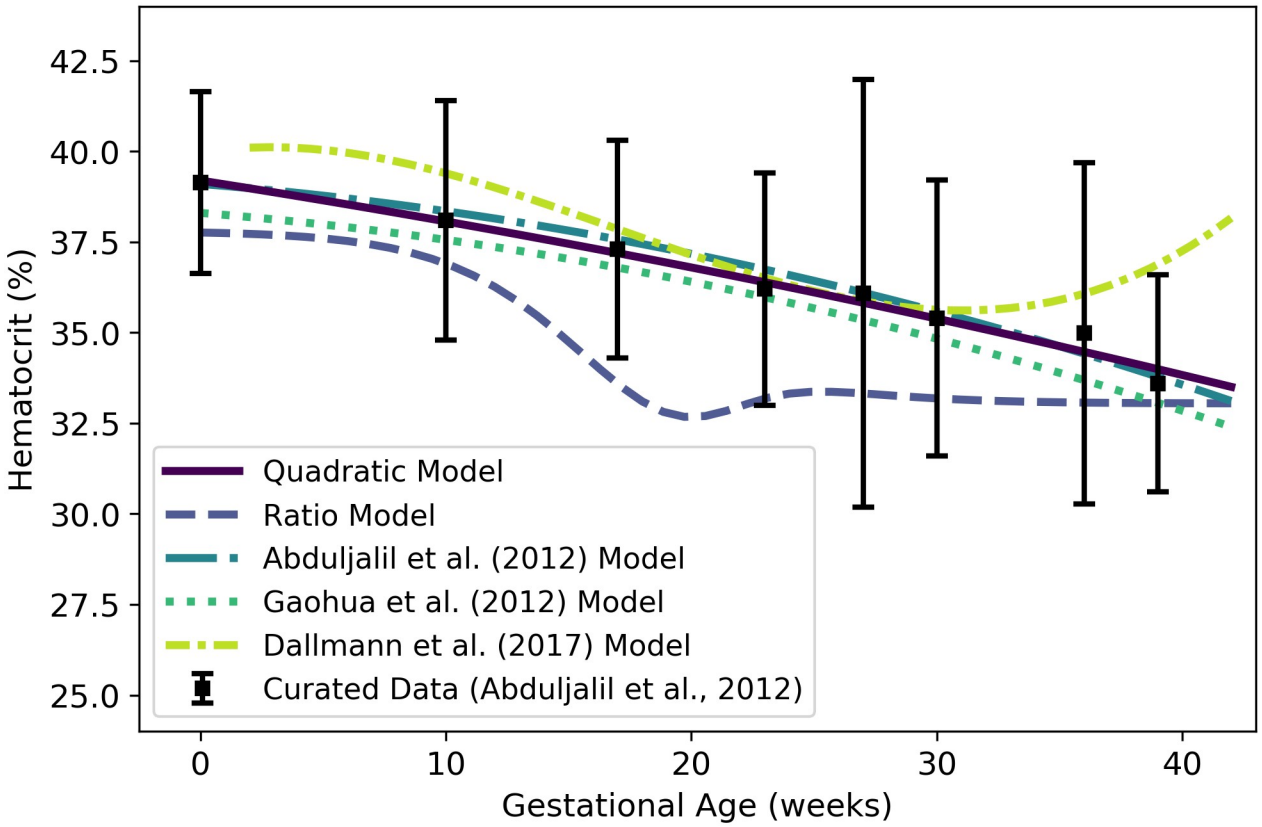

Fig 13. Maternal hematocrit vs. gestational age. The quadratic model (solid line) given by Eq 24 was selected as the most parsimonious model in our analysis. The "ratio model" given by Eq 25 is also shown. The models of Abduljalil et al. [28] and Gaohua et al. [29], both of which are quadratic models, were calibrated using the same curated data set [28] used by us. Dallmann et al. [3] calibrated their model with different data.

https://doi.org/10.1371/journal.pone.0215906.g013

yields a lower hematocrit than any of the other models (including the quadratic model of Eq 24). Note that this ratio model considers the volume of blood components other than plasma and RBCS to be negligible; if such components have a non-negligible volume, the hematocrit values predicted by this model should *over*estimate hematocrit.

We also note that some longitudinal studies of human subjects have shown that hematocrit typically increases at the end of pregnancy [56, 58]. When applied to the aggregated data set [28] our model selection process led us to choose a model for plasma volume (Eq 5) that does not predict such an increase. At least one alternative model [3] does predict an increase in hematocrit at the end of pregnancy.

Glomerular filtration rate. We used the curated data of Abduljalil et al. [28] to calibrate various models for glomerular filtration rate (GFR). The quadratic model given by

$$k^{\mathrm{m}}_{\mathrm{kidn}}(t) = 113.73 + 3.5784t - 0.067272t^2 \tag{26}$$

was selected as the most parsimonious model for GFR (mL/min) at gestational age t (weeks). Table 17 shows the maximum likelihood estimates of the parameter values for all models considered along with the associated log-likelihood and AIC values. The linear model of Eq 26 and two other models for maternal GFR [3, 28] are shown in Fig 14.

Pearce et al. [61] have used an allometric model for GFR. These authors assume that for a 70 kg human, GFR is 125 mL/min [62] and glomerular filtration can be computed as a

Table 17. Maternal GFR models (rate in mL/min vs. maternal mass in kg for power law models, rate in mL/min vs. gestational age in weeks for all other models).

Model	$\hat{\theta}_0$	$\hat{\theta}_1$	$\hat{\theta}_2$	$\hat{\theta}_3$	$\ell(\hat{\theta})$	AIC
Linear	122.82	1.3341	—	—	-1379.34	2762.68
Quadratic	**113.73**	**3.5784**	**-0.067272**	**—**	**-1363.91**	**2733.81**
Cubic	113.66	3.6732	-0.074784	1.4036×10^{-4}	-1363.90	2735.80
Modified Gompertz	2.6041×10^{-5}	4.4691	0.31100	113.87	-1363.38	2734.77
Modified Logistic	45.062	0.46667	10.026	113.59	-1363.25	2734.50
Power Law	0.41867	1.3891	—	—	-1384.28	2772.56
Luecke Power Law	8.9811×10^{-5}	5.4117	-0.47878	—	-1383.17	2772.34

For each model considered, the maximum likelihood parameter estimates ($\hat{\theta}$), log-likelihood ($\ell(\hat{\theta})$), and AIC are provided. The row describing the selected model is shown in boldface.

https://doi.org/10.1371/journal.pone.0215906.t017

multiple of body mass to the ¾ power [63]. Thus, one can compute the glomerular filtration as

$$k^{\mathrm{m}}_{\mathrm{kidn}}(t) = 125 \cdot \left(\frac{W^{\mathrm{m}}(t)}{70}\right)^{0.75}, \tag{27}$$

where t is the gestational age (in weeks) and $W^{\mathrm{m}}(t)$ represents the maternal mass given by Eq 1

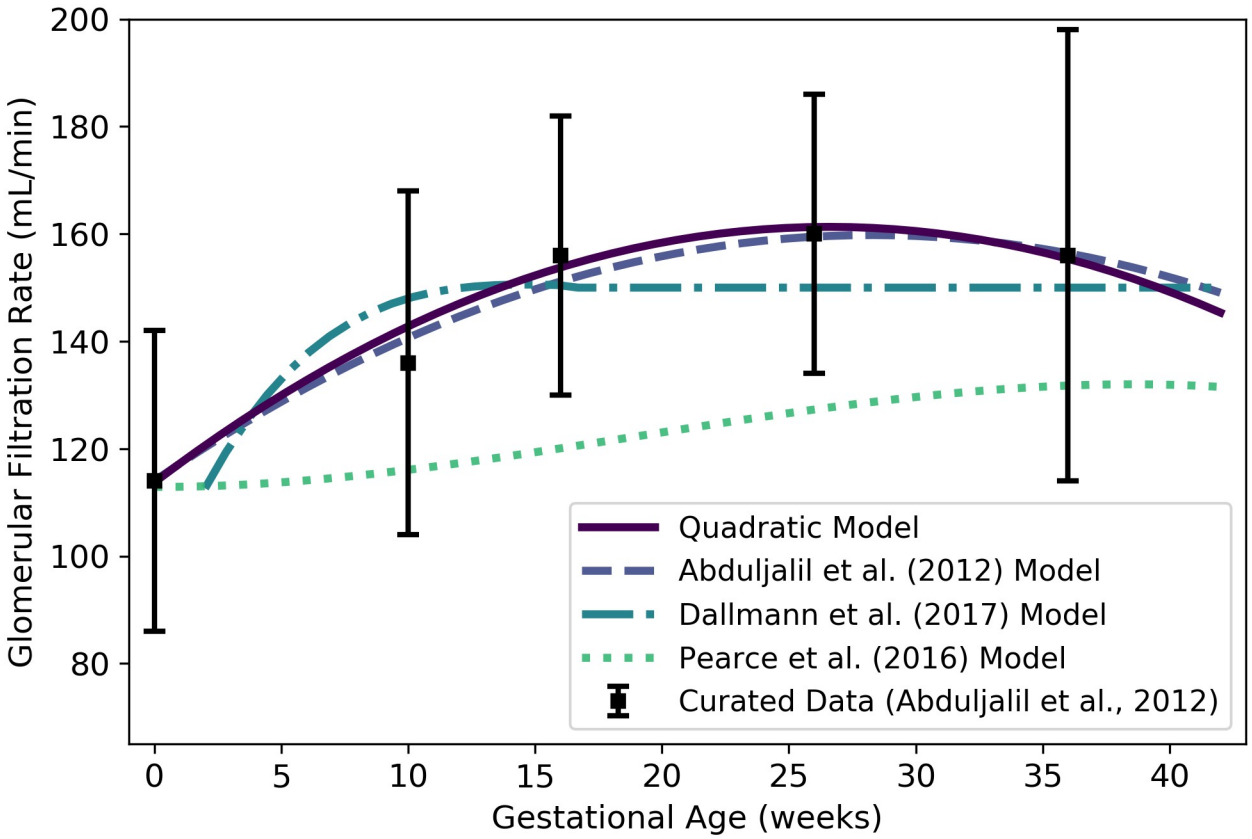

Fig 14. Maternal glomerular filtration rate vs. gestational age. The quadratic model (solid line) given by Eq 26 was selected as the most parsimonious model in our analysis. The model of Abduljalil et al. [28], also a quadratic model, was calibrated using the same curated data set [28] used by us. The Dallmann et al. [3] model depicted here has been modified from the published version, which contained typographical errors, based on personal correspondence with the lead author. The model attributed to Pearce et al. [61] is evaluated as described in the text.

https://doi.org/10.1371/journal.pone.0215906.g014

at gestational week t. For purposes of comparison, we show the plot of Equation 27 in Fig 14. It is labeled there as the "Pearce et al. (2016) Model".

Fetal Compartment Volumes

Brain. We used data curated by Abduljalil et al. [33] to calibrate various models for the brain mass of a human fetus during gestation. The cubic growth model given by

$$W^{\mathrm{f}}_{\mathrm{bran}}(t) = -2.1208t + 0.15645t^2 + 0.0034746t^3 \tag{28}$$

was selected as the most parsimonious model for fetal brain *mass* (g) at gestational age t (weeks); however, this model gives negative values for fetal brain mass during early gestation. The Gompertz model given by

$$W^{\mathrm{f}}_{\mathrm{bran}}(t) = 0.01574 \cdot \exp\left[\frac{0.70707}{0.064827}(1 - \exp[-0.064827t])\right], \tag{29}$$

has the next lowest AIC (21893.5 vs. 21861.4), but it yields strictly positive values for gestational ages greater than or equal to zero. Table 18 shows the maximum likelihood estimates of the parameter values for all models considered along with the associated log-likelihood and AIC values. The cubic growth model of Eq 28, the Gompertz model of Eq 29, three published models [15, 32, 33], and the curated summary data [33] are shown in Fig 15.

Since the mean density of human brain tissue is 1.04 g/mL [35], the *volume* (mL) of the fetal brain tissue can be computed as

$$V^{\mathrm{f}}_{\mathrm{bran}}(t) = \frac{1}{1.04} \cdot W^{\mathrm{f}}_{\mathrm{bran}}(t). \tag{30}$$

Liver. We used data curated by Abduljalil et al. [33] to calibrate various models for the liver mass of a human fetus during gestation. The cubic growth model given by

$$W^{\mathrm{f}}_{\mathrm{livr}}(t) = -0.69862t + 0.046670t^2 + 0.0013891t^3 \tag{31}$$

was selected as the most parsimonious model for fetal liver *mass* (g) at gestational week age t (weeks); however, this model gives negative values for fetal liver mass during early gestation. The Gompertz model given by

$$W^{\mathrm{f}}_{\mathrm{livr}}(t) = 0.0074774 \cdot \exp\left[\frac{0.65856}{0.061662}(1 - \exp[-0.061662t])\right], \tag{32}$$

Table 18. Fetal brain mass models (g vs. fetal mass in g for power law models, g vs. gestational age in weeks for all other models).

Model	$\hat{\theta}_0$	$\hat{\theta}_1$	$\hat{\theta}_2$	$\hat{\theta}_3$	$\ell(\hat{\theta})$	AIC
Linear Growth	2.9256	—	—	—	-21528.2	43058.5
Quadratic Growth	-3.9135	0.32870	—	—	-11008.6	22021.2
Cubic Growth	**-2.1208**	**0.15645**	**0.0034746**	**—**	**-10927.7**	**21861.4**
Gompertz	0.015740	0.70707	0.064827	—	-10943.7	21893.5
Logistic	462.90	0.19240	32.321	—	-11074.2	22154.4
Power Law	0.35659	0.85318	—	—	-10970.6	21945.2
Luecke Power Law	0.93210	0.55821	0.021936	—	-10956.8	21919.6

For each model considered, the maximum likelihood parameter estimates ($\hat{\theta}$), log-likelihood ($\ell(\hat{\theta})$), and AIC are provided. The row describing the selected model is shown in boldface.

https://doi.org/10.1371/journal.pone.0215906.t018

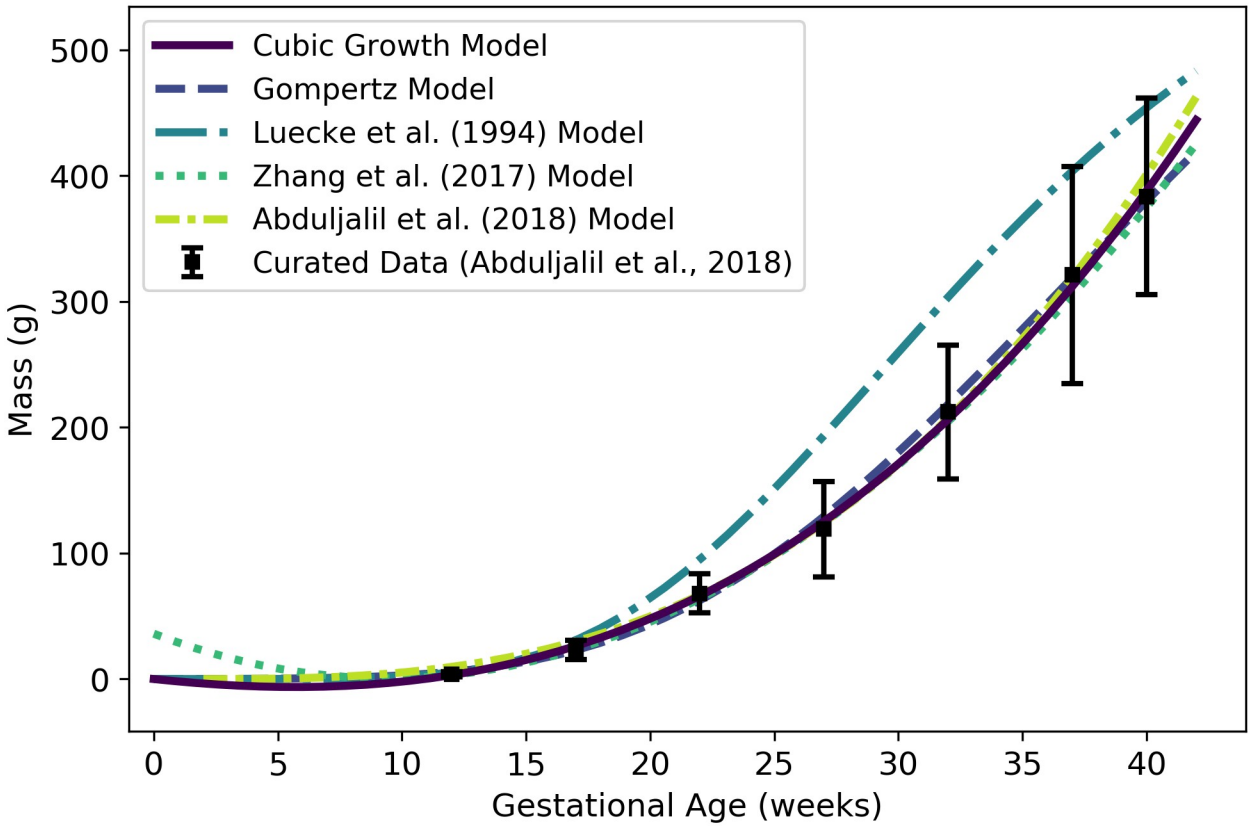

Fig 15. Fetal brain mass vs. gestational age. The quadratic growth model (solid line) given by Eq 28 was selected as the most parsimonious model in our analysis; however, that model gives negative brain mass values during early gestation. The Gompertz model (dashed line) given by Eq 29 is strictly positive on the time domain of interest. The model of Luecke et al. [15], which is a power law model based on fetal mass, was calibrated using a different data set [25]. The model of Zhang et al. [32] was also calibrated using a distinct compiled data set. The Zhang et al. [32] model describes brain volume, so the units were converted assuming a tissue density of 1 g/mL.

https://doi.org/10.1371/journal.pone.0215906.g015

yields strictly positive values for gestational ages greater than or equal to zero and has the next lowest AIC (16430.6 vs. 16402.1). Table 19 shows the maximum likelihood estimates of the parameter values for all models considered along with the associated log-likelihood and AIC values. The cubic growth model of Eq 31, the Gompertz model of Eq 32, three published models [15, 32, 33], and the curated summary data [33] are shown in Fig 16.

Since the mean density of human liver tissue is 1.05 g/mL [37], the *volume* (mL) of the fetal liver tissue can be computed as

$$\boldsymbol{V}^{\mathrm{f}}_{\mathrm{livr}}(\boldsymbol{t}) = \frac{\mathbf{1}}{\mathbf{1.05}} \cdot \boldsymbol{W}^{\mathrm{f}}_{\mathrm{livr}}(\boldsymbol{t}). \tag{33}$$

Kidneys. We used data curated by Abduljalil et al. [33] to calibrate various models for the kidney mass of a human fetus during gestation. The power law model given by

$$\boldsymbol{W}^{\mathrm{f}}_{\mathrm{kidn}}(\boldsymbol{t}) = \mathbf{0.016011} \cdot (\boldsymbol{W}^{\mathrm{f}}(\boldsymbol{t}))^{\mathbf{0.87512}}, \tag{34}$$

where $W^{\mathrm{f}}(t)$ denotes the fetal mass (g) given by Eq 2, was selected as the most parsimonious model for fetal kidney *mass* (g) at gestational age t (weeks). The power law relates fetal kidney mass to total fetal mass and thus requires an (intermediate) estimate of total fetal mass at each

Table 19. Fetal liver mass models (g vs. fetal mass in g for power law models, g vs. gestational age in weeks for all other models).

Model	$\hat{\theta}_0$	$\hat{\theta}_1$	$\hat{\theta}_2$	$\hat{\theta}_3$	$\ell(\hat{\theta})$	AIC
Linear Growth	1.0599	—	—	—	-12411.80	24825.6
Quadratic Growth	-1.4130	0.11397	—	—	-8241.18	16486.4
Cubic Growth	**-0.69862**	**0.046670**	**0.0013891**	**—**	**-8198.03**	**16402.1**
Gompertz	0.0074774	0.65856	0.061662	—	-8212.32	16430.6
Logistic	161.85	0.18771	32.712	—	-8275.32	16556.6
Power Law	0.10885	0.86562	—	—	-8231.05	16466.1
Luecke Power Law	0.38023	0.48526	0.028240	—	-8221.42	16448.8

For each model considered, the maximum likelihood parameter estimates ($\hat{\theta}$), log-likelihood ($\ell(\hat{\theta})$), and AIC are provided. The row describing the selected model is shown in boldface.

https://doi.org/10.1371/journal.pone.0215906.t019

time point of interest. The Gompertz model given by

$$W^{f}_{kidn}(t) = (6.3327 \times 10^{-5}) \cdot \exp\left[\frac{1.0409}{0.076435}(1 - \exp[-0.051995t])\right] \quad (35)$$

has an AIC that is only slightly larger (11838.3 vs. 11836.6) and does not require an

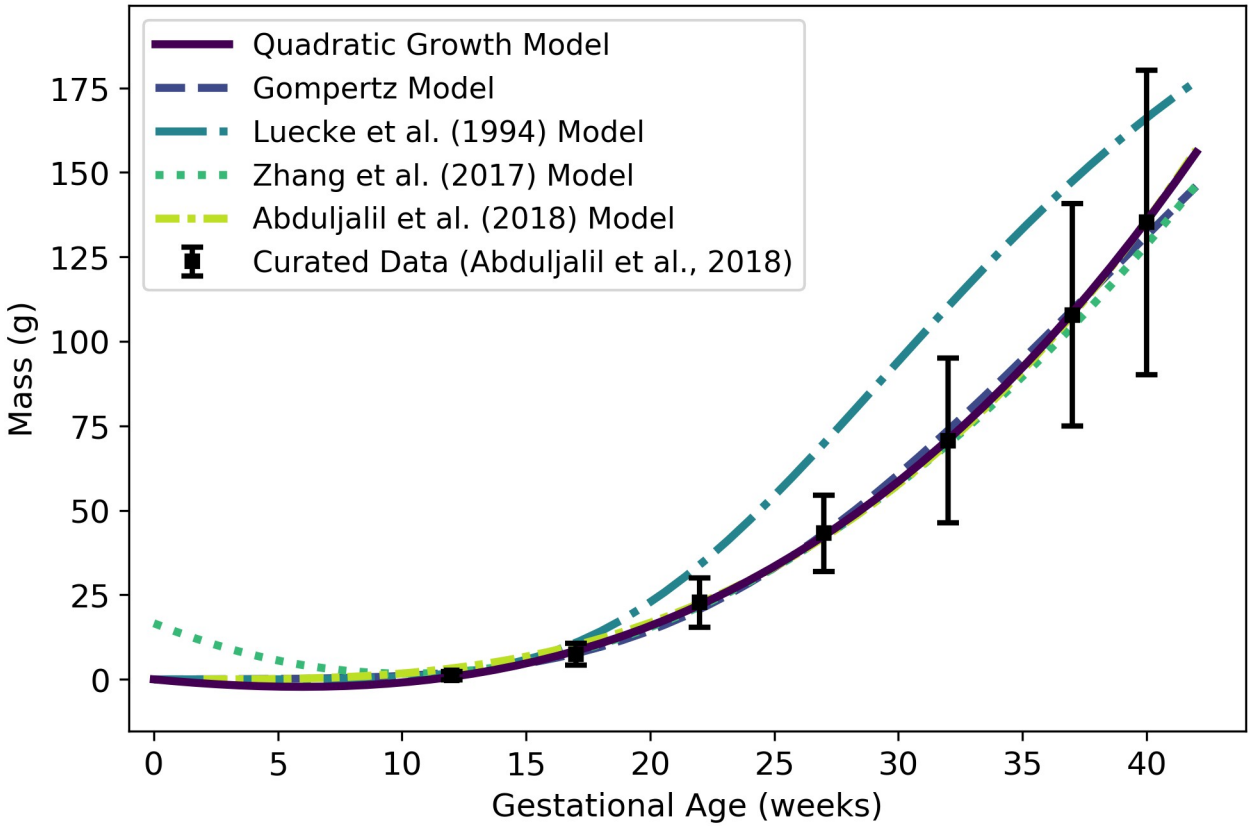

Fig 16. Fetal liver mass vs. gestational age. The cubic growth model (solid line) given by Eq 31 was selected as the most parsimonious model in our analysis; however, that model gives negative liver mass values during early gestation. The Gompertz model (dashed line) given by Eq 32 is strictly positive on the time domain of interest. The model of Luecke et al. [15], which is a power law model based on fetal mass, was calibrated using a different data set [25]. The model of Zhang et al. [32] was also calibrated using a distinct compiled data set. The Zhang et al. [32] model describes liver volume, so the units were converted assuming a tissue density of 1 g/mL.

https://doi.org/10.1371/journal.pone.0215906.g016

Table 20. Fetal kidney mass models (g vs. fetal mass in g for power law models, g vs. gestational age in weeks for all other models).

Model	$\hat{\theta}_0$	$\hat{\theta}_1$	$\hat{\theta}_2$	$\hat{\theta}_3$	$\ell(\hat{\theta})$	AIC
Linear Growth	0.10014	—	—	—	-12495.00	24992.0
Quadratic Growth	-0.26646	0.022757	—	—	-6097.13	12198.3
Cubic Growth	-0.093661	0.0043005	0.00040110	—	-5967.55	11941.1
Gompertz	6.33270×10^{-5}	1.0409	0.076435	—	-5916.16	11838.3
Logistic	29.583	0.23193	30.697	—	-5984.42	11974.8
Power Law	**0.016011**	**0.91410**	**—**	**—**	**-5916.29**	**11836.6**
Luecke Power Law	0.018129	0.87512	0.0029479	—	-5916.15	11838.3

For each model considered, the maximum likelihood parameter estimates ($\hat{\theta}$), log-likelihood ($\ell(\hat{\theta})$), and AIC are provided. The row describing the selected model is shown in boldface.

https://doi.org/10.1371/journal.pone.0215906.t020

intermediate calculation for total fetal mass. Table 20 shows the maximum likelihood estimates of the parameter values for all models considered along with the associated log-likelihood and AIC values. The power law model of Eq 34, the Gompertz model of Eq 35, three published models [15, 32, 33], and the curated summary data [33] are shown in Fig 17.

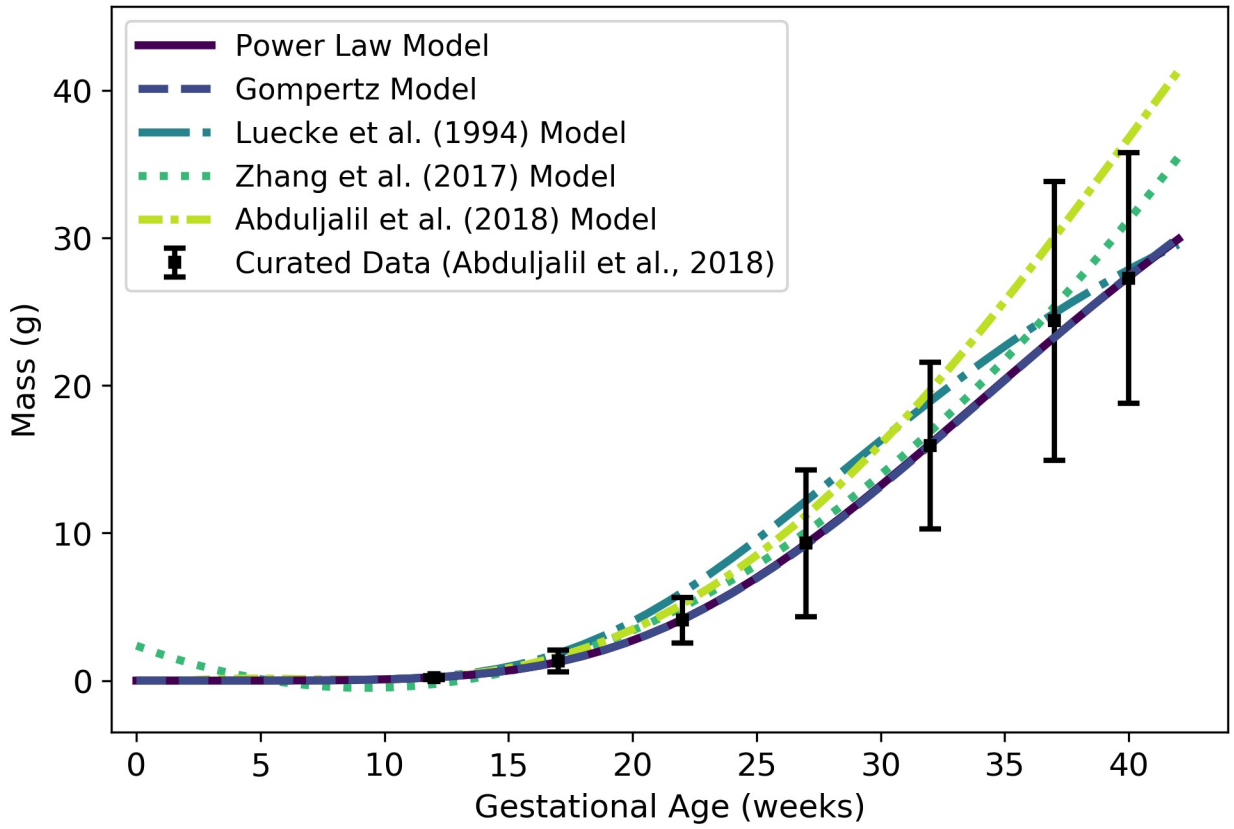

Fig 17. Fetal kidney mass vs. gestational age. The power law model (solid line) given by Eq 34 was selected as the most parsimonious model in our analysis; however, that model is a function of fetal mass. The Gompertz model (dashed line) given by Eq 35 may be preferred since it is a function of gestational age and does not require an intermediate model for fetal mass. Note that the Gompertz model and the power law model are virtually indistinguishable in this plot. The model of Luecke et al. [15], which is also a power law model based on fetal mass, was calibrated using a different data set [25]. The model of Zhang et al. [32] was also calibrated using a distinct compiled data set. The Zhang et al. [32] model describes kidney volume, so the units were converted assuming a tissue density of 1 g/mL. The apparently poor fit of the model of Abduljalil et al. [33] to their own curated data set is probably due to precision-related errors—they only reported the leading coefficient of their polynomial model to one significant figure.

https://doi.org/10.1371/journal.pone.0215906.g017

Table 21. Fetal lung mass models (g vs. fetal mass in g for power law models, g vs. gestational age in weeks for all other models).

Model	$\hat{\theta}_0$	$\hat{\theta}_1$	$\hat{\theta}_2$	$\hat{\theta}_3$	$\ell(\hat{\theta})$	AIC
Linear Growth	0.49354	—	—	—	-13910.20	27822.4
Quadratic Growth	-0.58156	0.053565	—	—	-8893.10	17790.2
Cubic Growth	-0.57275	0.052706	1.8119×10^{-5}	—	-8893.05	17792.1
Gompertz	**0.00030454**	**1.0667**	**0.084604**	**—**	**-8823.24**	**17652.5**
Logistic	59.996	0.22339	28.200	—	-8866.84	17739.7
Power Law	0.12888	0.75526	—	—	-8827.70	17659.4
Luecke Power Law	0.074365	0.92497	-0.012730	—	-8824.40	17654.8

For each model considered, the maximum likelihood parameter estimates ($\hat{\theta}$), log-likelihood ($\ell(\hat{\theta})$), and AIC are provided. The row describing the selected model is shown in boldface.

https://doi.org/10.1371/journal.pone.0215906.t021

Since the mean density of human kidney tissue is 1.05 g/mL [35], the *volume* (mL) of the fetal kidneys can be computed as

$$V^{\mathrm{f}}_{\mathrm{kidn}}(t) = \frac{1}{1.05} \cdot W^{\mathrm{f}}_{\mathrm{kidn}}(t). \tag{36}$$

Lungs. We used data curated by Abduljalil et al. [33] to calibrate various models for the lung mass of a human fetus during gestation. The Gompertz model given by

$$W^{\mathrm{f}}_{\mathrm{lung}}(t) = 0.00030454 \cdot \exp\left[\frac{1.0667}{0.084604}(1 - \exp[-0.084604t])\right], \tag{37}$$

was selected as the most parsimonious model for fetal lung *mass* (g) at gestational age t (weeks). Table 21 shows the maximum likelihood estimates of the parameter values for all models considered along with the associated log-likelihood and AIC values. The Gompertz model of Eq 37, two published models [15, 33], and the curated summary data [33] are shown in Fig 18.

The model of Luecke et al. [15] depicted in Fig 18 is a Luecke power law model (cf. Table 3) with coefficient values that have been modified from those that the authors show in their Table 3. When applied exactly as specified, that model over-predicts fetal lung masses by an order of magnitude, so we hypothesized that the first coefficient printed in their table (θ_0 = **0.09351**) may have been off by a factor of 10. We therefore decreased that coefficient by a factor of 10 (θ_0 = **0.009351**) to obtain the model version ("Luecke et al. (1994) Adjusted Model") shown in Fig 18.

Since the mean density of human lung tissue is 1.05 g/mL [35], the *volume* (mL) of the fetal lung tissue can be computed as

$$V^{\mathrm{f}}_{\mathrm{lung}}(t) = \frac{1}{1.05} \cdot W^{\mathrm{f}}_{\mathrm{lung}}(t). \tag{38}$$

Thyroid. We used data curated by Abduljalil et al. [33] to calibrate various models for the thyroid mass of a human fetus during gestation. The Gompertz model given by

$$W^{\mathrm{f}}_{\mathrm{thyr}}(t) = 0.0038483 \cdot \exp\left[\frac{0.30799}{0.039800}(1 - \exp[-0.039800t])\right) \tag{39}$$

was selected as the most parsimonious model for fetal thyroid *mass* (g) at gestational age t (weeks). We remark that the cubic growth model yielded a slightly lower AIC, but the AIC

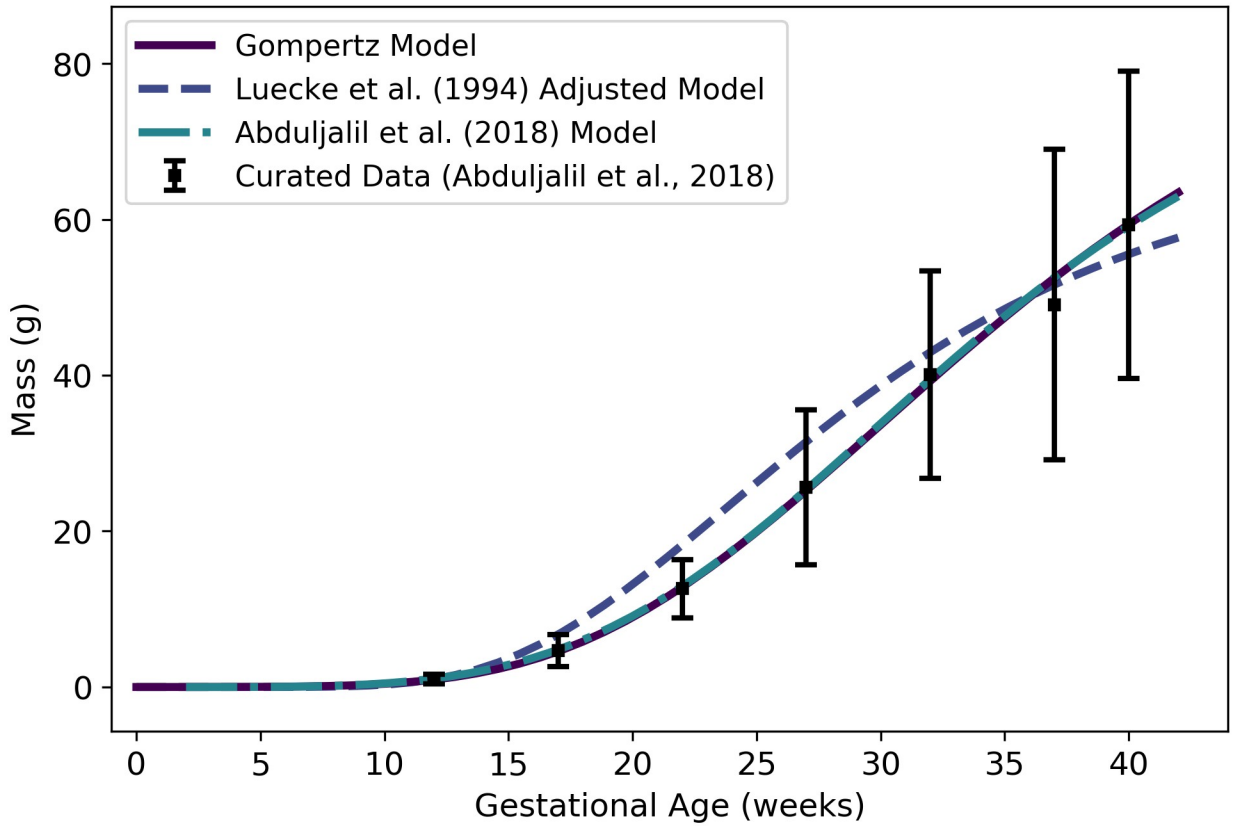

Fig 18. Fetal lung mass vs. gestational age. The Gompertz model (solid line) given by Eq 37 was selected as the most parsimonious model in our analysis. The model of Luecke et al. [15], which is a power law model based on fetal mass, was calibrated using a different data set [25]. The version of the Luecke et al. [15] model depicted here has been adjusted as described in the text. Note that our Gompertz model and the model of Abduljalil et al. [33] are virtually indistinguishable in this plot.

https://doi.org/10.1371/journal.pone.0215906.g018

difference (-334.07 vs. -334.16) is too small to recommend one model over the other. Because the Gompertz model yields strictly positive values for gestational ages greater than or equal to zero, we selected that model over the cubic growth model.

Table 22 shows the maximum likelihood estimates of the parameter values for all models considered along with the associated log-likelihood and AIC values. The Gompertz model

Table 22. Fetal thyroid mass models (g vs. fetal mass in g for power law models, g vs. gestational age in weeks for all other models).

Model	$\hat{\theta}_0$	$\hat{\theta}_1$	$\hat{\theta}_2$	$\hat{\theta}_3$	$\ell(\hat{\theta})$	AIC
Linear Growth	0.014960	—	—	—	28.2108	-54.42
Quadratic Growth	-0.015229	0.0014665	—	—	168.39	-332.78
Cubic Growth	-0.0029982	0.00043792	1.9641×10^{-5}	—	170.08	-334.16
Gompertz	**0.0038483**	**0.30799**	**0.039800**	**—**	**170.035**	**-334.07**
Logistic	2.6022	0.14914	34.613	—	169.644	-333.29
Power Law	0.0050755	0.71057	—	—	164.447	-324.89
Luecke Power Law	0.10683	-0.25045	0.073247	—	169.579	-333.16

For each model considered, the maximum likelihood parameter estimates ($\hat{\theta}$), log-likelihood ($\ell(\hat{\theta})$), and AIC are provided. The row describing the selected model is shown in boldface.

https://doi.org/10.1371/journal.pone.0215906.t022

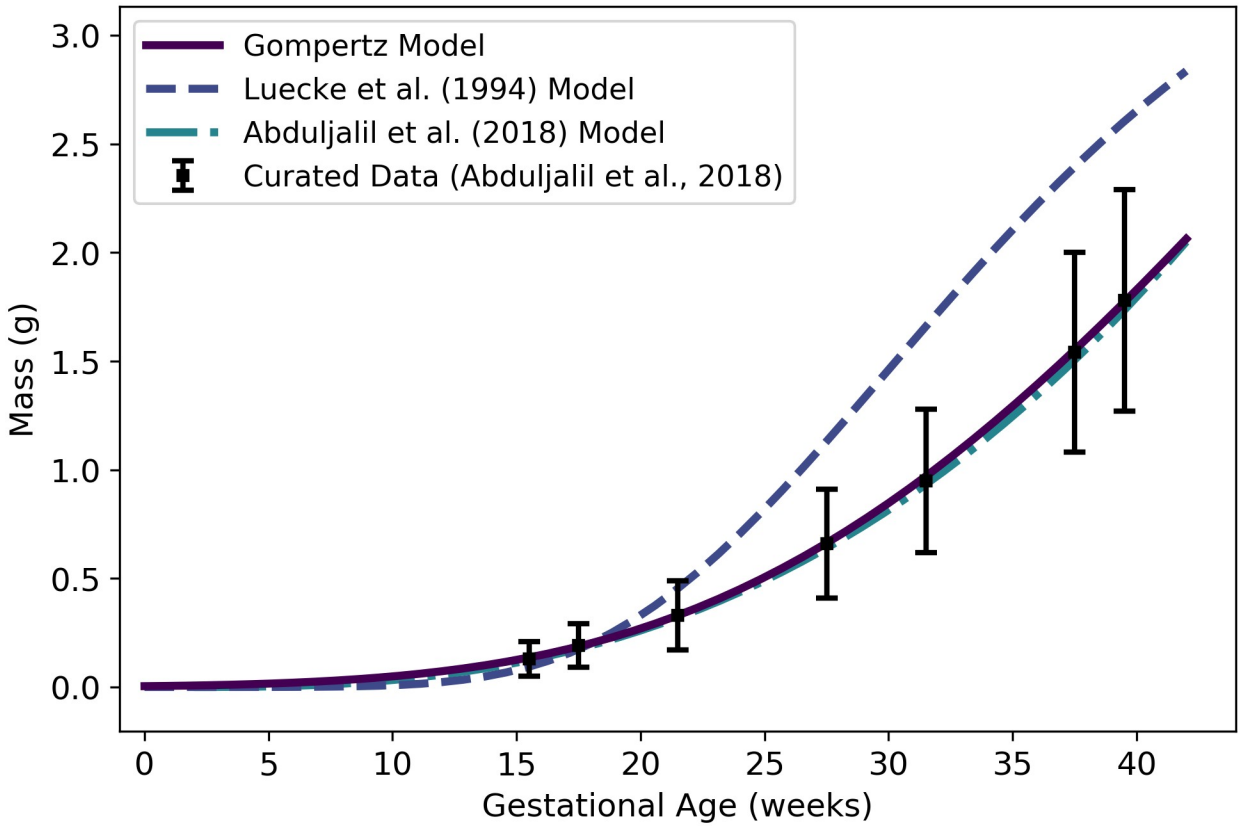

Fig 19. Fetal thyroid mass vs. gestational age. The Gompertz model (solid line) given by Eq 39 was selected as the most parsimonious model in our analysis. The model of Luecke et al. [15], which is a power law model based on fetal mass, was calibrated using a different data set [25].

https://doi.org/10.1371/journal.pone.0215906.g019

of Eq 39, two published models [15, 33], and the curated summary data [33] are shown in Fig 19.

Since the mean density of human thyroid tissue is 1.05 g/mL [35], the *volume* (mL) of the fetal thyroid can be computed as

$$V^{\mathrm{f}}_{\mathrm{thyr}}(t) = \frac{1}{1.05} \cdot W^{\mathrm{f}}_{\mathrm{thyr}}(t). \tag{40}$$

Gut. We used data curated by Abduljalil et al. [33] to calibrate various models for mass of the gastrointestinal tract (or "gut") of a human fetus during gestation. The Gompertz model given by

$$W^{\mathrm{f}}_{\mathrm{gutx}}(t) = 0.00081828 \cdot \exp\left[\frac{0.65028}{0.047724}\left(1 - \exp[-0.047724t]\right)\right] \tag{41}$$

was selected as the most parsimonious model for fetal thyroid *mass* (g) at gestational age t (weeks). Table 23 shows the maximum likelihood estimates of the parameter values for all models considered along with the associated log-likelihood and AIC values. The Gompertz model of Eq 41, two published models [32, 33], and the curated summary data [33] are shown in Fig 20.

Table 23. Fetal gut mass models (g vs. fetal mass in g for power law models, g vs. gestational age in weeks for all other models).

Model	$\hat{\theta}_0$	$\hat{\theta}_1$	$\hat{\theta}_2$	$\hat{\theta}_3$	$\ell(\hat{\theta})$	AIC
Linear Growth	0.0059272	—	—	—	-125.99	253.98
Quadratic Growth	-0.10234	0.015358	—	—	-58.46	120.93
Cubic Growth	0.14024	-0.032080	0.0018327	—	-11.68	29.37
Gompertz	**0.00081828**	**0.65028**	**0.047724**	**—**	**-7.3947**	**20.79**
Logistic	81.648	0.30673	31.545	—	-15.16	36.32
Power Law	0.026604	0.93314	—	—	-20.31	44.62
Luecke Power Law	0.038437	0.48413	0.056261	—	-9.00	23.99

For each model considered, the maximum likelihood parameter estimates ($\hat{\theta}$), log-likelihood ($\ell(\hat{\theta})$), and AIC are provided. The row describing the selected model is shown in boldface.

https://doi.org/10.1371/journal.pone.0215906.t023

Since the mean density of human gut tissue is 1.045 g/mL [35], the *volume* of the fetal gut (in mL) can be computed as

$$V^{\mathrm{f}}_{\mathrm{gutx}}(t) = \frac{1}{1.045} \cdot W^{\mathrm{f}}_{\mathrm{gutx}}(t). \tag{42}$$

Rest of body. We used the principle of mass balance to obtain a formula for the volume of a "rest of body" compartment comprising all mass in the fetal body that has not been accounted

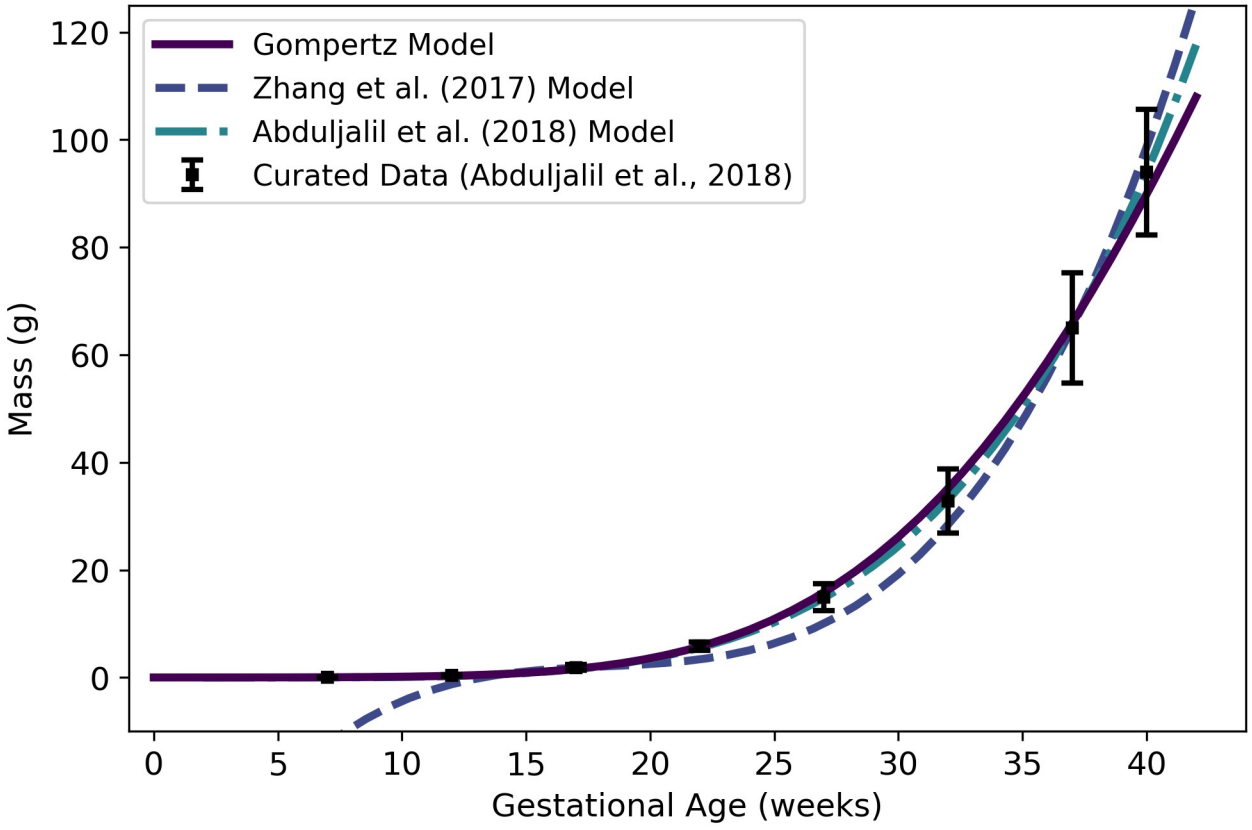

Fig 20. Fetal gut mass vs. gestational age. The Gompertz model (solid line) given by Eq 41 was selected as the most parsimonious model in our analysis. The model of Zhang et al. [32] was calibrated using a different data set. The Zhang et al. [32] model describes gut volume, so the units were converted assuming a tissue density of 1 g/mL.

https://doi.org/10.1371/journal.pone.0215906.g020

for in one of the specific compartments already described. The volume (mL) of the rest of body can be calculated as

$$\begin{aligned} \boldsymbol{V}^{\mathrm{f}}_{\mathrm{rest}}(\boldsymbol{t}) = \quad & \boldsymbol{W}^{\mathrm{f}}(\boldsymbol{t}) - \left(\frac{\mathbf{1}}{\mathbf{1.04}}\boldsymbol{W}^{\mathrm{f}}_{\mathrm{bran}}(\boldsymbol{t})\right) + \frac{\mathbf{1}}{\mathbf{1.05}}\boldsymbol{W}^{\mathrm{f}}_{\mathrm{livr}}(\boldsymbol{t}) + \frac{\mathbf{1}}{\mathbf{1.05}}\boldsymbol{W}^{\mathrm{f}}_{\mathrm{kidn}}(\boldsymbol{t}) \\ & + \frac{\mathbf{1}}{\mathbf{1.05}}\boldsymbol{W}^{\mathrm{f}}_{\mathrm{lung}}(\boldsymbol{t}) + \frac{\mathbf{1}}{\mathbf{1.05}}\boldsymbol{W}^{\mathrm{f}}_{\mathrm{thyr}}(\boldsymbol{t}) + \left(\frac{\mathbf{1}}{\mathbf{1.045}}\boldsymbol{W}^{\mathrm{f}}_{\mathrm{gutx}}(\boldsymbol{t})\right), \end{aligned} \tag{43}$$

where W^{f}, $W^{\mathrm{f}}_{\mathrm{bran}}$, $W^{\mathrm{f}}_{\mathrm{livr}}$, $W^{\mathrm{f}}_{\mathrm{kidn}}$, $W^{\mathrm{f}}_{\mathrm{lung}}$, $W^{\mathrm{f}}_{\mathrm{thyr}}$, and $W^{\mathrm{f}}_{\mathrm{gutx}}$ are given by Eqs 2, 29, 32, 35, 37, 39 and 41 respectively, and the scalars represent appropriate densities (cf. Table 8). Note that we assume the average density of the fetus is 1 g/mL throughout gestation, so the total mass (g) of the fetus equals the total volume (mL) of the fetus. Eq 43 yields negative values until about 8 weeks of gestational age, so it should not be used for predictions before that time. In fact, because several of the models upon which Eq 43 depends were derived from data sets that contain no observations from the first trimester, we recommend that this model only be applied for gestational ages greater than 13 weeks. As shown in Fig 21, Eq 43 results in volumes for the fetal rest of body compartment that increase from about 15 mL at 13 weeks to about 2800 mL at 40 weeks.

Fetal blood flow rates

Doppler ultrasound studies provide a non-invasive means for determining cardiac output and distribution of blood flow in an organism at various stages of development. We examined

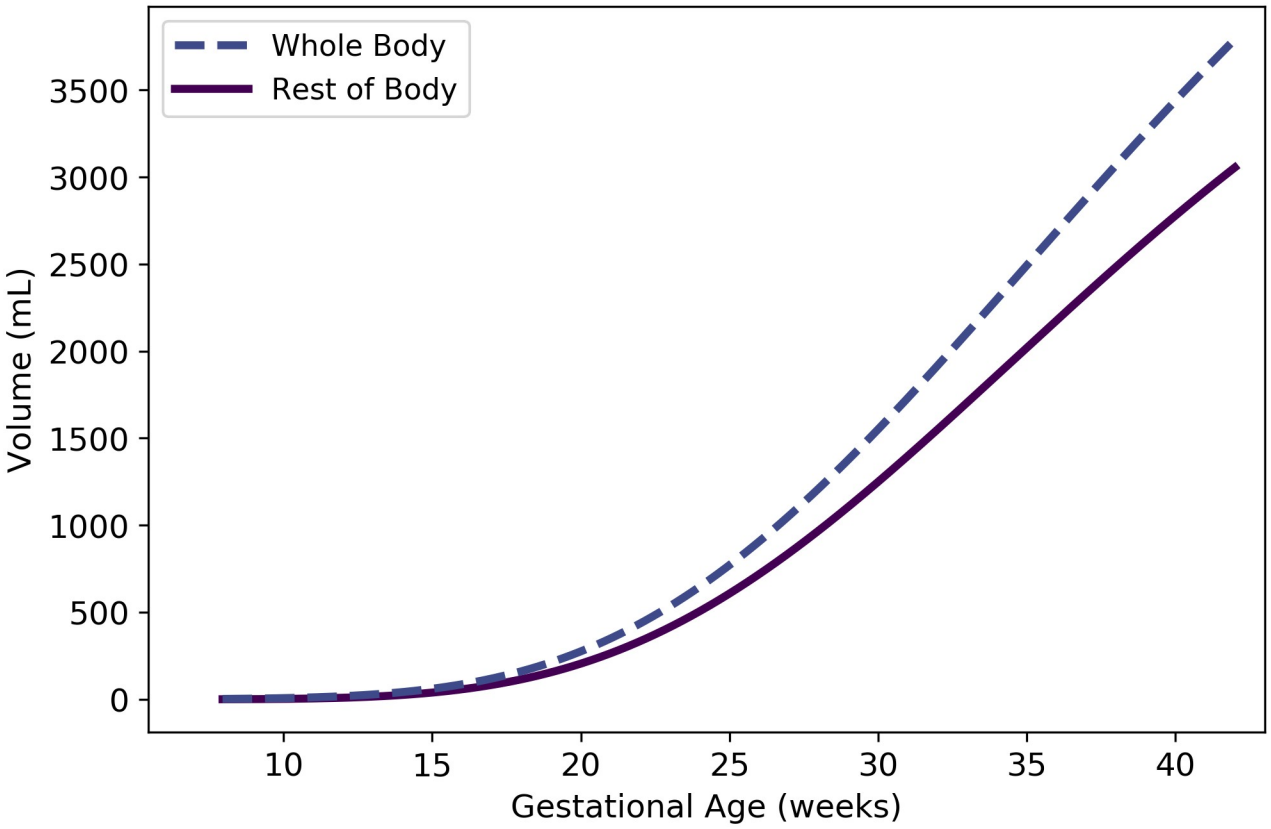

Fig 21. Fetal rest of body vs. gestation age (cf. Eq 43). The volume of the whole fetal body (cf. Eq 2) is shown for comparison.

https://doi.org/10.1371/journal.pone.0215906.g021

Table 24. Fetal right ventricle blood flow models (mL/min vs. fetal mass in g for power law models, mL/min vs. gestational age in weeks for all other models).

Model	$\hat{\theta}_0$	$\hat{\theta}_1$	$\hat{\theta}_2$	$\hat{\theta}_3$	$\ell(\hat{\theta})$	AIC
Linear Growth	3.265	—	—	—	-1563.53	3129.07
Quadratic Growth	-19.697	1.0498	—	—	-964.06	1932.13
Cubic Growth	11.755	-1.0908	0.034829	—	-940.55	1887.09
Gompertz	1.0138	0.27387	0.025665	—	-940.51	1887.02
Logistic	**2466.5**	**0.14837**	**43.108**	**—**	**-940.14**	**1886.29**
Power Law	0.024935	1.2908	—	—	-956.00	1915.99
Luecke Power Law	16619	-2.2943	0.23852	—	-941.29	1888.57

For each model considered, the maximum likelihood parameter estimates ($\hat{\theta}$), log-likelihood ($\ell(\hat{\theta})$), and AIC are provided. The row describing the selected model is shown in boldface.

https://doi.org/10.1371/journal.pone.0215906.t024

several studies that rely on such measurements to obtain formulae for blood flow rates to fetal tissues and through various components of the fetal circulatory system.

Right ventricle. We extracted data from Fig 5A of Kiserud et al. [38] and used it to calibrate various models for blood flow rate through the right ventricle of the fetal heart. The logistic model given by

$$Q^{f}_{rvtl}(t) = \frac{2466.5}{1 + \exp[-0.14837(t - 43.108)]} \tag{44}$$

was selected as the most parsimonious model for fetal right ventricle flow (mL/min) at gestational age t (weeks). Table 24 shows the maximum likelihood estimates of the parameter values for all models considered along with the associated log-likelihood and AIC values. Fig 22 shows the logistic model of Eq 44 along with the published model of Kiserud et al. [38].

Left ventricle. We extracted data from Fig 4A of Kiserud et al. [38] and used it to calibrate various models for blood flow rate through the left ventricle of the fetal heart. The logistic model given by

$$Q^{f}_{lvtl}(t) = \frac{506.30}{1 + \exp[-0.21916(t - 30.231)]} \tag{45}$$

was selected as the most parsimonious model for fetal left ventricle flow (mL/min) at gestational age t (weeks). Table 25 shows the maximum likelihood estimates of the parameter values for all models considered along with the associated log-likelihood and AIC values. Fig 23 shows the logistic model of Eq 45 along with the published model of Kiserud et al. [38].

Ductus arteriosus. We extracted data from Fig 8 of Mielke and Benda [39] and used it to calibrate various models for blood flow rate through ductus arteriosus of the human fetus. The logistic model given by

$$Q^{f}_{DA}(t) = \frac{1125.3}{1 + \exp[-0.18031(t - 35.939)]} \tag{46}$$

was selected as the most parsimonious model for fetal ductus arteriosus flow (mL/min) at gestational age t (weeks). Table 26 shows the maximum likelihood estimates of the parameter values for all models considered along with the associated log-likelihood and AIC values. Fig 24 shows the logistic model of Eq 46 and the data of Mielke and Benda [39].

Arterial blood. We define the flow rate into the fetal "arterial blood compartment" as the flow through the aorta just beyond its junction with the ductus arteriosus [64]. This flow

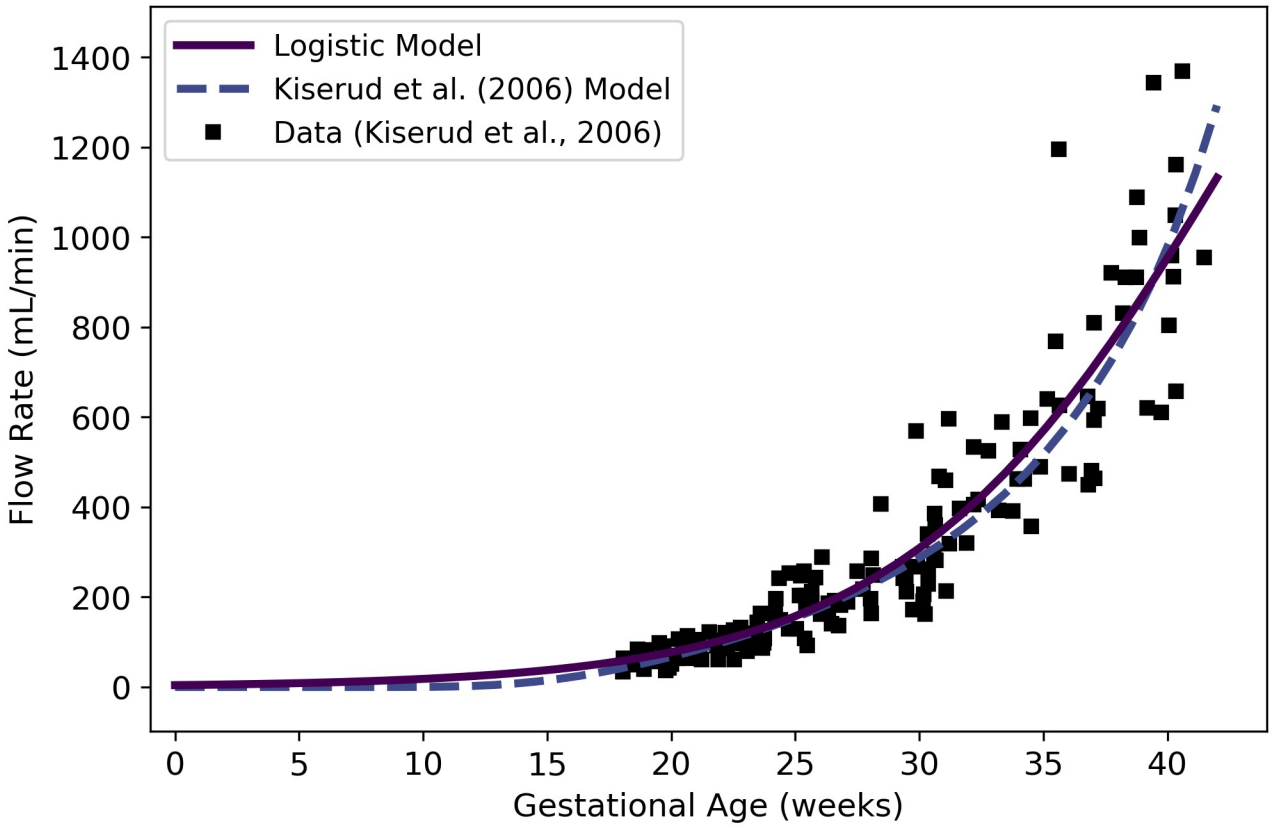

Fig 22. Fetal blood flow through the right ventricle vs. gestational age. The logistic model (solid line) given by Eq 44 was selected as the most parsimonious model in our analysis. The model of Kiserud et al. [38] was calibrated using the same data set [38] used by us.

https://doi.org/10.1371/journal.pone.0215906.g022

(mL/min) can be computed as

$$\boldsymbol{Q}^{\mathrm{f}}_{\mathrm{artb}}(\boldsymbol{t}) = \boldsymbol{Q}^{\mathrm{f}}_{\mathrm{lvtl}}(\boldsymbol{t}) + \boldsymbol{Q}^{\mathrm{f}}_{\mathrm{DA}}(\boldsymbol{t}). \tag{47}$$

Note that this formula represents a composite model, and it is not based directly upon measured time-course data for flow into the fetal arterial blood compartment.

Lung. The flow rate into the lungs equals the flow rate out of the left ventricle minus the flow that is shunted away from the lungs by the ductus arteriosus [64]. This flow (mL/min) is

Table 25. Fetal left ventricle blood flow models (mL/min vs. fetal mass in g for power law models, mL/min vs. gestational age in weeks for all other models).

Model	$\hat{\boldsymbol{\theta}}_0$	$\hat{\boldsymbol{\theta}}_1$	$\hat{\boldsymbol{\theta}}_2$	$\hat{\boldsymbol{\theta}}_3$	$\boldsymbol{\ell}(\hat{\boldsymbol{\theta}})$	AIC
Linear Growth	8.2127	—	—	—	-1328.70	2659.41
Quadratic Growth	-6.4372	0.46894	—	—	-1002.69	2009.38
Cubic Growth	-18.700	1.3115	-0.013824	—	-992.93	1991.86
Gompertz	2.4461×10^{-5}	1.5891	0.092460	—	-989.10	1984.20
Logistic	**506.30**	**0.21916**	**30.231**	**—**	**-985.42**	**1976.84**
Power Law	0.42909	0.86053	—	—	-991.64	1987.28
Luecke Power Law	0.0024511	2.2736	-0.095998	—	-989.07	1984.14

For each model considered, the maximum likelihood parameter estimates ($\hat{\theta}$), log-likelihood ($\ell(\hat{\theta})$), and AIC are provided. The row describing the selected model is shown in boldface.

https://doi.org/10.1371/journal.pone.0215906.t025

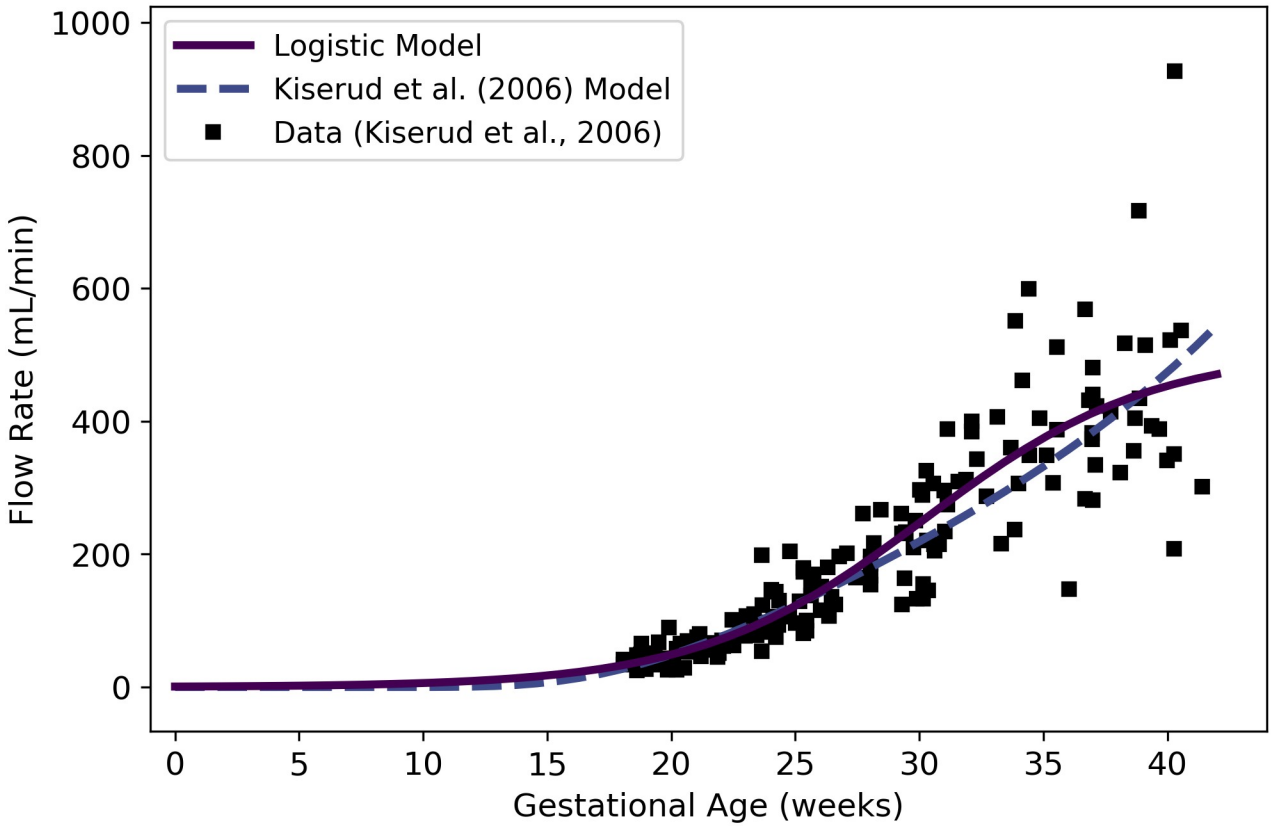

Fig 23. Fetal blood flow through the left ventricle vs. gestational age. The logistic model (solid line) given by Eq 45 was selected as the most parsimonious model in our analysis. The model of Kiserud et al. [38] was calibrated using the same data set [38] used by us.

https://doi.org/10.1371/journal.pone.0215906.g023

given by

$$\boldsymbol{Q}^{\mathrm{f}}_{\mathrm{lung}}(\boldsymbol{t}) = \boldsymbol{Q}^{\mathrm{f}}_{\mathrm{rvtl}}(\boldsymbol{t}) - \boldsymbol{Q}^{\mathrm{f}}_{\mathrm{DA}}(\boldsymbol{t}). \tag{48}$$

Note that this formula represents a composite model, and it is not based directly upon measured time-course data for flow into the fetal lung.

Foramen ovale. Assuming a conservation of flow, the total flow rate returning to the heart from the body via the "venous blood compartment" should be equal to the total flow rate

Table 26. Fetal ductus arteriosus blood flow models (mL/min vs. fetal mass in g for power law models, mL/min vs. gestational age in weeks for all other models).

Model	$\hat{\boldsymbol{\theta}}_0$	$\hat{\boldsymbol{\theta}}_1$	$\hat{\boldsymbol{\theta}}_2$	$\hat{\boldsymbol{\theta}}_3$	$\ell(\hat{\boldsymbol{\theta}})$	AIC
Linear Growth	13.401	—	—	—	-1714.79	3431.58
Quadratic Growth	-13.001	0.79207	—	—	-1258.10	2520.21
Cubic Growth	-3.2054	0.079383	0.012051	—	-1252.88	2511.76
Gompertz	0.011836	0.71885	0.058724	—	-1249.89	2505.78
Logistic	**1125.3**	**0.18031**	**35.939**	**—**	**-1247.00**	**2499.99**
Power Law	0.068851	1.1419	—	—	-1251.60	2507.2
Luecke Power Law	23.030	-0.41319	0.10352	—	-1249.07	2504.15

For each model considered, the maximum likelihood parameter estimates ($\hat{\theta}$), log-likelihood ($\ell(\hat{\theta})$), and AIC are provided. The row describing the selected model is shown in boldface.

https://doi.org/10.1371/journal.pone.0215906.t026

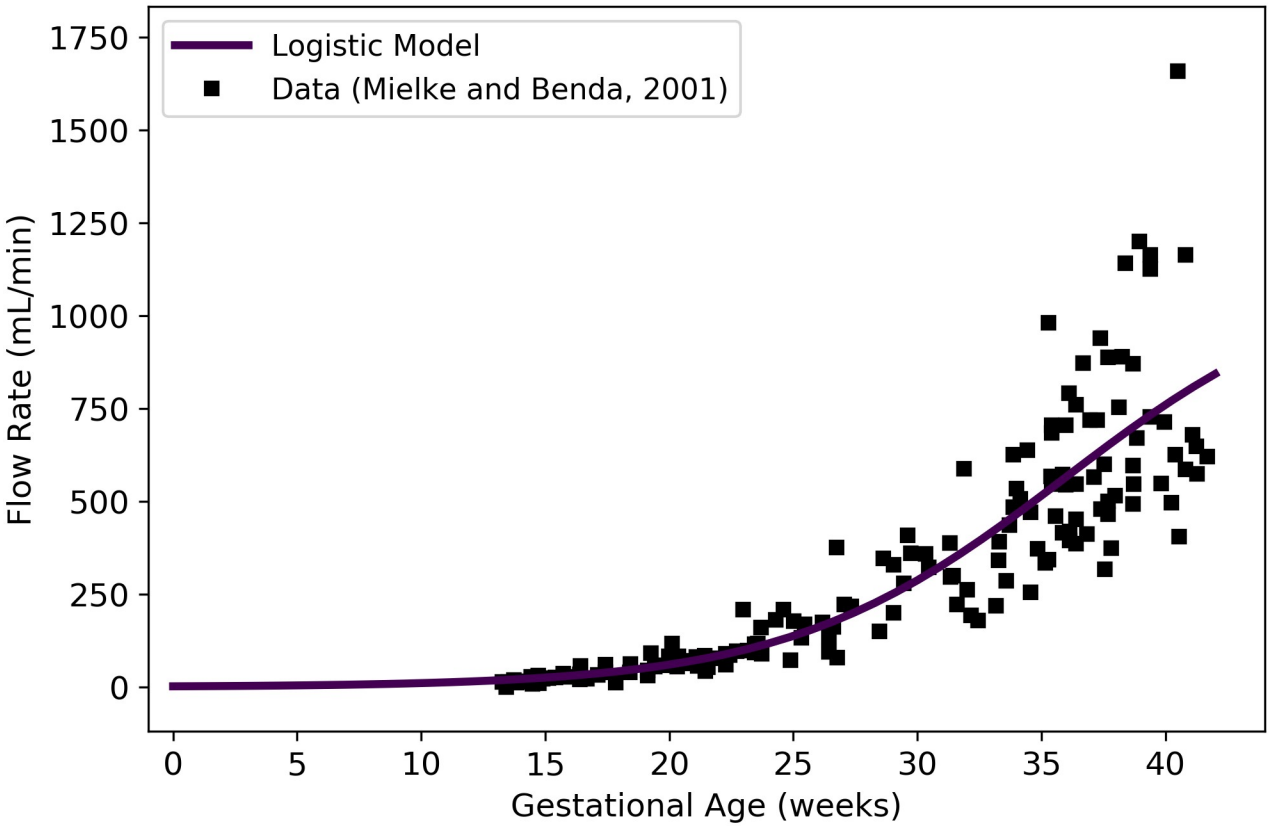

Fig 24. Fetal blood flow through the ductus arteriosus vs. gestational age. The logistic model (solid line) given by Eq 46 was selected as the most parsimonious model in our analysis, which utilized data of Mielke and Benda [39].

https://doi.org/10.1371/journal.pone.0215906.g024

leaving the heart and entering the "arterial blood compartment". This flow enters the right atrium of the heart, and part of the flow is directed to the right ventricle, while the remaining part is directed through the foramen ovale [64]. Thus, the flow (mL/min) through the foramen ovale can be computed as

$$\boldsymbol{Q}^{\mathrm{f}}_{\mathrm{FO}}(\boldsymbol{t}) = \boldsymbol{Q}^{\mathrm{f}}_{\mathrm{artb}}(\boldsymbol{t}) - \boldsymbol{Q}^{\mathrm{f}}_{\mathrm{rvtl}}(\boldsymbol{t}). \tag{49}$$

Note that this formula represents a composite model, and it is not based directly upon measured time-course data for flow through the foramen ovale.

Placenta. We extracted data from Fig 5A of Kiserud et al. [40] and used it to calibrate various models for the fetal blood flow rate through the placenta. The data depicted in the aforementioned figure are for blood flow in the "intra-abdominal umbilical vein", and so they measure rates of blood flowing from the placenta toward the liver and the ductus venosus [40]. The logistic model given by

$$\boldsymbol{Q}^{\mathrm{f}}_{\mathrm{plac}}(\boldsymbol{t}) = \frac{\mathbf{262.20}}{\mathbf{1} + \exp[\mathbf{-0.22183}(\boldsymbol{t} - \mathbf{28.784})]} \tag{50}$$

was selected as the most parsimonious model for fetal flow (mL/min) through the placenta at gestational age t (weeks). Table 27 shows the maximum likelihood estimates of the parameter values for all models considered along with the associated log-likelihood and AIC values.

Table 27. Models for fetal blood flow to the placenta (mL/min vs. fetal mass in g for power law models, mL/min vs. gestational age in weeks for all other models).

Model	$\hat{\theta}_0$	$\hat{\theta}_1$	$\hat{\theta}_2$	$\hat{\theta}_3$	$\ell(\hat{\theta})$	AIC
Linear Growth	4.716	—	—	—	-1343.40	2688.80
Quadratic Growth	-2.1512	0.21963	—	—	-1092.25	2188.49
Cubic Growth	-12.892	0.95321	-0.011962	—	-1066.27	2138.54
Gompertz	2.4281×10^{-5}	1.6159	0.098127	—	-1065.14	2136.28
Logistic	**262.20**	**0.22183**	**28.784**	**—**	**-1059.02**	**2124.04**
Power Law	0.59874	0.74324	—	—	-1070.75	2145.51
Luecke Power Law	6.1120×10^{-4}	2.6388	-0.12945	—	-1064.47	2134.93

For each model considered, the maximum likelihood parameter estimates ($\hat{\theta}$), log-likelihood ($\ell(\hat{\theta})$), and AIC are provided. The row describing the selected model is shown in boldface.

https://doi.org/10.1371/journal.pone.0215906.t027

Fig 25 shows the logistic model of Eq 50, two published models [32, 40], and the data extracted from Kiserud et al. [40].

Ductus venosus. We extracted data from Fig 5B of Kiserud et al. [40] and used it to calibrate various models for the fetal blood flow rate through the ductus venosus. The Gompertz model given by

$$Q^{\mathrm{f}}_{\mathrm{DV}}(t) = \mathbf{1.892} \cdot \exp\left[\frac{\mathbf{0.098249}}{\mathbf{0.0064374}}\left(1 - \exp[-\mathbf{0.0064374}t]\right)\right] \tag{51}$$

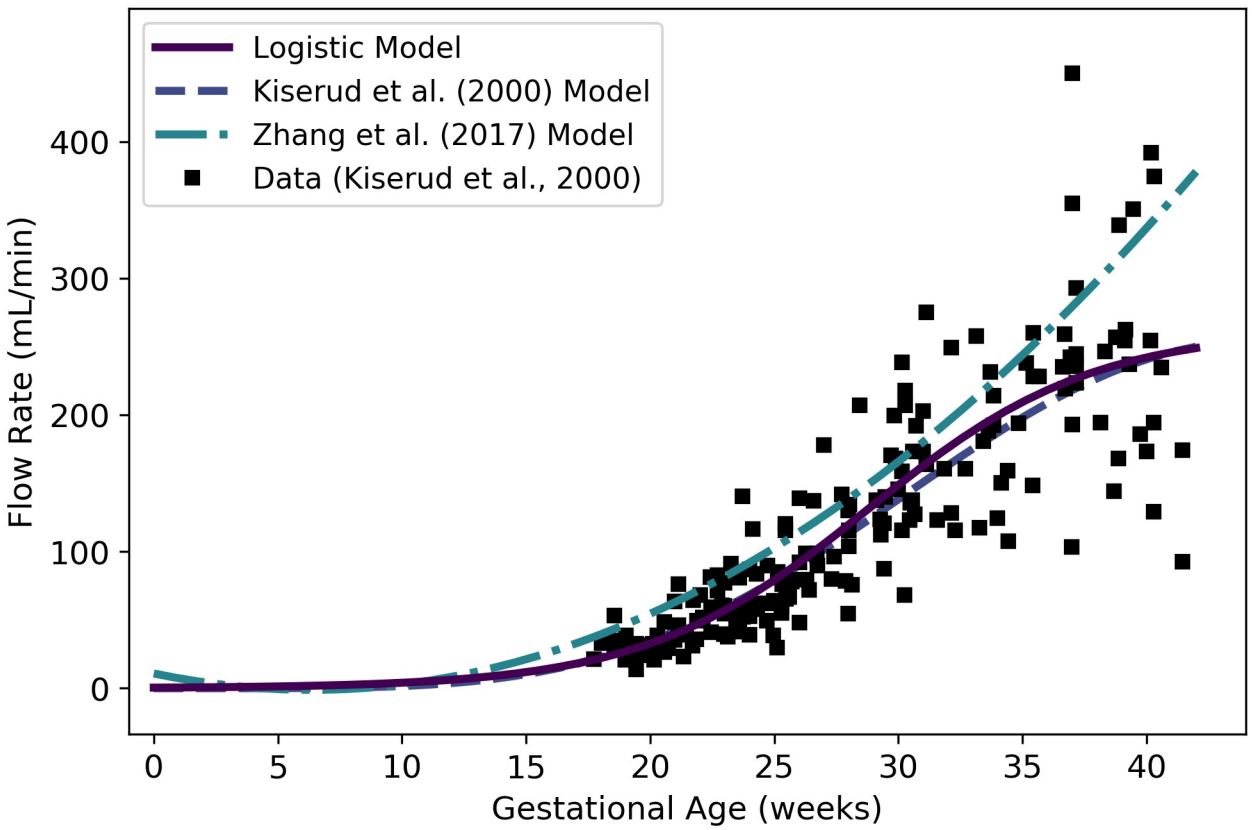

Fig 25. Fetal blood flow through the placenta vs. gestational age. The logistic model (solid line) given by Eq 50 was selected as the most parsimonious model in our analysis. The model of Kiserud et al. [40] was calibrated using the same data set [40] used by us, whereas the model of Zhang et al. [32] was calibrated using a different compiled data set.

https://doi.org/10.1371/journal.pone.0215906.g025

Table 28. Models for fetal blood flow through the ductus venosus (mL/min vs. fetal mass in g for power law models, mL/min vs. gestational age in weeks for all other models).

Model	$\hat{\theta}_0$	$\hat{\theta}_1$	$\hat{\theta}_2$	$\hat{\theta}_3$	$\ell(\hat{\theta})$	AIC
Linear Growth	1.0214	—	—	—	-1578.25	3158.5
Quadratic Growth	-0.41055	0.046294	—	—	-1330.9	2665.8
Cubic Growth	0.39477	-0.0095095	9.2087×10^{-4}	—	-1327.59	2661.18
Gompertz	**1.8920**	**0.098249**	**0.0064374**	**—**	**-1326.87**	**2659.75**
Logistic	2072.9	0.081565	82.890	—	-1327.09	2660.18
Power Law	0.14986	0.72500	—	—	-1347.34	2698.68
Luecke Power Law	180.87	-1.2763	0.13957	—	-1335.16	2676.32

For each model considered, the maximum likelihood parameter estimates ($\hat{\theta}$), log-likelihood ($\ell(\hat{\theta})$), and AIC are provided. The row describing the selected model is shown in boldface.

https://doi.org/10.1371/journal.pone.0215906.t028

was selected as the most parsimonious model for fetal blood flow (mL/min) through the ductus venosus at gestational age t (weeks). Table 28 shows the maximum likelihood estimates of the parameter values for all models considered along with the associated log-likelihood and AIC values. Fig 26 shows the Gompertz model of Eq 51, two published models [32, 40], and the data extracted from Kiserud et al. [40].

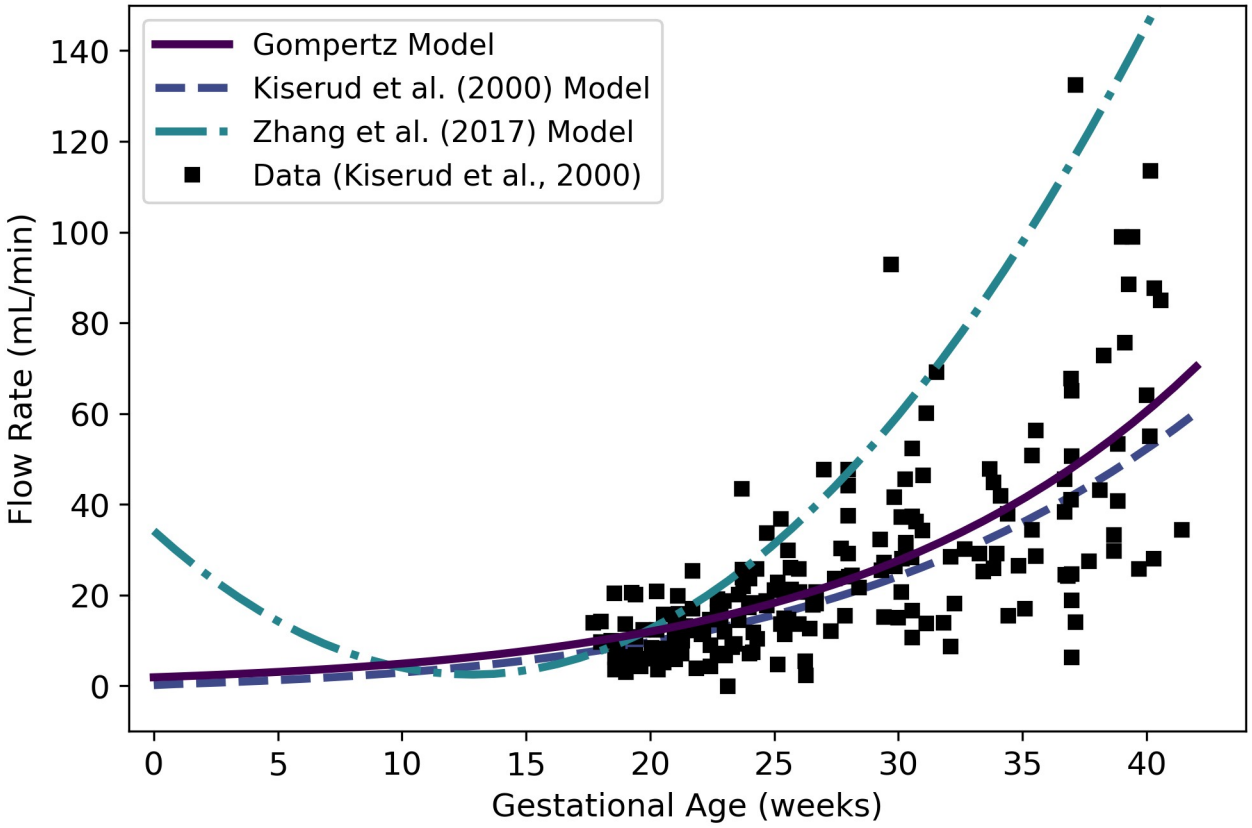

Fig 26. Fetal blood flow through the ductus venosus vs. gestational age. The Gompertz model (solid line) given by Eq 51 was selected as the most parsimonious model in our analysis. The model of Kiserud et al. [40] was calibrated using the same data set [40] used by us, whereas the model of Zhang et al. [32] was calibrated using a different compiled data set.

https://doi.org/10.1371/journal.pone.0215906.g026

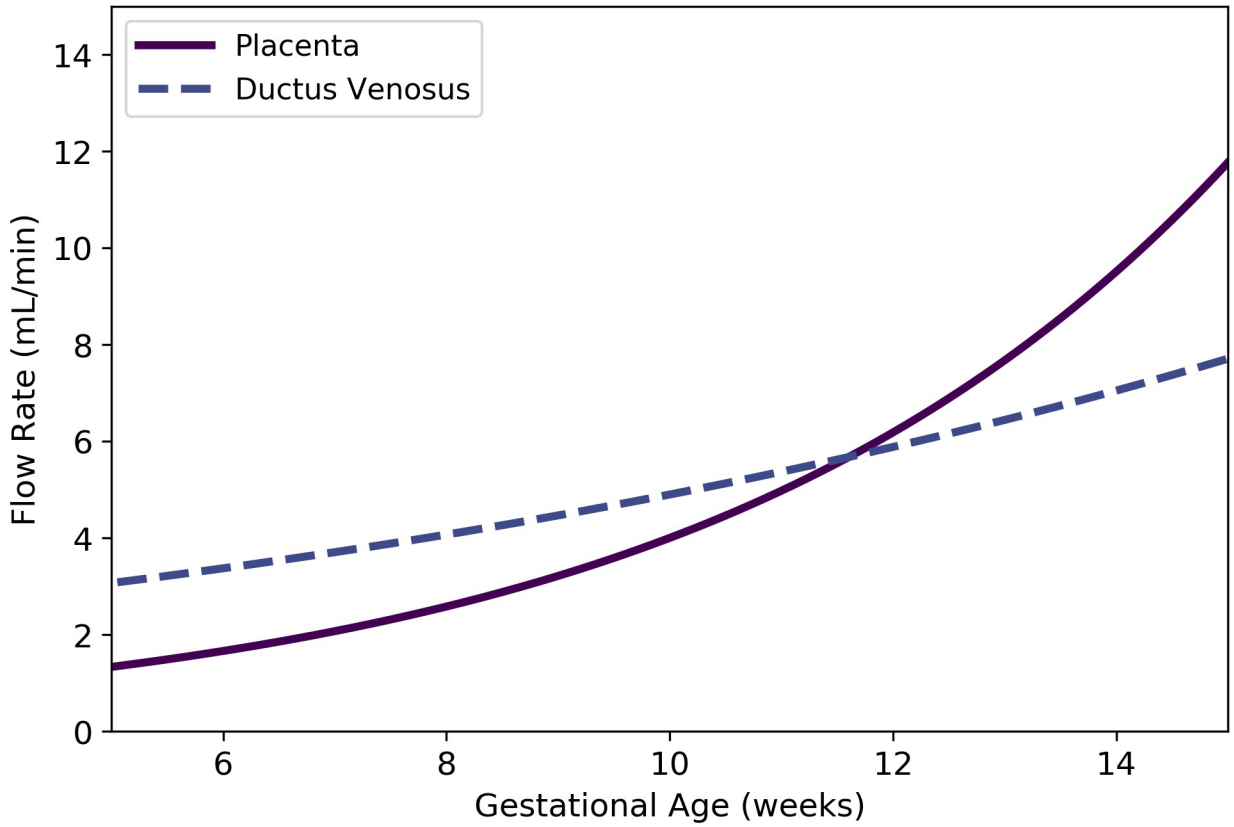

Fig 27. Comparison of flow rates through the placenta and through the ductus venosus vs. gestational age (cf. Eqs 50 and 51). Because blood flow through the ductus venosus should always be less than blood flow through the placenta, these models should not be used prior to gestational age 12 weeks.

https://doi.org/10.1371/journal.pone.0215906.g027

When using the models for flow to the placenta (Eq 50) and through the ductus venosus (Eq 51) together, one should exercise caution. The ductus venosus effectively diverts a portion of the blood traveling through the umbilical vein directly to the venous blood compartment, whereas the rest of that blood is carried to the liver [40]. Thus, the flow through the ductus venosus should always be less than the flow to (and from) the placenta. As shown in Fig 27, our models ensure that $Q^{\mathrm{f}}_{\mathrm{DV}}(t) < Q^{\mathrm{f}}_{\mathrm{plac}}(t)$ for gestational ages t greater than 12 weeks, but for some earlier gestational ages this is not the case.

Other specific compartments. We compute flow rates to other specific compartments in the fetus using proportions of the total flow to the arterial blood compartment, $Q^{\mathrm{f}}_{\mathrm{artb}}(t)$, which is given in Eq 47. Rudolph et al. [65] measured blood flow rates to various organs in 33 previable human fetuses with masses ranging from 12 to 272 grams (and estimated gestational ages between 10 and 20 weeks). Using this data, we generated the mean flow rate data shown in Table 29. To compute the fetal blood flows to the various sites other than the placenta (for which we already have Eq 50), we made the following assumptions:

- The proportion of blood flow to the placenta is not a constant, but depends on gestational age. This proportion can be computed as $Q^{\mathrm{f}}_{\mathrm{plac}}(t)/Q^{\mathrm{f}}_{\mathrm{artb}}(t)$ using Eqs 47 and 50.
- All arterial blood that does not flow to the placenta flows to the other tissues and tissue groups listed in Table 29. The total proportion of arterial blood flowing to these other tissues can be computed as $1 - Q^{\mathrm{f}}_{\mathrm{plac}}(t)/Q^{\mathrm{f}}_{\mathrm{artb}}(t)$.

Table 29. Average blood flow rates to various fetal tissues.

Tissue	Relevant Symbol	% CO
Placenta	Q^{f}_{plac}	23.9
Gut	Q^{f}_{gutx}	6.8
Kidneys	Q^{f}_{kidn}	5.4
Adrenals	—	4.8
Lower Body	—	27.1
Heart	—	3.0
Brain	Q^{f}_{bran}	14.3
Upper Body	—	13.6
Total		98.9

The values shown indicate mean percentages of total cardiac output (% CO), and are based upon data of Rudolph et al. [65]. In some cases, these authors made multiple measurements for a single fetus; for the purposes of computing the means in this table we only used the first measurement for each fetus. For many of the individual fetuses measured by Rudolph et al. [65], the percentages summed to 99 or 101; this can be explained by the fact that percentage values were rounded to the nearest unit. In some cases, however, the percentages for an individual fetus summed to a total less than 99 (and, in one case, as low as 88). The reason for these larger discrepancies is unclear, but they were rare and we decided to use the values from all 33 fetuses to compute the averages reported here.

https://doi.org/10.1371/journal.pone.0215906.t029

- The blood flow rates to compartments other than the placenta maintain constant proportions according to the values listed in Table 29. Since the total percentage of cardiac output flowing to tissues other than the placenta equals 75 (according to Table 29), all proportions from the table are scaled by this value.

Thus, blood flows (mL/min) to the gut, kidneys, and brain can be computed as

$$\boldsymbol{Q}^{f}_{gutx}(\boldsymbol{t}) = \frac{\mathbf{6.8}}{\mathbf{75}}\left(\mathbf{1} - \frac{\boldsymbol{Q}^{f}_{plac}(\boldsymbol{t})}{\boldsymbol{Q}^{f}_{artb}(\boldsymbol{t})}\right)\boldsymbol{Q}^{f}_{artb}(\boldsymbol{t}), \tag{52}$$

$$\boldsymbol{Q}^{f}_{kidn}(\boldsymbol{t}) = \frac{\mathbf{5.4}}{\mathbf{75}}\left(\mathbf{1} - \frac{\boldsymbol{Q}^{f}_{plac}(\boldsymbol{t})}{\boldsymbol{Q}^{f}_{artb}(\boldsymbol{t})}\right)\boldsymbol{Q}^{f}_{artb}(\boldsymbol{t}), \tag{53}$$

and

$$\boldsymbol{Q}^{f}_{bran}(\boldsymbol{t}) = \frac{\mathbf{14.3}}{\mathbf{75}}\left(\mathbf{1} - \frac{\boldsymbol{Q}^{f}_{plac}(\boldsymbol{t})}{\boldsymbol{Q}^{f}_{artb}(\boldsymbol{t})}\right)\boldsymbol{Q}^{f}_{artb}(\boldsymbol{t}), \tag{54}$$

respectively.

Several fetal tissue compartments were not examined by Rudolph et al. [65], and are therefore not listed in Table 29. To determine blood flow rates to these fetal compartments, we relied on published *adult* blood flow proportions [35]. In a typical adult (averaging male and female values), the total proportion of cardiac output *not* flowing to the gut, kidneys, or brain is 54% [35]. (We assume that the "gut" includes the stomach and esophagus, the small intestine, and the large intestine.) Also, in the fetus, the proportion of the arterial blood flow ($Q^{f}_{artb}(t)$) that goes to the gut, kidneys, and brain is $\frac{26.5}{75}\left(1 - Q^{f}_{plac}(t)/Q^{f}_{artb}(t)\right)$ (where 26.5 is the sum of the percentages flowing to gut, kidneys, and brain in Table 29). Thus, the proportion of arterial

blood flow not going to the gut, kidneys, brain, or placenta is $\left(1-\frac{26.5}{75}\right)\left(1-Q^{\mathrm{f}}_{\mathrm{plac}}(t)/Q^{\mathrm{f}}_{\mathrm{artb}}(t)\right)$. Since the adult proportions of cardiac output flowing to the liver and thyroid are 6.5% and 1.5%, respectively [35], we can estimate blood flows (mL/min) to the *fetal* liver and thyroid as

$$\boldsymbol{Q}^{\mathrm{f}}_{\mathrm{livr}}(\boldsymbol{t}) = \frac{\mathbf{6.5}}{\mathbf{54}}\left(\mathbf{1}-\frac{\mathbf{26.5}}{\mathbf{75}}\right)\left(\mathbf{1}-\frac{\boldsymbol{Q}^{\mathrm{f}}_{\mathrm{plac}}(\boldsymbol{t})}{\boldsymbol{Q}^{\mathrm{f}}_{\mathrm{artb}}(\boldsymbol{t})}\right)\boldsymbol{Q}^{\mathrm{f}}_{\mathrm{artb}}(\boldsymbol{t}) \tag{55}$$

and

$$\boldsymbol{Q}^{\mathrm{f}}_{\mathrm{thyr}}(\boldsymbol{t}) = \frac{\mathbf{1.5}}{\mathbf{54}}\left(\mathbf{1}-\frac{\mathbf{26.5}}{\mathbf{75}}\right)\left(\mathbf{1}-\frac{\boldsymbol{Q}^{\mathrm{f}}_{\mathrm{plac}}(\boldsymbol{t})}{\boldsymbol{Q}^{\mathrm{f}}_{\mathrm{artb}}(\boldsymbol{t})}\right)\boldsymbol{Q}^{\mathrm{f}}_{\mathrm{artb}}(\boldsymbol{t}), \tag{56}$$

respectively.

Rest of body. We used the principle of conservation of flow to obtain a formula for the blood flow rate to the fetal rest of body compartment. Thus, the flow rate to the rest of body compartment (in mL/min) is given by

$$\begin{aligned} Q^{\mathrm{f}}_{\mathrm{rest}}(t) = \; & Q^{\mathrm{f}}_{\mathrm{artb}}(t) - (Q^{\mathrm{f}}_{\mathrm{plac}}(t)) + Q^{\mathrm{f}}_{\mathrm{gutx}}(t) + Q^{\mathrm{f}}_{\mathrm{livr}}(t) + Q^{\mathrm{f}}_{\mathrm{thyr}}(t) \\ & + Q^{\mathrm{f}}_{\mathrm{kidn}}(t) + (Q^{\mathrm{f}}_{\mathrm{bran}}(t)), \end{aligned} \tag{57}$$

where t is the gestational age (weeks) and $Q^{\mathrm{f}}_{\mathrm{artb}}$, $Q^{\mathrm{f}}_{\mathrm{lung}}$, $Q^{\mathrm{f}}_{\mathrm{plac}}$, $Q^{\mathrm{f}}_{\mathrm{gutx}}$, $Q^{\mathrm{f}}_{\mathrm{kidn}}$, $Q^{\mathrm{f}}_{\mathrm{bran}}$, $Q^{\mathrm{f}}_{\mathrm{livr}}$, and $Q^{\mathrm{f}}_{\mathrm{thyr}}$ are given by Eqs 47, 48, 50, 52, 53, 54, 55, and 56, respectively. As shown in Fig 28, Eq 57 results in

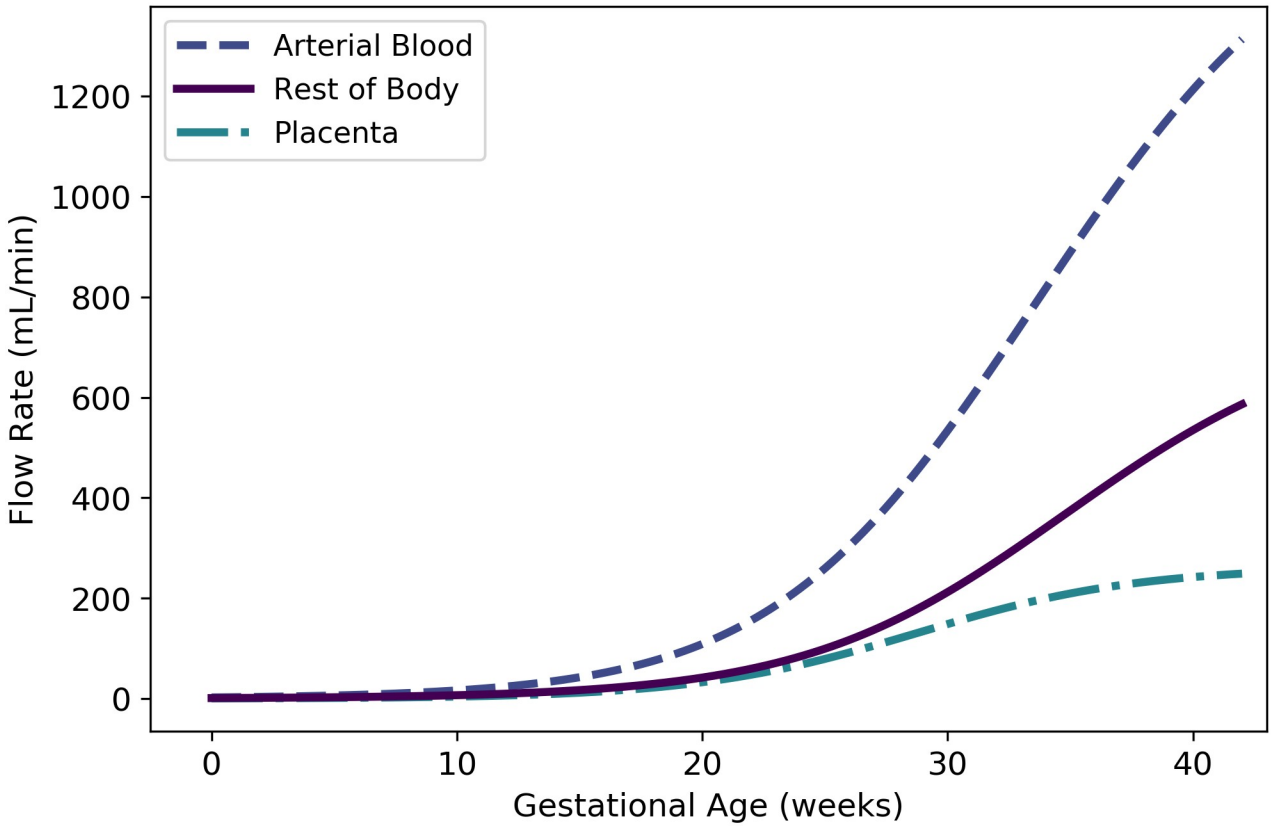

Fig 28. Fetal blood flow to the "rest of body" compartment vs. gestational age (cf. Eq 57). Fetal blood flow to the arterial blood compartment (cf. Eq 47) and the placenta (cf. Eq 50) are shown for comparison.

https://doi.org/10.1371/journal.pone.0215906.g028

Table 30. Fetal hematocrit models (percentage vs. gestational age in weeks).

Model	$\hat{\theta}_0$	$\hat{\theta}_1$	$\hat{\theta}_2$	$\hat{\theta}_3$	$\ell(\hat{\theta})$	AIC
Linear Growth	1.5067	—	—	—	-17.65	37.29
Quadratic Growth	**2.1113**	**-0.020268**	**—**	**—**	**-15.99**	**35.98**
Cubic Growth	4.5061	-0.18487	0.0026766	—	-15.13	36.27
Gompertz	1.4852	0.37866	0.10624	—	-16.33	38.36
Logistic	48.265	0.18901	15.372	37.316	-16.92	39.85
Power Law	11.579	0.18622	—	—	-16.65	37.29
Luecke Power Law	9.8655	0.27410	-0.0091527	—	-16.20	38.41

For each model considered, the maximum likelihood parameter estimates ($\hat{\theta}$), log-likelihood ($\ell(\hat{\theta})$), and AIC are provided. The row describing the selected model is shown in boldface.

https://doi.org/10.1371/journal.pone.0215906.t030

flow rates to the fetal rest of body compartment that increase from approximately 12 mL/min at 13 weeks to approximately and 535 mL/min at 40 weeks. The model produces strictly positive values for all gestational ages greater than zero; however, because the models upon which Eq 57 depends were derived from data sets that contain no observations prior to the second trimester, we recommend that this model only be applied for gestational ages greater than 13 weeks.

Other fetal physiological parameters

Hematocrit. Ohls [41] reported means and standard deviations for hematocrits of fetuses at gestational ages 18–21, 22–25, 26–29, and ">30" weeks, as well as at "term". To calibrate our models using these data, we assumed these periods correspond to 20, 24, 28, and 35 weeks of gestational age. Ohls [41] also reported that "term hematocrit values range from 50% to 63%," so we included an additional data point of 56.5% +/- 6.5% (the midpoint +/- half the difference of these two values) at 40 weeks. To incorporate an assumption that the embryo has no red blood cells at the time of conception (0 weeks gestational age), we included a data point for 0.0% +/- 4.0% at 0 weeks. As shown in Table 30, the quadratic growth model given by

$$H^{\mathrm{f}}(t) = 2.1113t - 0.020268t^2 \tag{58}$$

is the most parsimonious model based on the AIC; however, the cubic growth model

$$H^{\mathrm{f}}(t) = 4.5061t - 0.18487t^2 + 0.0026766t^3 \tag{59}$$

gives a better visual fit to the data and its AIC is only 0.8% larger. Both models allow for prediction of the fetal hematocrit (as a percentage) at gestational t (weeks) and are shown in Fig 29. The cubic model of Dallmann et al. [3] is also shown in Fig 29.

Discussion

Here we have presented a comprehensive collection of empirical models for anatomical and physiological changes related to human pregnancy and gestation. (See Table 2 for our list of preferred models.) Several similar repositories have been published [3, 15, 25, 28, 29, 31–33], but in evaluating each of these we found shortcomings that we sought to address in our own set of empirical models. One distinguishing feature of the current collection of models derives from our recognition that the fetal circulatory system differs fundamentally from the adult circulatory system. Thus, in addition to describing models for those pregnancy- and gestation-

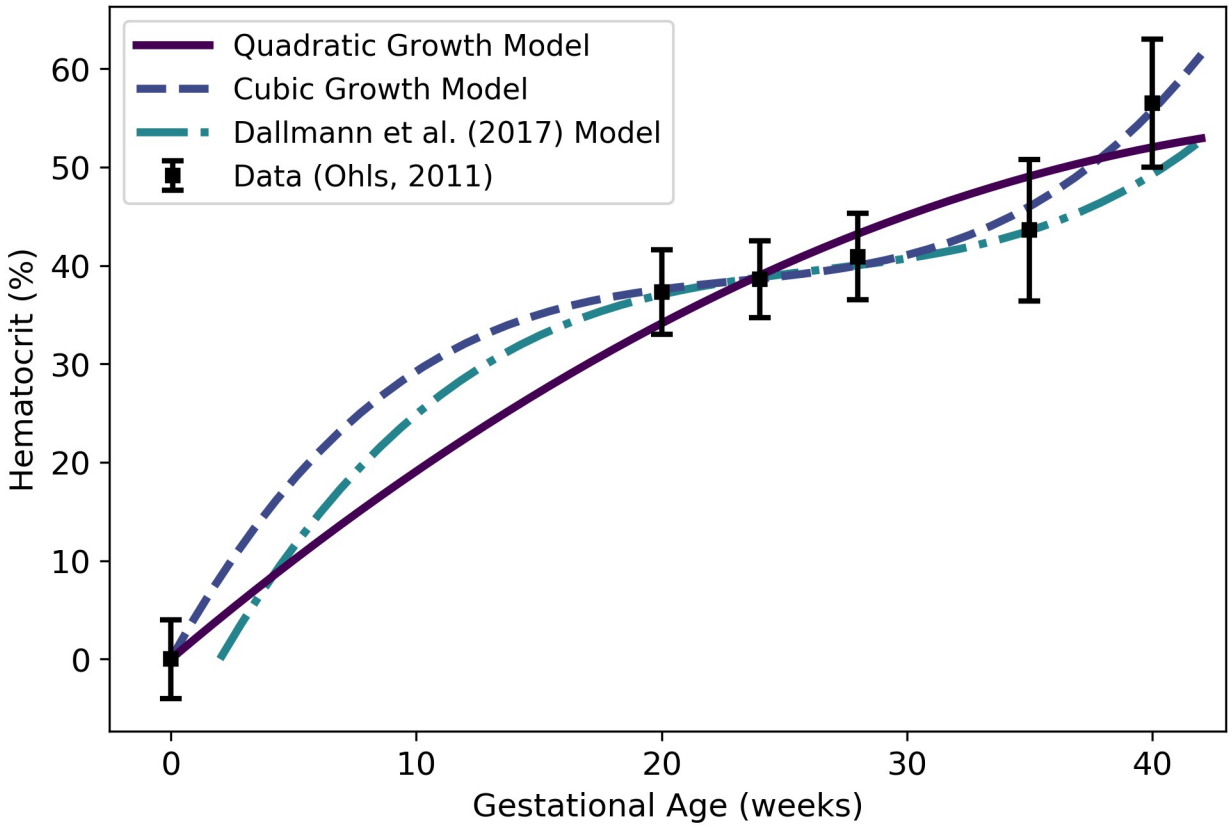

Fig 29. Fetal hematocrit vs. gestational age. The quadratic growth model (solid line) given by Eq 58 was selected as the most parsimonious model in our analysis, but the cubic growth model given by Eq 59 gives a better visual fit to the data while yielding only a slightly (0.8%) larger AIC score. We calibrated our models using the data curated by Ohls [41]. Dallmann et al. [3] calibrated their model with different data.

https://doi.org/10.1371/journal.pone.0215906.g029

related changes that have been included in other collections, we have provided models for blood flow rates in the fetus that do not have analogs in the adult; in particular, we have included models for blood flow rates through the ductus venosus, the ductus arteriosus, and the foramen ovale of the human fetus. To establish a single best model for each quantity of interest, we applied a rigorous set of statistical and mathematical procedures for calibrating a variety of models and selecting an optimal model. Finally, to better inform potential users of the models described herein, we have compared our models to previously-published alternative models wherever possible.

Some of the published models for fetal and maternal changes in anatomical and physiological quantities [15, 25, 28, 29, 31, 32, 38–40] are based on gestational age, or time since the last menstruation, while others [3, 33] are based on fetal age, or time since fertilization of the ovum. We have used gestational age as the basis for all the models reported herein since it seems to represent the more standard time scale in descriptions of pregnancy. It is generally acknowledged that a fetal age of zero weeks, or fertilization, coincides with a gestational age of 2 weeks [3, 33, 42]; thus, none of our models describing fetal quantities or products of conception (e.g., the placenta or amniotic fluid) should be used for predictions prior to gestational age 2 weeks! Whenever necessary (i.e., for data analysis or model comparison), we assumed that gestational age equals fetal age plus two weeks to convert between the two time scales.

One of our primary concerns with previously published repositories of human pregnancy and gestation models is that they tend to neglect models for changes in the developing fetus,

and most did not include models for those fetal blood flow rates that do not have analogs in the adult. There were exceptions, however. Luecke et al. [15] provided models for changes in maternal and fetal blood flow rates that were based upon allometric scaling of corresponding tissue masses, but did not describe the methods and data that were used to calibrate these models. Zhang et al. [32] acknowledged differences between adult and fetal circulation in their overall PBPK model schematic, and they did provide models for flow through the ductus arteriosus and the umbilical vein (which are components of the circulatory system special to the fetus); however, they did not provide models for blood flow through the ductus venosus or the foramen ovale (which are also important components of the fetal circulatory system). Similarly, El-Masri et al. [31] presented a PBPK model schematic demonstrating differences between the fetal and adult circulatory systems, and provided models for flow rates through many of the components of the fetal circulatory system, but omitted a model for blood flow through the umbilical vein. Also, El-Masri et al. [31] did not describe the methods they used to "fit" their models, and they did not verify the domains of applicability of the models (e.g., by identifying times at which the placenta flow model yields values less than the ductus arteriosus blood flow model).

In examining the models for human pregnancy- and gestation-related changes that are available in the literature, we discovered that some of the models give results that are clearly incorrect and/or substantially different from available data. For example, the maternal plasma volume model of Luecke et al. [15] predicts only small increases (~9%) in plasma volume during pregnancy. Our model and the curated data set we used for calibrating it predict considerably larger increases (~50%) in plasma volume (cf. Fig 4). Also, the amniotic fluid volume model of Luecke et al. [15] predicts volumes approximately an order of magnitude lower that those seen in the curated data set we used for calibrating our models. We hypothesize that one of the model parameters provided by those authors may have been in error by a factor of 10 (cf. Fig 7 and its caption). In the model collection published by Dallmann et al. [3], we found that the maternal glomerular filtration model (see their Eq 27) contains typographical and scaling errors. Through personal correspondence with the lead author of this work, we confirmed this finding and obtained a corrected version of the formula (cf. Fig 14 and its caption). The Luecke et al. (1994) models for fetal brain mass, liver mass, and thyroid mass tend to greatly exceed compiled data values for these quantities [33] during later gestational weeks (cf. Figs 15, 16 and 19). Several other examples of published models yielding unreasonable values were provided in the Introduction.

Besides various situations in which previously published models seem to contain errors, we discovered a few instances in which potential users of those models might need to exercise caution. For example, although the careful reader will note that the placenta volume model of Luecke et al. (1994) is only intended for use from days 25 to 300 of gestation, extrapolating to earlier times leads to unreasonably large values for placenta volume (cf. Fig 6). Thus, researchers needing estimates of placenta volume prior to the 3rd week of gestation should avoid using that model. Similarly, Zhang et al. [32] propose models for several fetal parameters (e.g., fetal brain blood flow and fetal small intestine) with limited domains of applicability (e.g., "10–20 weeks" and "12–25 weeks"), though they apparently apply these models for much broader time domains (i.e., up to 40 weeks) when conducting simulations using their full PBPK model for gestation.

In an apparent discrepancy with the curated data set [28] we used for calibrating our models for maternal hematocrit, the maternal hematocrit model of Dallmann et al. [3] predicts an increase in hematocrit in late pregnancy. Dallmann et al. [3] used a different curated data set to calibrate their model, and this data does seem to suggest an increase in maternal hematocrit starting at about 31 weeks. Some longitudinal studies of human subjects have shown that

hematocrit does typically increase at the end of pregnancy [56, 58]. Thus, applying our model parameterization and selection methods to aggregated data may in some cases lead to models that do not accurately represent anatomical and physiological changes experienced by *individuals* during pregnancy. Nevertheless, we believe the "preferred" models presented herein (cf. Table 2) are suitable for representing an *average* mother-fetus pair throughout gestation and pregnancy. We emphasize here that some published models that we have cited and reproduced graphically in our figures were constructed using data sets different from those used by us. Under these circumstances, two comparable models will inevitably be different even when both were constructed using appropriate and rigorous methods.

Most of the previously-published collections of human pregnancy and gestation models we've identified do not explicitly consider mass balance, flow balance, or "rest of body" compartments (cf. Table 1). In the present work, we have applied the principle of mass balance to provide models for volumes of and flow rates to rest of body compartments for both the mother and the fetus. With the exception of the fetal rest of body volume model, all of these models yield positive values on the entire time domain of interest (i.e., for gestational ages between 0 and 42 weeks), and the fetal rest of body volume model predicts positive volumes for gestational ages greater than 8 weeks. However, as discussed in the Results section, we recommend that the fetal flow rate and volume models not be used for gestational ages prior to 13 weeks due to the general sparsity of fetal data for the first trimester. (It is worth noting here that at least one study has demonstrated that maternal blood flow to the placental intervillous space may not be established until the end of the first trimester [60].) We have also endeavored evaluate consistency of the flow rate models. For example, based on the basic anatomy of the fetal circulatory system, the flow rate through the ductus venosus should always be less than the flow rate through the placenta. As shown in Fig 27, our models (Eqs 50 and 51) satisfy this requirement for gestational ages greater than 13 weeks.

While our collection of models offers many advantages and improvements over similar collections that have been published previously, it does still have some shortcomings. For one, we have provided no description of active transport across the placenta and how this might change throughout pregnancy. Understanding movement of a chemical across the placenta that is not based on passive diffusion may be critically important in assessing the levels of that chemical in both mother and fetus during pregnancy and gestation. Also, while we have provided models for many of the time-varying anatomical and physiological quantities relevant to pharmacokinetics, there are other potentially time-varying quantities that we have not considered that might also be relevant. For example, Dallmann et al. [3] point out that maternal serum albumin levels vary during pregnancy and they include a model for these variations in their model repository. Another limitation of our treatment is that most data sets we have used (and therefore most of the models we have presented) describe "healthy" women from predominantly Caucasian populations that were experiencing singleton, low-risk, uncomplicated pregnancies [28, 33]. Such women (and their fetuses) may not be adequately representative of *all* pregnant (and gestating) humans. Furthermore, we have offered no account of population variability in the time-dependent anatomical and physiological quantities we have analyzed. Dallmann et al. [3] attempted to do this by providing empirical models of both a "mean" and "standard deviation" for each quantity of interest they considered; however, using such models of component variability to account for whole-system variability (e.g., in a PBPK model for a mother and her fetus) may lead to unrealistic or unreasonable results, as the individual models for various components (e.g., maternal mass and maternal cardiac output) do not take into account the interdependencies inherent in the corresponding anatomical and physiological parameters [66, 67]. One subtle weakness of our analysis is that many of our fetal models tacitly assume the existence of functional organ systems in the embryo and fetus at early

gestational weeks. In constructing a PBPK model of human pregnancy and gestation, such assumptions should be carefully evaluated; in fact, in any such modeling effort, perhaps the best strategy would be to model the embryo/fetus as a single "compartment" up until the end of the first trimester, at which time distinct organs and tissues certainly exist in the fetus [42] and can be more reliably characterized. Finally, our repository of models is only valid for *human* mothers and their developing fetuses. For PBPK modeling applications involving intra-species extrapolation, it would be helpful to have a repository of models comparable to the one contained herein but specific to various non-human animals.

Conclusions

All PBPK models involve parameters that describe the anatomy and physiology of an organism, but defining values for these parameters requires special care when designing a PBPK model to represent a mother and fetus during the period from conception to birth. Because pregnancy and gestation represent a time of dramatic changes, many of the PBPK model parameters that are traditionally treated as constants for adult organisms or shorter-duration simulations must be described by time-varying functions in any PBPK model intended for studying this period, either in its entirety or for shorter time periods during which pregnancy- and gestation-related changes might be substantial. To facilitate the development of human pregnancy and gestation PBPK models, we have provided a repository of empirical models describing tissue volumes, blood flow rates, hematocrits, and glomerular filtration rates in an "average" mother and fetus. This collection of models offers advantages over similar repositories in that it includes descriptions for many fetal parameters that have previously been neglected and it uses rigorous and well-defined methods for model calibration and selection. We anticipate that the formulae provided in this collection will provide an improved basis for PBPK models of human pregnancy and gestation, and ultimately support decision-making with respect to optimal pharmacological dosing and risk assessment for pregnant women and their developing fetuses. In fact, we are currently preparing a manuscript that describes a high-throughput toxicokinetic (HTTK) model for pregnancy and gestation that is based upon the formulae provided herein.

Supporting information

S1 File. Model calibration details.
(PDF)

S2 File. Python source code and data files.
(ZIP)

Acknowledgments

The authors are grateful to Elaina Kenyon and Paul Schlosser for their careful review of any early draft of this manuscript. They would also like to thank the *PLOS ONE* editors and anonymous peer reviewers, whose comments and suggestions significantly enhanced the final version of this manuscript.

Author Contributions

Formal analysis: Dustin F. Kapraun.

Methodology: Dustin F. Kapraun.

Project administration: John F. Wambaugh.

Software: Dustin F. Kapraun.

Supervision: R. Woodrow Setzer, Richard S. Judson.

Visualization: Dustin F. Kapraun.

Writing – original draft: Dustin F. Kapraun, John F. Wambaugh.

Writing – review & editing: Dustin F. Kapraun, R. Woodrow Setzer, Richard S. Judson.

References

1. Congress US. Frank R. Lautenberg Chemical Safety for the 21st Century Act. Pub L 114–182 (114th Congress, 22 June 2016). 2016.
2. Corley RA, Mast TJ, Carney EW, Rogers JM, Daston GP. Evaluation of physiologically based models of pregnancy and lactation for their application in children's health risk assessments. Critical reviews in toxicology. 2003; 33(2):137–211. https://doi.org/10.1080/713611035 PMID: 12708613
3. Dallmann A, Ince I, Meyer M, Willmann S, Eissing T, Hempel G. Gestation-Specific Changes in the Anatomy and Physiology of Healthy Pregnant Women: An Extended Repository of Model Parameters for Physiologically Based Pharmacokinetic Modeling in Pregnancy. Clinical Pharmacokinetics. 2017; 56 (11):1303–30. https://doi.org/10.1007/s40262-017-0539-z PMID: 28401479
4. Judson R, Richard A, Dix DJ, Houck K, Martin M, Kavlock R, et al. The Toxicity Data Landscape for Environmental Chemicals. Environmental Health Perspectives. 2009; 117(5):685–95. https://doi.org/10.1289/ehp.0800168 PMID: 19479008
5. Breyer S. Breaking the Vicious Circle: Toward Effective Risk Regulation: Harvard University Press; 2009.
6. Egeghy PP, Judson R, Gangwal S, Mosher S, Smith D, Vail J, et al. The exposure data landscape for manufactured chemicals. Sci Total Environ. 2012; 414:159–66. Epub 2011/11/23. https://doi.org/10.1016/j.scitotenv.2011.10.046 PMID: 22104386.
7. National Research Council. Risk Assessment in the Federal Government: Managing the Process. Washington (DC): National Academies Press; 1983.
8. O'Flaherty EJ. Toxicants and drugs: kinetics and dynamics: John Wiley & Sons; 1981.
9. Young JF, Branham WS, Sheehan DM, Baker ME, Wosilait WD, Luecke RH. Physiological "constants" for PBPK models for pregnancy. Journal of toxicology and environmental health. 1997; 52(5):385–401. https://doi.org/10.1080/00984109708984072 PMID: 9388532
10. Rowlands JC, Sander M, Bus JS, Committee FO. FutureTox: building the road for 21st century toxicology and risk assessment practices. toxicological sciences. 2013; 137(2):269–77. https://doi.org/10.1093/toxsci/kft252 PMID: 24204016
11. Centers for Disease Control and Prevention. National Health and Nutrition Examination Survey Webpage: About the National Health and Nutrition Examination Survey 2016 [cited 2016 28 July]. http://www.cdc.gov/nchs/nhanes/about_nhanes.htm.
12. Barton HA. Computational pharmacokinetics during developmental windows of susceptibility. Journal of Toxicology and Environmental Health, Part A. 2005; 68(11–12):889–900.
13. Gentry PR, Covington TR, Clewell HJ. Evaluation of the potential impact of pharmacokinetic differences on tissue dosimetry in offspring during pregnancy and lactation. Regulatory Toxicology and Pharmacology. 2003; 38(1):1–16. PMID: 12878049
14. Wilson JG. Environment and birth defects: Academic Pr; 1973.
15. Luecke RH, Wosilait WD, Pearce BA, Young JF. A physiologically based pharmacokinetic computer model for human pregnancy. Teratology. 1994; 49:90–103. https://doi.org/10.1002/tera.1420490205 PMID: 8016750
16. Chiu WA, Barton HA, DeWoskin RS, Schlosser P, Thompson CM, Sonawane B, et al. Evaluation of physiologically based pharmacokinetic models for use in risk assessment. Journal of Applied Toxicology. 2007; 27(3):218–37. https://doi.org/10.1002/jat.1225 PMID: 17299829
17. Clark LH, Woodrow Setzer R, Barton HA. Framework for evaluation of physiologically-based pharmacokinetic models for use in safety or risk assessment. Risk analysis. 2004; 24(6):1697–717. https://doi.org/10.1111/j.0272-4332.2004.00561.x PMID: 15660623
18. Coecke S, Pelkonen O, Leite SB, Bernauer U, Bessems JG, Bois FY, et al. Toxicokinetics as a key to the integrated toxicity risk assessment based primarily on non-animal approaches. Toxicology in Vitro. 2013; 27(5):1570–7. https://doi.org/10.1016/j.tiv.2012.06.012 PMID: 22771339

19. Dourson ML, Felter SP, Robinson D. Evolution of science-based uncertainty factors in noncancer risk assessment. Regulatory Toxicology and Pharmacology. 1996; 24(2):108–20.
20. EPA U. Approaches for the application of physiologically based pharmacokinetic (PBPK) models and supporting data in risk assessment. National Center for Environmental Assessment, Washington, DC. 2006.
21. Espié P, Tytgat D, Sargentini-Maier M-L, Poggesi I, Watelet J-B. Physiologically based pharmacokinetics (PBPK). Drug metabolism reviews. 2009; 41(3):391–407. https://doi.org/10.1080/10837450902891360 PMID: 19601719
22. Grech A, Brochot C, Dorne J-L, Quignot N, Bois FY, Beaudouin R. Toxicokinetic models and related tools in environmental risk assessment of chemicals. Science of The Total Environment. 2017; 578:1–15. https://doi.org/10.1016/j.scitotenv.2016.10.146 PMID: 27842969
23. Barton HA, Chiu WA, Setzer RW, Andersen ME, Bailer AJ, Bois FY, et al. Characterizing uncertainty and variability in physiologically based pharmacokinetic models: state of the science and needs for research and implementation. Toxicological Sciences. 2007; 99(2):395–402. https://doi.org/10.1093/toxsci/kfm100 PMID: 17483121
24. Clewell RA, Merrill EA, Gearhart JM, Robinson PJ, Sterner TR, Mattie DR, et al. Perchlorate and radioiodide kinetics across life stages in the human: using PBPK models to predict dosimetry and thyroid inhibition and sensitive subpopulations based on developmental stage. Journal of Toxicology and Environmental Health, Part A. 2007; 70(5):408–28.
25. Luecke RH, Wosilait WD, Young JF. Mathematical representation of organ growth in the human embryo/fetus. International Journal of Bio-Medical Computing. 1995; 39:337–47. PMID: 7490167
26. Luecke RH, Wosilait WD, Young JF. Mathematical modeling of human embryonic and fetal growth rates. Growth, development, and aging: GDA. 1999; 63(1–2):49–59. PMID: 10885857
27. Wosilait WD, Luecke RH, Young JF. A mathematical analysis of human embryonic and fetal growth data. Growth, development, and aging: GDA. 1992; 56(4):249–57. Epub 1992/01/01. PMID: 1487363.
28. Abduljalil K, Furness P, Johnson TN, Rostami-Hodjegan A, Soltani H. Anatomical, Physiological and Metabolic Changes with Gestational Age during Normal Pregnancy. Clinical Pharmacokinetics. 2012; 51(6):365–96. https://doi.org/10.2165/11597440-000000000-00000 PMID: 22515555
29. Gaohua L, Abduljalil K, Jamei M, Johnson TN, Rostami-Hodjegan A. A pregnancy physiologically based pharmacokinetic (p-PBPK) model for disposition of drugs metabolized by CYP1A2, CYP2D6 and CYP3A4. British journal of clinical pharmacology. 2012; 74(5):873–85. Epub 2012/06/26. https://doi.org/10.1111/j.1365-2125.2012.04363.x PMID: 22725721.
30. Spiess A-N, Neumeyer N. An evaluation of R2 as an inadequate measure for nonlinear models in pharmacological and biochemical research: a Monte Carlo approach. BMC Pharmacology. 2010; 10(6).
31. El-Masri H, Kleinstreuer N, Hines RN, Adams L, Tal T, Isaacs K, et al. Integration of Life-Stage Physiologically Based Pharmacokinetic Models with Adverse Outcome Pathways and Environmental Exposure Models to Screen for Environmental Hazards. Toxicological sciences: an official journal of the Society of Toxicology. 2016; 152(1):230–43. Epub 2016/05/22. https://doi.org/10.1093/toxsci/kfw082 PMID: 27208077 mc5009469.
32. Zhang Z, Imperial MZ, Patilea-Vrana GI, Wedagedera J, Gaohua L, Unadkat JD. Development of a Novel Maternal-Fetal Physiologically Based Pharmacokinetic Model I: Insights into Factors that Determine Fetal Drug Exposure through Simulations and Sensitivity Analyses. Drug Metabolism and Disposition. 2017; 45:920–38. https://doi.org/10.1124/dmd.117.075192 PMID: 28588050
33. Abduljalil K, Jamei M, Johnson TN. Fetal Physiologically Based Pharmacokinetic Models: Systems Information on the Growth and Composition of Fetal Organs. Clin Pharmacokinet. 2018. Epub 2018/07/11. https://doi.org/10.1007/s40262-018-0685-y PMID: 29987449.
34. Rohatgi A. WebPlotDigitizer 2018. https://automeris.io/WebPlotDigitizer.
35. ICRP. Basic Anatomical and Physiological Data for Use in Radiological Protection: Reference Values, ICRP Publication 89. Annals of the ICRP. 2002; 32:1–277. https://doi.org/10.1016/S0146-6453(03)00002-2
36. Wang Y, Zhao S. Placental Blood Circulation. 2010.
37. Overmoyer BA, McLaren CE, Brittenham GM. Uniformity of liver density and nonheme (storage) iron distribution. Archives of pathology & laboratory medicine. 1987; 111(6):549–54. Epub 1987/06/01. PMID: 3579513.
38. Kiserud T, Ebbing C, Kessler J, Rasmussen S. Fetal cardiac output, distribution to the placenta and impact of placental compromise. Ultrasound in obstetrics & gynecology: the official journal of the International Society of Ultrasound in Obstetrics and Gynecology. 2006; 28(2):126–36. Epub 2006/07/11. https://doi.org/10.1002/uog.2832 PMID: 16826560.

39. Mielke G, Benda N. Cardiac output and central distribution of blood flow in the human fetus. Circulation. 2001; 103:1662–8. PMID: 11273994

40. Kiserud T, Rasmussen S, Skulstad S. Blood flow and the degree of shunting through the ductus venosus in the human fetus. American journal of obstetrics and gynecology. 2000; 182(1 Pt 1):147–53. Epub 2000/01/29. PMID: 10649170.

41. Ohls RK. Developmental Erythropoiesis. In: Polin RA, Fox WW, Abman SH, editors. Fetal and Neonatal Physiology. 4 ed: Elsevier; 2011. p. 1495–520.

42. O'Rahilly R, Müller F. Human Embryology and Teratology. 2 ed: Wiley; 1996.

43. Gompertz B. On the Nature of the Function Expressive of the Law of Human Mortality, and on a New Mode of Determining the Value of Life Contingencies. Philosophical Transactions of the Royal Society of London. 1825; 115:513–83.

44. Laird AK. Dynamics of relative growth. Growth. 1965; 29(3):249–63. Epub 1965/09/01. PMID: 5865687.

45. Laird AK. Dynamics of embryonic growth. Growth. 1966; 30(2):263–75. Epub 1966/06/01. PMID: 5963700.

46. Verhulst PF. Recherches mathématiques sur la loi d'accroissement de la population. Nouveaux mémoires de l'Académie Royale des Sciences et Belles-Lettres de Bruxelles. 1845; 18:14–54.

47. Burnham KP, Anderson DR. Model Selection and Multimodel Inference: A practical information-theoretic approach. 2 ed: Springer-Verlag; 2002.

48. Hytten FE, Leitch I. The physiology of human pregnancy: Blackwell Scientific Publications Ltd; 1971 1971. 622 p.

49. Hytten FE. Weight gain in pregnancy. Clinical physiology in obstetrics. Second ed. Oxford: Blackwell Scientific Publications; 1991.

50. Meban C. The surface area and volume of the human fetus. Journal of Anatomy. 1983; 137(Pt 2):271–8.

51. Martin AD, Daniel MZ, Drinkwater DT, Clarys JP. Adipose tissue density, estimated adipose lipid fraction and whole body adiposity in male cadavers. International journal of obesity and related metabolic disorders: journal of the International Association for the Study of Obesity. 1994; 18(2):79–83. Epub 1994/02/01. PMID: 8148928.

52. CDC. National Health and Nutrition Examination Survey 2018. http://www.cdc.gov/nchs/nhanes.htm.

53. Del Nero U, Rudge MVC, Novo NF, Calderon IdMP, Brasil MAM. Metodologia para estudo do volume e densidade absoluta da placenta humana de termo. Revista Brasileira de Ginecologia e Obstetrícia. 2002; 24:212–6.

54. Uyeno D. The Physical Properties and Chemical Composition of Human Amniotic Fluid. Journal of Biological Chemistry. 1919; 37(1):77–103.

55. Hytten FE, Paintin DB. Increase in plasma volume during normal pregnancy. BJOG: An International Journal of Obstetrics & Gynaecology. 1963; 70(3):402–7. https://doi.org/10.1111/j.1471-0528.1963.tb04922.x

56. Weir RJ, Paintin DB, Brown JJ, Fraser R, Lever AF, Robertson JI, et al. A serial study in pregnancy of the plasma concentrations of renin, corticosteroids, electrolytes and proteins and of haematocrit and plasma volume. The Journal of obstetrics and gynaecology of the British Commonwealth. 1971; 78 (7):590–602. Epub 1971/07/01. PMID: 5558849.

57. Caton WL, Roby CC, et al. Plasma volume and extravascular fluid volume during pregnancy and the puerperium. American journal of obstetrics and gynecology. 1949; 57(3):471–81. Epub 1949/03/01. PMID: 18110652.

58. Low JA, Johnston EE, McBride RL. Blood volume adjustments in the normal obstetric patient with particular reference to the third trimester of pregnancy. American journal of obstetrics and gynecology. 1965; 91:356–63. Epub 1965/02/01. PMID: 14258262.

59. Widen EM, Gallagher D. Body composition changes in pregnancy: measurement, predictors and outcomes. European journal of clinical nutrition. 2014; 68(6):643–52. https://doi.org/10.1038/ejcn.2014.40 PMID: 24667754

60. Hustin J, Schaaps J-P. Echocardiograhic and anatomic studies of the maternotrophoblastic border during the first trimester of pregnancy. American Journal of Obstetrics & Gynecology. 1987; 157(1):162–8. https://doi.org/10.1016/S0002-9378(87)80371-X

61. Pearce R, Setzer W, Strope C, Sipes N, Wambaugh J. httk: R Package for High-Throughput Toxicokinetics. Journal of Statistical Software (accepted). 2016.

62. Davies B, Morris T. Physiological parameters in laboratory animals and humans. Pharmaceutical research. 1993; 10(7):1093–5. Epub 1993/07/01. PMID: 8378254.

63. Anderson BJ, Holford NH. Mechanistic basis of using body size and maturation to predict clearance in humans. Drug metabolism and pharmacokinetics. 2009; 24(1):25–36. Epub 2009/03/03. PMID: 19252334.

64. Barclay AE, Franklin KJ, Prichard MML. The foetal circulation and cardiovascular system, and the changes that they undergo at birth. Oxford, UK: Blackwell Scientific Publication; 1944.

65. Rudolph AM, Heymann MA, Teramo KAW, Barrett CT, Raiha NCR. Studies on circulation of the previable human fetus. Pediatric Research. 1971; 5:452–65.

66. Ring CL, Pearce RG, Setzer RW, Wetmore BA, Wambaugh JF. Identifying populations sensitive to environmental chemicals by simulating variability. 2017.

67. McNally K, Cotton R, Hogg A, Loizou G. Reprint of PopGen: A virtual human population generator. Toxicology. 2015; 332:77–93. Epub 2015/04/30. https://doi.org/10.1016/j.tox.2015.04.014 PMID: 25921244.